Journal of Double Star Observations

VOLUME 16 NUMBER 1 JANUARY 1, 2020

Inside this issue:

Inside this issue:

Catalog Access and New Lists of Neglected Doubles

Brian D. Mason

U.S. Naval Observatory
3450 Massachusetts Avenue, NW, Washington, DC, 20392-5420
brian.d.mason@navy.mil

1. Catalog Access

The US Naval Observatory Websites are undergoing modernization and will be offline starting Thursday, 24 October 2019. The expected completion of work and return of service is estimated as 30 April 2020. Until that time, the only access to double star catalogs will be via our website mirrors:

- The Washington Double Star Catalog: http://www.astro.gsu.edu/wds/
- Sixth Catalog of Orbits of Visual Binary Stars: http://www.astro.gsu.edu/wds/orb6.html
- Second Catalog of Rectilinear Elements: http://www.astro.gsu.edu/wds/lin2.html
- Fourth Catalog of Interferometric Measurements of Binary Stars: http://www.astro.gsu.edu/wds/int4.html
- The Third Photometric Magnitude Difference Catalog: http://www.astro.gsu.edu/wds/dm3.html
- IAU Commission G1 (Binary and Multiple Stars) webpage: http://www.astro.gsu.edu/wds/bsl/
- Double Star Astronomy at the U.S. Naval Observatory: http://www.astro.gsu.edu/wds/ds_history.html

2. Growth of the WDS and Data Mining

The availability of large astrometric catalogs and the admirable acumen of users has led to the republishing of the same measures and identification of the same "new" systems by multiple data-miners. This has significantly increased the amount of work needed to properly incorporate these data into the USNO double star catalogs. Therefore, in the future, data mining results will be added to the Washington Double Star (WDS) and Washington Double Star Supplement (WDSS) Catalogs at the discretion of the catalogers.

Furthermore, preference will be given to data prepared by those specifically associated with the original catalog project.

As can be seen in Figure 1, the WDS and the other catalogs we maintain are being added to at a prodigious rate. A great deal of this work is coming from data mining, most recently from Gaia (DR2). While this can be useful, it is always there to be mined and based on some private discussions it is possible that the best and final Gaia astrometric solution will not be producted until DR4 or later, so to avoid current data mining efforts being eventually superseded and replaced, data mining of Gaia results is not recommended at this time.

3. What Needs to be Done?

Observe. Actual observations cannot be replicated. The observations you make tonight cannot be made tomorrow night or next week. Due to the slow motion of many of the pairs in the WDS and WDSS, to first order, the claim is absurd: the motion of most known visual pairs are insignificant and well below the measurement error on consecutive nights.

However, it does get to the crux of the issue: your observations are a unique dataset which cannot be replicated.

As a result, lists have been generated of pairs which need to be observed. These lists include pairs which either are unconfirmed or pairs which have not been measured in many years ("many" set arbitrarily at 20 years). In the initial formulation two lists have been generated:

- https://ad.usno.navy.mil/wds/Webtextfiles/neglected list1.txt: List 1: Unconfirmed or (*date - last*) > 20*yrs*., V_a < 12, No X or K code systems.
- https://ad.usno.navy.mil/wds/Webtextfiles/neglected list2.txt: List 2: as above, but no magnitude restrictions.

Catalog Access and New Lists of Neglected Doubles

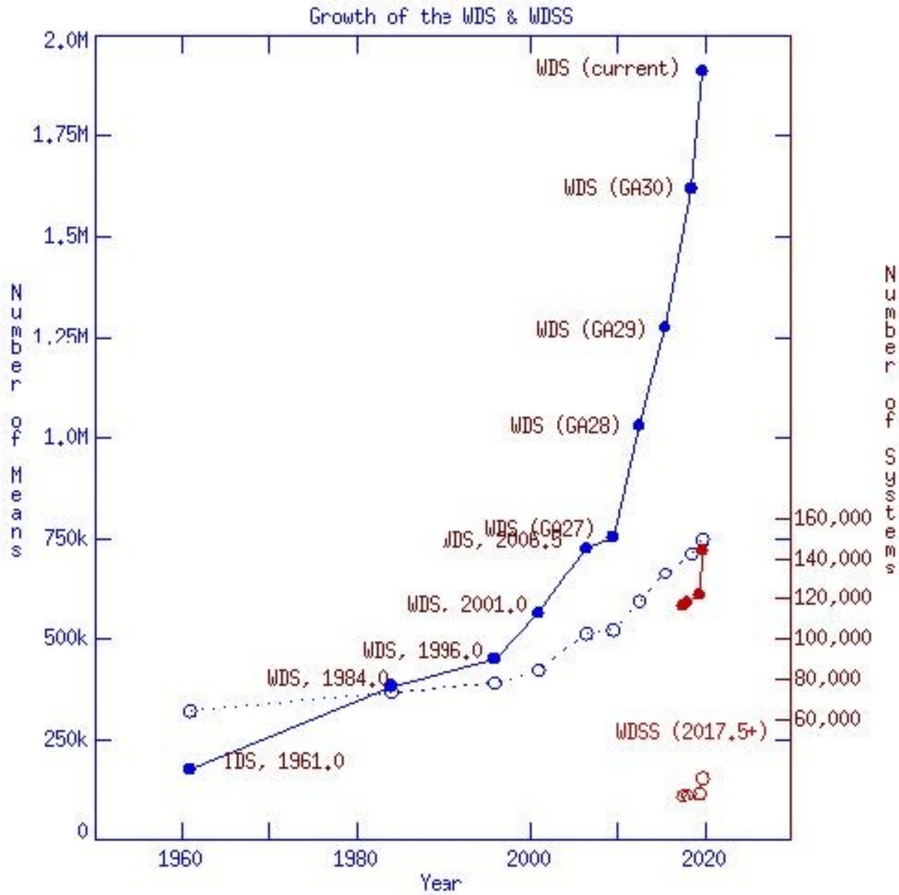

Figure 1. Growth of the WDS. The solid blue line and dots indicates the number of mean positions in the WDS, indicated on the left margin, at certain key dates. Indicated are publication of the IDS (1961), the major WDS data releases (1984, 1996, 2001, 2006.5), more recent dates corresponding to IAU General Assemblies (2009.5, 2012.5, 2015.5, 2018.5) and now (2019.75). The dashed blue line and open circles indicates the number of systems on those same dates and is indicated on the right margin. The solid/dashed red lines and filled/open red dotes indicates growth of the new WDS Supplement at inception and later (2017.5, 2018.0, 2019.41, 2019.75), on the same scales as the WDS plots.

The above lists are in WDS summary line format and are also available at the WDS mirror website at the weblinks below. These files will be automatically updated from the WDS as new observations and systems are added. The update of the lists will occur at least monthly, but may occur more often.

- http://www.astro.gsu.edu/wds/Webtextfiles/neglected_list1.txt
- http://www.astro.gsu.edu/wds/Webtextfiles/neglected_list2.txt

For these neglected pairs, even a non-detection can be useful if your observing capability is much greater than the parameters of the pair in question. For the neglected pairs where (*date* - *last*) is a very large number, the pair may be lost or miscataloged, and it may involve detective work or the perusal of old articles. This type of investigative work may be found especially appealing.

Good observing!

CCD Astrometric Measurements and Historical Data Summary of Double Stars WDS 05548-2527 and WDS 00177+2630

Ana Parra[1], Alexander Beltzer-Sweeney[1], Irena Stojimirovic[1], Pat Boyce[2], and Grady Boyce[2]

1. San Diego Mesa Community College
2. Boyce Research Initiatives and Education Foundation (BRIEF)

Abstract: We report CCD astrometric measurements of the double star system WDS 00548-2527 (B 92AB) and WDS 00177+2630 (BUP 5AB) using the iTelescope network. A position angle of 309.7° ± 0.03° and an angular separation of 7.33" ± 0.004" was determined for B 92AB. A position angle of 200.7° ± 0.007° and angular separation of 77.53" ± 0.02" was determined for BUP 5AB. Based on our new measurements and historic data on the systems we see no clear evidence that either system is binary.

Introduction

Astrometry is a branch of astronomy that measures a celestial body's position in the sky and its movement. Through astrometry, we can track the movement of the secondary star relative to the primary star of a double star system by recording its position angle (theta), measured in degrees from the celestial north, and angular separation (rho) between the two stars in arcseconds. By fixing the position of the primary star, the secondary star's movement can be tracked based on the pair's relative position angle and angular separation over time. The linear separation between binary pairs determines the time needed to complete one orbit by the secondary star (third Kepler's law). Binary components in a pair with a large separation may exhibit a linear motion with respect to each other over a long period of time. In this case even if the stars are true binaries, we may not see the signature of elliptical orbits in a few hundred years of observing. Small separation between binary components may quickly yield curvature in the motion of the secondary component confirming their binary nature. Optical pairs can display a linear/flat trend or random motion over extended time. Additionally, a double star's properties, such as common proper motion, parallax, and spectral type, can be inspected to further investigate its binary or optical identity.

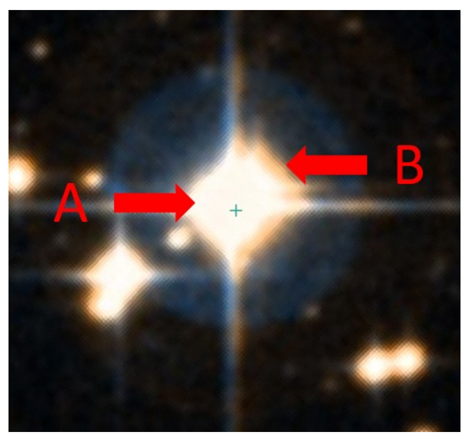

Figure 1. SIMBAD's optical image of B 92AB.

We selected two double star systems with unknown status: WDS 00548-2527 (B 92AB) and WDS 00177+2630 (BUP 5AB). The pairs meet the following criteria per the Washington Double Star (WDS) Catalog, accessible through Stelle Doppie: (a) observable during the fall in the northern and southern hemisphere by having a right ascension between 00 and 06 hours, (b) a magnitude difference (Δm) of 6 or less, (c) and an angular separation of 6" or more. We then (1) measured position angle and angular separation for each selected pair by the analysis of CCD images provided by the iTelescope network, and (2) investigated the double star's binary or optical properties by examining its historical data provided by The United States Naval Observatory (USNO), the WDS catalog, and SIMBAD, an astronomical database.

Historical Measurements of B 92AB				
Epoch	Position Angle (deg)	Angular Separation (arcseconds)	Source	Measurement Type
1911.01	314.1°	7.88"	WFC1998	Pa - Photographic with an astrograph
1926.00	310.2°	7.30"	B__1928b	Ma - Micrometer with refractor
1965.44	310.0°	7.10"	Knp1996a	Ma - Micrometer with refractor
1965.67	309.8°	7.28"	B__1968	Ma - Micrometer with refractor
1999.02	309.2°	7.38"	TMA2003	E2 - 2MASS Survey
1999.14	309.2°	7.32"	UC_2013b	EU - UCAC Catalog

Table 1. Historic measurements and data available on B 92AB; measurements are courtesy of the WDS catalog.

B 92AB Historical Background

B 92AB, Figure 1, found in Lepus, was discovered by Willem Hendrik van den Bos, a Dutch-South African astronomer, using a micrometer and a 0.7-meter refracting telescope in 1926. However, there was an earlier observation in 1911 not noted until 1998 by the Washington Fundamental Catalog (Wycoff, Mason, Urban 2006). Van den Bos recorded a position angle of 309.8° and angular separation of 7.28". The most recent observation was by USNO CCD Astrograph Catalog (UCAC) in 1999 and recorded a position angle of 309.2° and an angular separation of 7.32". There are currently seven observations of B 92AB in the WDS and it has been 18 years since its last observation. The historic observations for B 92AB are summarized in Table 1 (Mason, Hartkopf 2015).

B 92AB's A component is a star similar to our Sun, with a spectral class G1/2V and a magnitude of 8.67, and its B component has magnitude of 11.20 (Mason, Hartkopf 2015). Gaia DR2 reported the A component to have a proper motion of [-98.428 -33.771] and a parallax 15.1665 (±0.0353) milli-arcseconds (Gaia 2018b). For the B component Gaia DR2 reported a proper motion of [-96.864 -23.442] and a parallax 16.0971 (±0.1873) milli-arcseconds (Gaia 2018b). The small angular separation of 7.3" may appear challenging to image, Figure 1, however its 2.53 difference in magnitude grants leverage to the resolution capabilities of the iTelescope network.

BUP 5AB Historical Background

BUP 5AB, Figure 2, located in Andromeda, was discovered by Sherburne Wesley Burnham, an American astronomer, using a micrometer and a 1-meter refractor telescope of the Yerkes observatory in 1910. There was an earlier observation in 1895; however, it was not noted until 1998 by the Washington Fundamental Catalogue (Wycoff, Mason, Urban 2006). Burnham recorded a position angle of 199.7° and angular separation of 80.2" for BUP 5AB. The most recent observation was by USNO CCD Astrograph Catalog (UCAC) in 1999 and recorded a position angle of 200.5° and an angular separation of 77.90". There are currently seven observations of BUP 5AB in the WDS and it has been 16 years since its last observation. We summarize the historic observations for BUP 5AB in Table 2 (Mason, Hartkopf 2015).

BUP 5AB's A component has magnitude of 10.52 and was reported from Gaia DR2 to have a proper motion of [+40.024 -10.851] and a parallax 3.2695 (±0.0570) milli-arcseconds (Gaia 2018b). The B component has a 12.27 magnitude and was reported from Gaia DR2 to have a proper motion of [+33.598 +16.084] and a parallax 4.5776 (±0.0557) milli-arcseconds (Gaia 2018b). Having an 77.9" angular separation and 1.75 delta magnitude makes it a good candidate to observe without challenge to the iTelescope network. Different proper motions and parallaxes suggest an optical system.

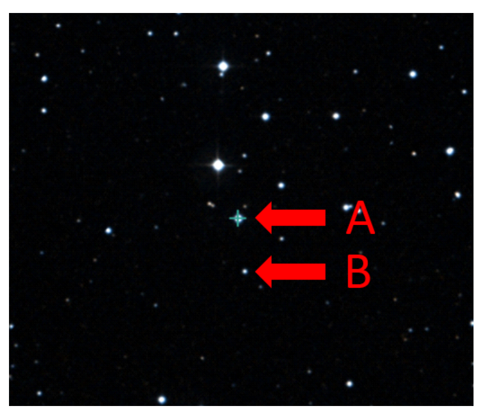

Figure 2. SIMBAD's optical image of BUP 5AB.

Historical Measurements of BUP 5AB				
Epoch	Position Angle (deg)	Angular Separation (arcseconds)	Source	Measurement Type
1895.76	199.2°	80.49"	WFC1998	Pa - Photographic with an astrograph
1897.77	199.6°	79.83"	WFC1998	Pa - Photographic with an astrograph
1907.78	199.6°	80.41"	WFC1998	Pa - Photographic with an astrograph
1910.56	199.7°	80.02"	Bu_1913	Ma - Micrometer with refractor
1991.47	200.5°	78.34"	TYC2002	Ht - Tycho
1997.80	200.5°	78.08"	TYC2003	E2 - 2MASS Survey
2001.58	200.5°	77.90"	UC_2013b	EU - UCAC Catalog

Table 2. Historic measurements and data available on BUP 5AB; measurements are courtesy of the WDS catalog.

Equipment

B 92AB images were acquired by Telescope T32, Figure 3, located in Siding Springs, Australia at an elevation of 1,122 meters. The CCD camera for T32 is a FLI Proline 16803 with a resolution of 0.63" per pixel housing an array 4096 by 4096 with a FOV of 43.2 by 43.2 arcminutes. The CCD camera is mounted on a Planewave 17" Corrected Dall-Kirkham (CDK) with a focal length of 2,912 mm, an aperture of 431 mm, and a focal ratio of f/6.8.

BUP 5AB images were acquired by Telescope T11, Figure 4, located in Mayhill, New Mexico at an elevation of 2,225 meters. The CCD camera for T11 is a FLI Proline PL1102M with a resolution of 0.81" per pixel housing an array 4008 by 2672 with a FOV of 36.2 by 54.3 arcminutes. The CCD camera is mounted on a Planewave 20" CDK with a focal length of 2,280 mm, an aperture of 510 mm, and a focal ratio of f/4.5. All images were saved as FITS files.

Figure 3. T32 17" PlaneWave f/6.8 CDK Astrograph with FLI Proline 16803 CCD in Siding Springs, Australia.

Methods and Procedures

Through the iTelescope network, we requested images of B 92AB and BUP 5AB at various exposure times and filters. The images B 92AB were observed at an exposure times of 60 seconds and 90 seconds with the Blue, OIII, and Hydrogen-alpha filters, and 90 seconds for the Ionized Sulfur filters. The images of BUP 5AB were captured at an exposure length of 45 seconds and 90 seconds with two filters: Luminance and Red.

The FITS files were individually uploaded to Astrometry.net for an astrometric calibration. The Right Ascension and Declination coordinates were calculated for the stars in the FITS images by comparing them to catalog images. Right Ascension and Declination grid of the image creates World Coordinate System (WCS) and was saved in the FITS file header. The down-

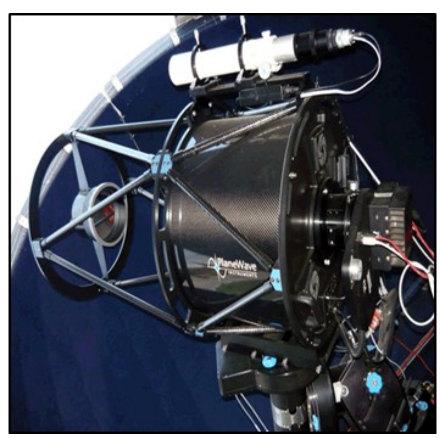

Figure 4. T11 20“ PlaneWave f/4.58 CDK Astrograph with FLI Proline PL1102M CCD Mayhill, New Mexico.

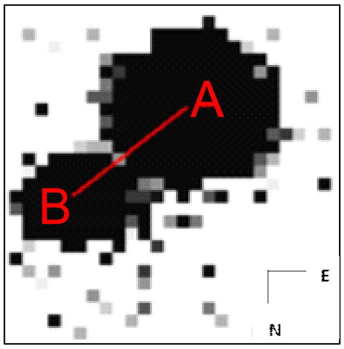

Figure 5. B 92AB under Hydrogen Alpha Filter-60 seconds. Image was processed in Mira Pro x64.

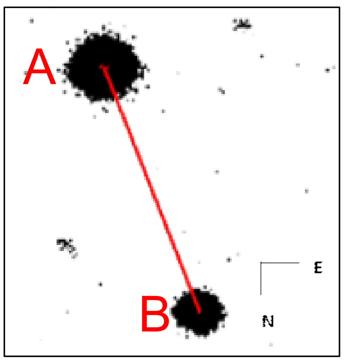

Figure 6. BUP 5AB under Luminance Filter-45 seconds. Image was processed in Mira Pro x64

loadable calibrated images were transferred to Mira Pro x64, an image processing software developed by Mirametrics, Inc.

Each image was processed in Mira Pro x64 (Mira) to calculate position angle and angular separation. The WDS catalog and SIMBAD were referenced to verify the A and B component's location on the calibrated images. Mira's Vertical Transfer Function and Vertical Palette granted better star visibility. With Mira's Distance and Angle tool, a line was drawn to connect the primary and secondary star's centroid and astrometric measurements were generated.

Results

Nine images of B 92AB were acquired on November 22, 2017, Table 3, and a sample image (Hydrogen Alpha filter with 60 second exposure) is provided in Figure 5. Four images of BUP 5AB were acquired on November 11, 2017 by T11, Table 4. A sample image (Luminance filter with 45 second exposure) of BUP 5AB is provided in Figure 6. Mira measurement of position angle and angular separation for each exposure and filter were exported to Microsoft Excel. Excel was used to calculate the mean, standard deviation, and

WDS 00548-2527 (B 92AB) Astrometry		
Telescope T32	**Epochs 2017.89**	
Filter Type-Exposure Time (seconds)	**Position Angle (degrees)**	**Angular Separation (arcseconds)**
Red-60s	309.58°	7.362"
Red-90s	309.65°	7.33"
OIII-60s	309.91°	7.31"
OIII-90s	310.11°	7.24"
Hydrogen Alpha-60s	309.08°	7.32"
Hydrogen Alpha-90s	310.00°	7.33"
Blue-60s	309.87°	7.32"
Blue-90s	309.76°	7.35"
SII-90s	309.66°	7.37"
Mean	**309.7°**	**7.33"**
Std. Deviation	**0.3**	**0.04"**
SEM	**0.03**	**0.004"**

Table 3. Position angle, angular separation and uncertainties for B 92AB.

WDS 05548-2527 (BUP 5AB) Astrometry		
Telescope T11	**Epochs 2017.87**	
Filter Type-Exposure Time (seconds)	**Position Angle (deg)**	**Angular Separation (arcsec)**
Luminance-45s	200.69°	77.47"
Luminance-90s	200.68°	77.52"
Red-45s	200.75°	77.53"
Red-90s	200.72°	77.62"
Mean	**200.7°**	**77.53"**
Std. Deviation	**0.03**	**0.06"**
SEM	**0.007°**	**0.02"**

Table 4. Position angle, angular separation, and uncertainties for BUP 5AB.

standard error of mean for position angle and angular separation. The results are summarized for B 92AB in Table 3, and BUP 5AB in Table 4.

To determine if the pair's components had similar proper motion, we generated a Richard Harshaw (Harshaw 2014) rating, a classification system for common proper motion pairs (CPMs), by dividing the difference in the vectors by the sum of the vectors. The

Harshaw Rating for B 92AB				
WDS	COMP	PM Ra (mas)	PM Dec (mas)	Rating %
05548 -2527	A	-98.428 ± 0.038	-33.771 ± .051	0.05128
	B	-96.864 ± 0.198	-23.442 ± .272	

Table 5. Proper motion of B 92AB Components; measurements are courtesy of Gaia DR2.

Harshaw Rating for BUP 5AB				
WDS	COMP	PM Ra (mas)	PM Dec (mas)	Rating %
00177 +2630	A	+40.024 ± 0.061	-10.851 ± 0.062	0.351773
	B	+33.598 ± 0.062	+16.084 ± .061	

Table 6. Proper motion of BUP 5AB Components; measurements are courtesy of Gaia DR2.

rating value range from 0 for CPMs and 1 for optical pairs. In the interest of obtaining accurate data with cited sources, the proper motion values for B 92AB, Table 5, and BUP 5AB, Table 6, were obtained from Gaia DR2 rather than the WDS catalog.

Discussion

Is B 92AB a physical pair?

Historic trends for the angular separation, Figure 7, range from 7.1" to 8". In 1999, the 2MASS Survey in 1999 reported a 7.38" separation and UCAC reported a 7.32" separation (Mason, Hartkopf 2015) and our measurement is at 7.33" of separation. Within the limits of our camera resolution, these data agree indicating constant separation between components and not much motion, not just the last twenty years but possibly from the very first measurement in 1911.

Position angle vs. time, Figure 7 bottom panel, shows somewhat random behavior. The largest position angle is reported in the first measurement (1911) to be around 314 degrees and in the following measurement (1926) measured 310 degrees consistent with our measurements. Most historical observations of this pair were performed using a micrometer, which has lower precision than our current measurement or the 1999 measurements (2 MASS Survey and UCAC Catalog). Both 2MASS Survey and UCAC report the same measurements for the position angle of 309.2°, very close to our measurement is 309.7°. With the first historic observational point excluded, we would get flat line fit, indicating no change in position angle in the last hundred years.

The orbital plot for the B 92 AB system is shown in

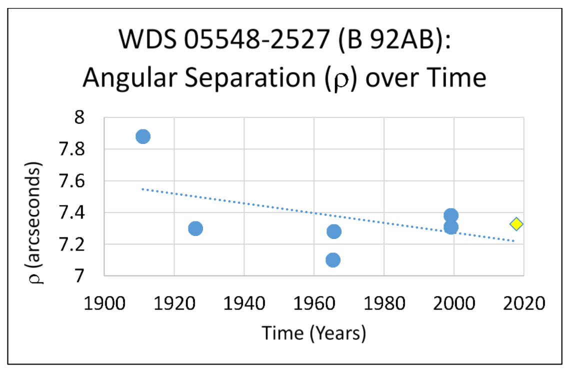

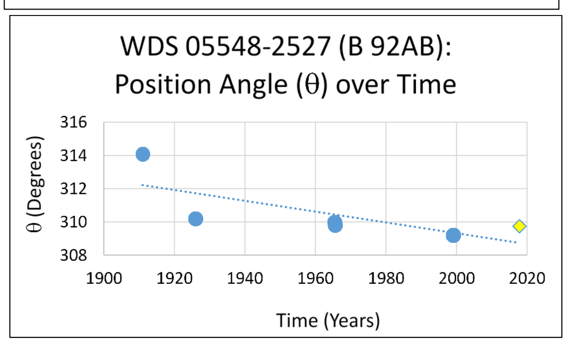

Figure 7. Angular separation versus time (top) and position angle versus time of B 92AB. The yellow diamond symbol represents our measurement.

Figure 8. In the top panel B 92 A is fixed in the origin (0,0) position, and motion of the B component is shown by blue dots. As expected, based on position and angular separation vs time plots, not much motion is apparent. Most points cluster in the same spot, with first his-

toric point slightly offset. In the bottom panel of Figure 8, we zoom into the motion of the secondary component and each historic point is labeled. The trend displays somewhat random movement over time.

By analyzing B 92A's A parallax (15.1665 milli-arcseconds) and its error (±0.0353), we calculated its minimum distance (214.45 light years), mid-point distance (214.95 light years), and maximum distance (215.45 light years) from our Sun. We analyzed component B's parallax (16.0971 milli-arcseconds) and its error (±0.1873) and calculated a minimum distance (200.19 light years), mid-point distance (202.52 light years), and maximum distance (204.91 light years) from our Sun. Even at three standard deviations from the mean measurements, the two stars would be almost four light years apart. A 0.051 Harshaw rating per Table 5, a value closer to 0 than 1 is suggestive of a common proper motion pair. A large separation suggests that they may be a physical pair traveling in the same direction in space, Table 5.

Is BUP 5AB a physical pair?

Using historical data and our new measurements, position angle and separation of the A and B components are plotted as a function of time, Figure 9. The data indicate clear trend in the decrease in the separation, Figure 9 top, and increase in position angle, Figure 9 top, since 1907.

In Figure 10 we show the orbital plot for the BUP 5AB system. In the top panel, A is fixed in the origin (0,0) position, and motion of the B component is shown by blue dots. This image doesn't reveal a long stretch of the secondary star's path relative to the primary star. Most data points are clustered close together. In the bottom panel of Figure 10, we zoom more into the motion of the secondary component, where we label each historic data point. The secondary star appears to be moving from southeast to northwest direction. Data points fluctuate around the line that connects first and last position and this may be attributed to the measurement errors. Overall the secondary star appears to be moving along the straight line with respect to the primary which is consistent with both long term binary and/or physically unrelated systems.

By analyzing BUP 5A's parallax (3.2695 milli-arcseconds) and its error (±0.057), we calculated its minimum distance (980.01 light years), mid-point distance (997.09 light years), and maximum distance (1014.79 light years) from our Sun. We analyzed component B's parallax (4.5776 milli-arcseconds) and its error (±0.0557) and calculated a minimum distance (703.60 light years), mid-point distance (712.16 light years), and maximum distance (720.94 light years) from our Sun.

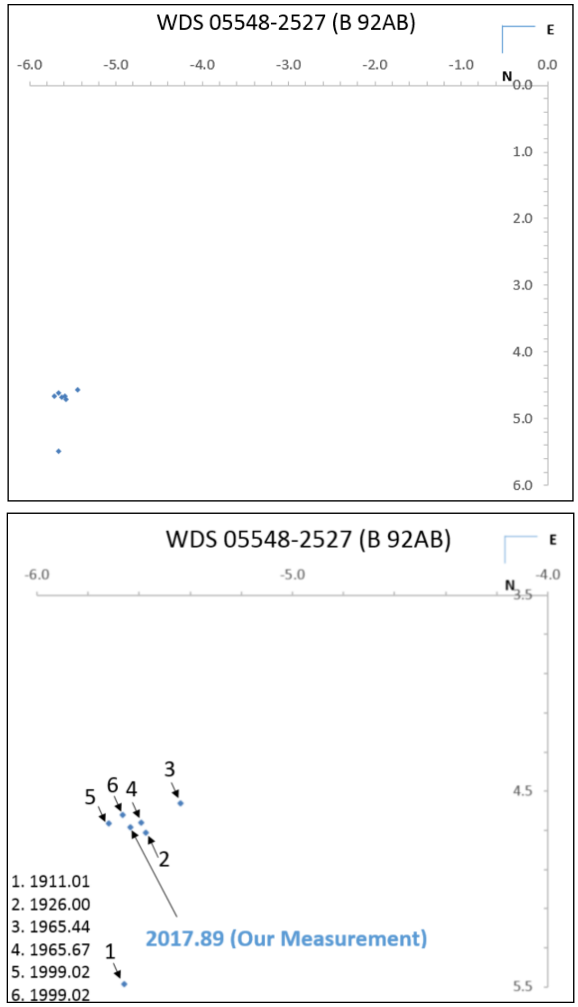

Figure 8. XY plot of the historical and new astrometric data of B 92AB with B 92A at (0,0) (top). The difference between these two panels is the level of zoom applied. In the bottom panel B 92A is not present, but details of B 92B motion are more obvious.

A Harshaw rating of 0.352, a value settled between 0 and 1, is suggestive of not being a common proper motion pair, Table 6. Our astrometric data in combination with historical data, its Harshaw rating and very wide distance between components essentially eliminates the possibility that these are a physical pair.

Conclusion

B 92AB's separation and position angle did not change much in the last hundred years. In our astrometric data we see no indication of the gravitationally bound orbit of the secondary star B around the primary star A. However, with similar parallaxes and proper motion, they may be physical with orbital motion not observable in a few hundred years but possibly tens of

CCD Astrometric Measurements and Historical Data Summary of Double Stars WDS 05548-2527 ...

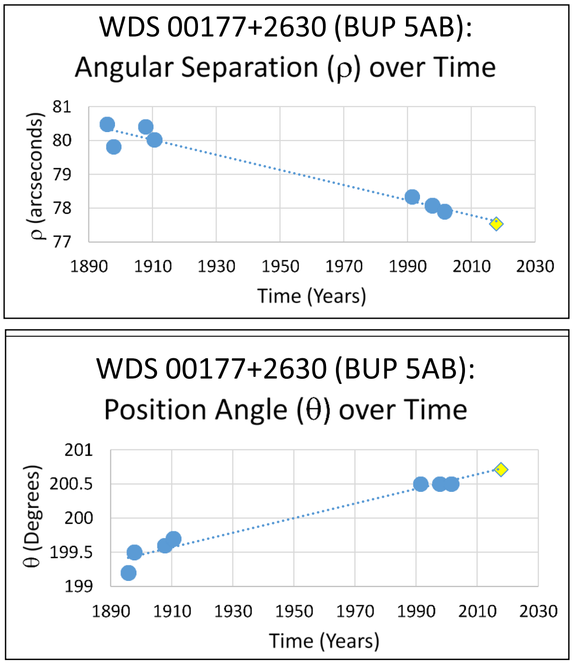

Figure 9. Angular separation vs time (top) and position angle versus time of BUP 5AB. The diamond symbol represents our measurement (bottom).

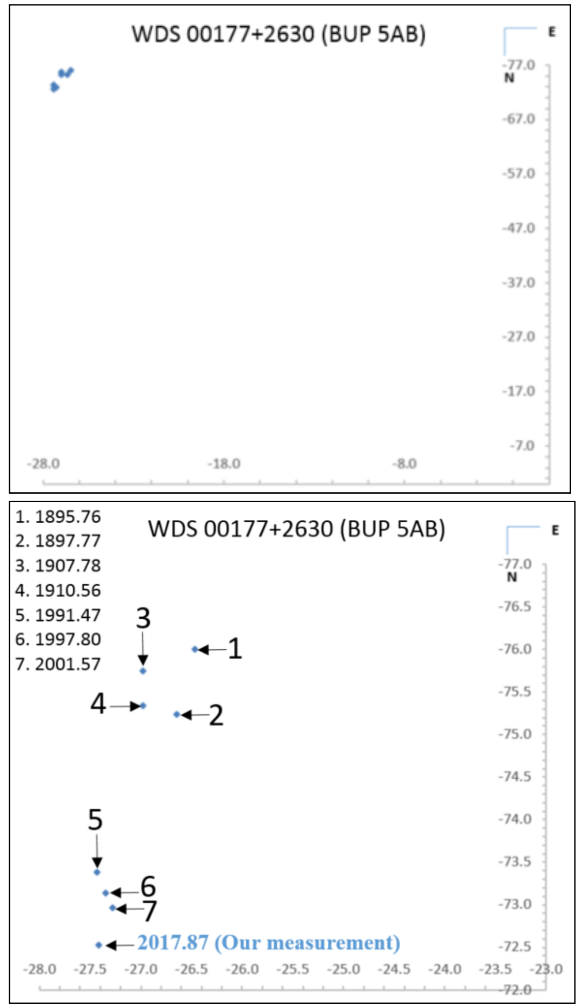

Figure 10. XY plot of the historical and new astrometric data of BUP 5AB with BUP 5A at (0,0) (top). The difference between the two panels is the level of zoom applied. In the bottom panel BUP 5A is not present, but details of BUP 5B motion is more obvious.

thousands of years from present day. Therefore, additional observational methods are encouraged to reveal the target's true nature.

BUP 5AB's 2017 measurements are close to its most recent WDS values from 2001 and combined with the historic data we see some consistent trends in change of position angle and separation. Common proper motion values are not suggestive of traveling in the same direction. This and parallax data from Gaia suggest these have no physical relationship.

Acknowledgements

We thank Brian Mason from USNO for helping the Fall 2017 semester research teams and past teams obtain the historical data of our elected double star systems. Additionally, we thank Pat and Grady Boyce of the Boyce Research Initiative and Education Foundation (B.R.I.E.F) for their instructional support and financial donation that allowed us access to the iTelescope network and the software tools on the BARC server. This research has made use of the Washington Double Star catalog maintained by the USNO, Aladin Sky Atlas software developed at CDS, Strasbourg Observatory, France, and the SIMBAD database operated by CDS, Strasbourg Observatory, France. This work has made use of data from the European Space Agency (ESA) mission Gaia (https:www.cosmos.esa.int/gaia), processed by the Gaia Data Processing and Analysis Consortium (DPAC, https://www.cosmos.esa.int/web/gaia/dpac/consortium). Funding for the DPAC has been provided by national institutions, in particular the institutions participating in the Gaia Multilateral Agreement. This research made use of data provided by Stelle Doppie and Astrometry.net.

References

Gaia Collaboration, 2016, "The Gaia misson", *Astronomy & Astrophysics*, **595**, A1.

Gaia Collaboration, 2018b, "Gaia Data Release 2: Summary of the contents and survey properties", *A & A*, **616**, A1.

Genet, R., Johnson, J., Buchheim, R., and Harshaw, R, 2016, *Small Telescope Astronomical Research Handbook*. Ed. Collins, D.

Harshaw, R., 2014, "Another Statistical Tool for Evaluating Binary Stars", *Journal for Double Star Observations*,**10** (1), 32-51.

Mason, B. and Hartkopf, W., 2015, The Washington Double Star Catalog, Astrometry Department, U.S. Naval Observatory.

Skrutskie, M.F., et al., 2006, "The Two Micron All Sky Survey (2MASS)", *The Astronomical Journal*, **131**, 1163-1183. http://adsabs.harvard.edu/abs/2006AJ....131.1163S

Wycoff, G.L., Mason, B.D., and Urban S. E., 2006, "Data Mining for Double Stars in Astrometric Catalogs", *The Astronomical Journal*, **132**, 50-60. http://adsabs.harvard.edu/abs/2006AJ....132...50W

Ana Veronica Parra received a Bachelor's degree in Cellular/Molecular Biology from Humboldt State University in 2013 and is a full-time Research Associate (Cancer Biology) at a biopharmaceutical company in San Diego, CA. Her curiosity for Astronomy soon began after watching "Cosmos: A Spacetime Odyssey", narrated by Neil deGrasse Tyson, in 2016. She enthusiastically began her education and research experience in Astronomy at San Diego Mesa Community College in 2017.

Double Star System WDS 02229+5835 BLL 7 (S Per)

Olivia Ho[1], Kieran Saucedo[1], Alani Bayha[1], Eliana Meza-Ehlert[1], Shakara Tilghman[1], Brian Delgado[1], Pat Boyce[2], and Grady Boyce[2]

1. High Tech High School
2. Boyce Research Initiatives and Education Foundation (BRIEF)

Abstract: Research regarding the Double Star System WDS 02229+5835 BLL 7 (S Per)] was conducted to contribute to the previous observations of the system, determine the nature of this system, and to further the science and data regarding double stars. Data was collected through careful observations of BLL 7, using Charge-Coupled Device cameras from the Las Cumbres Observatory. Researchers were able to find the current theta 20.34° and rho 69.10", on epoch 2018.832. The collected measurements and data show that this system is most likely an optical double.

Introduction

Referencing the Washington Double Star Catalog (WDS), students searched through lists of Double Star systems that met the following criteria: the right ascension (RA) of the systems were between 00 and 08 hours, the stars had a separation of at least 5" arcseconds, and magnitudes between 7 and 12. Data was requested for star systems that met these requirements, and the system WDS 02229+5835 BLL 7 was picked from those candidates.

This star was chosen due to the uncertainty regarding the gravitational nature of BLL 7 based on research using GAIA data. Thus, this unknown, as well as the extensive historical value of the system, made it an intriguing system to study. It's stellar location with an RA of 02h, and a declination (Dec) of about +57° made it visible during the time of year this study was conducted. The delta magnitude is 0.63, with S Persei as the primary star having a magnitude of 10.76 and the secondary star having a magnitude of 11.39. The separation angle (theta) from the last measurement taken in 2010 is about 69.3°, changing by 1.1° from the initial measurement in 1880 of, 68.2°.

Methods and Materials

The images were taken using a 0.4-meter telescope with an SBIG CCD requested through Las Cumbres Observatory (LCO) Observing Portal (LCO Web).

Figure 1. SDSS r' Filtered Image of BLL 7 processed through the OSS Pipeline.

LCO is a conglomeration of twenty-one telescopes across eight global locations, tasked with keeping a constant eye on the night sky. An SBIG CCD camera was used to take the images of BLL 7, Figure 1, in order to enable precise measurements.

Thirty images in total were requested from LCO, 15 using the SDSS r' filter, isolating red wavelengths, with an exposure time of eight seconds, and 15 using

Double Star System WDS 02229+5835 BLL 7 (S Per)

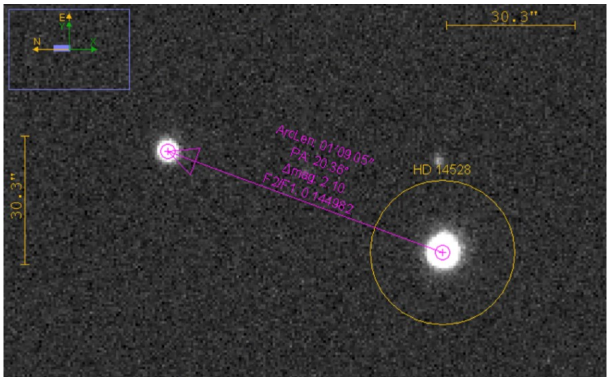

Figure 2. Image of AIJ Measurement.

the SDSS g' filter, isolating green wavelengths, with an exposure time of 12 seconds. The images were all taken on BJD 2458422.7025 using the Teide 1 telescope in Tenerife.

The images were taken and initially processed through LCO, then through the OSS Pipeline, (Fitzgerald, 2018 accepted). After getting the files from the OSS Pipeline, AstroImageJ (AIJ) was used as astrometric software that provided further information on all 30 images. Starting from the center of the primary star, a line was drawn to the rough center of the secondary star. The position angle, separation in arcseconds, RA and Dec, were then calculated by AIJ, Figure 2. This process was repeated, with each image being measured with the same method.

Data and Results

The data is exhibited in Tables 1 - 5. Table 1 shows the average position angle (theta) of the 15 SDSS r' filtered images, the 15 SDSS g' filtered images, and the compiled data from all 30 of the images together. Table 2 shows the average length of separation in arcseconds (rho). Table 3 displays the historical data on this double star with this paper's 2018 measurement included for reference. Table 4 provides Effective Temperature and Luminosity Values reported by GAIA. Figure 3 provides Proper Motion vectors provided by ALADIN10 using GAIA data.

Discussion

After an in-depth analysis, using new data brought forth by this study compared with previous measurements of this system, it was concluded that this system is most likely an optical double star system with no gravitational bond. Gravitationally bound double stars display similar parallax and proper motions, whereas these values for BLL 7 are significantly different, Table 4, when comparing the minimum, middle, and maximum possible values of both stars parallaxes. This il-

Filter	**SDSS r′**	**SDSS g′**	**Across All Filters/ Images**
Mean	20.32°	20.36°	20.34°
Standard Deviation	0.02	0.03	0.05
Standard Deviation of the Mean	0.013	0.003	0.009

Table 1. Theta measurements

Filter	**SDSS r′**	**SDSS g′**	**Across All Filters/ Images**
Mean	69.08"	69.12"	69.10"
Standard Deviation	0.06"	0.06"	0.06"
Standard Deviation of the Mean	0.015"	0.015"	0.011"

Table 2. Rho Measurements

Epoch	**Position Angle**	**Separation**
1880	20°	68.2"
1908.05	19.6°	69.193"
1908.87	19.8°	69.04"
1919.95	19.5°	69.008"
1929.89	19.4°	69.583"
1956.77	20.2°	67.206"
1989	20.2°	68.751"
1991.64	20.1°	69.08"
1999.71	20.1°	69.16"
2000.87	20.5°	69.42"
2003.652	20.5°	69.3"
2018.832	*20.34 ± .009°*	*69.10″ ± 0.011″*

Table 3. Historical Data.

Star	**Temperature Effective Value**	**Luminosity Value**
Primary	3293 Kelvin	Not Reported
Secondary	5899.50 Kelvin	25.366

Table 4. Luminosity / Temperature

Double Star System WDS 02229+5835 BLL 7 (S Per)

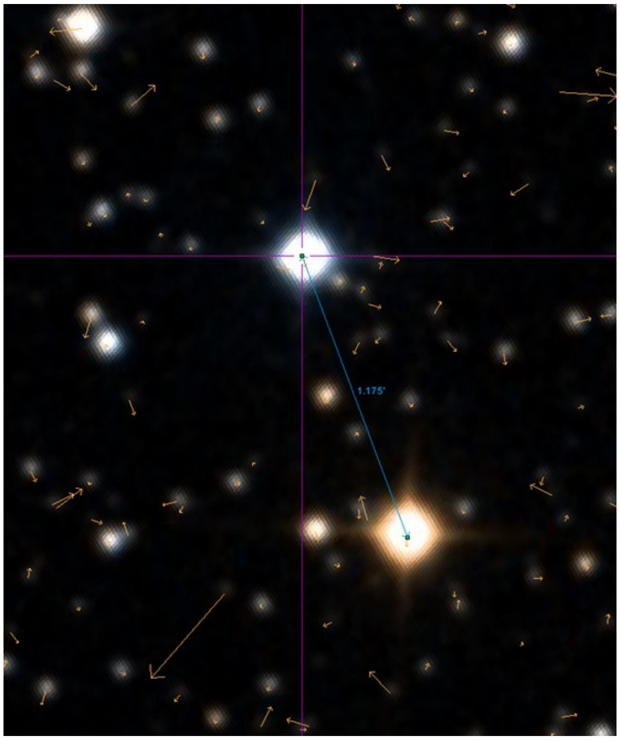

Figure 3. Image of Aladin 10 Proper Motion Vectors.

Star	Right Ascension (Proper Motion)	Declination (Proper Motion)
Primary	-0.010 ± 0.295	-2.570 ± 0.307
Secondary	-0.177 ± .081	-1.617 ± 0.083

Table 5. Proper Motion

lustrates that the smallest possible distance between these two stars is 1818.83 parsecs (calculated by taking the minimum parallax of the primary star, maximum parallax of the secondary star, and finding the difference between the two). Two stars with such a vast amount of (minimum) distance between them are most likely not gravitationally bound—especially when other data regarding this system is taken into account.

Considering the proper motion measurements from GAIA under 3 mas/year, Table 5, the analysis indicates the probability that these stars have different proper motions as well. While there is a possibility that the RA motion of both stars could be equal, the GAIA data, in its current state, points to the possibility that there may not be an overlap between the Dec motion of both stars.

Viewing the historical measurements, Table 3, shows that from the first recorded measurement in 1880 to the most recent measurements in 2018, there is only a minor difference in the position angle (20° to 20.34° ± 0.009°) with common variations through measurement history (e.g. from 1908 to 1929 the position angle drops from 19.8° to 19.4°, before increasing to 20.5° in 2000). These variations can be attributed to variations in astronomers and the methods they employed. The separation shows a change in 1" between the first recorded measurement in 1880 to the most recent measurements in 2018 (68.2" to 69.10" ± 0.011"), providing too little data to discern a distinguishable pattern. The totality of data points is plotted, Figure 4, showing no evi-

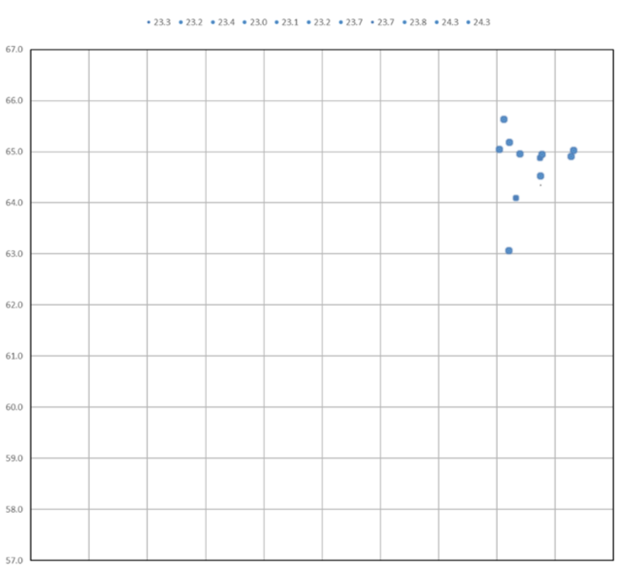

Figure 4. Historical data star positions.

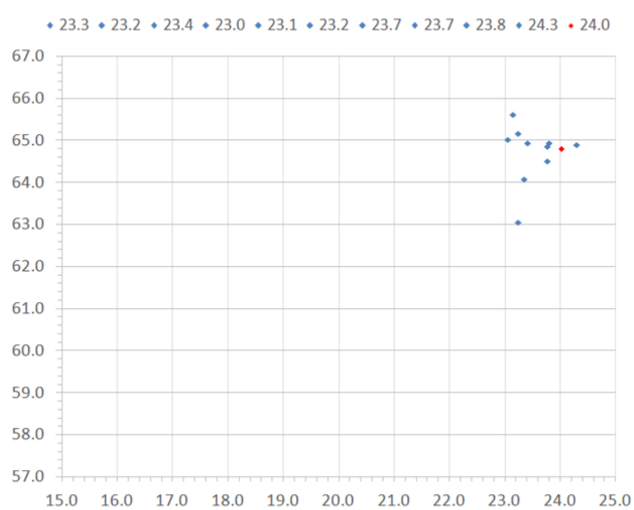

Figure 5. Historical data plotted with conducted observation marked in red.

dence of a trend line. When the 2018 data was plotted along with the historical data, shown in Figure 5, it appears evident that there has been little change over time.

The data garnered from the historical measurements as well as the recent measurement are confirmed with data from GAIA—showing that the parallax of the primary star and the parallax of the secondary star are different (putting the stars over 1818.83 parsecs apart), the proper motion of the primary star and the proper motion of the secondary star are different (the RA have a small overlap but the Dec are definitely different), the systems position angle is constantly changing (decreasing and increasing seemingly randomly), and the system's separation shows no discernable pattern (decreasing and increasing seemingly randomly)—this data helps to provide us with the conclusion that this double star system is not gravitationally bound or a common proper motion pair, but optical.

Conclusion:

WDS 02229+5835 BLL 7 is a double star system that was first measured in 1880 and most recently measured in 2018. Using CCD camera technology and the assistance of several heavily experienced mentors, this double star system was measured and researched. Considering this new data as well as historical data, it is unlikely these two stars are gravitationally bound given both stars' RA, Dec and proper motions.

Acknowledgments

The authors of this paper would like to thank Dr. Michael Fitzgerald, Richard Harshaw, and Bob Buchheim for their contributions to the seminar classes provided by BRIEF. They would also like to thank the L.C.O. network for the time and resources they spent helping make the writing of this paper a possibility. Lastly, the authors of this paper would like to thank Brian Delgado, a physics teacher from High Tech High San Diego for introducing this scientific opportunity.

References

Chapman, Allan, "Sir Robert Stawell Ball (1840-1913): Royal Astronomer in Ireland and Astronomy's Public Voice", *Journal of Astronomical History and Heritage*, **10**, 198-210, 2007.

"About LCO." Parallax and Distance Measurement | Las Cumbres Observatory, http://www.lco.global/about/.

"02229+5835 BLL 7 (S Per)." Stelle Doppie - Double Star Database, http://www.stelledoppie.it/index2.php?iddoppia=8633.

Mason, B., Wycoff, G., and Hartkopf, W. The Washington Double Star Catalog. Astrometry Department, U.S. Naval Observatory.

Double Star Photometry – March 2019

Wilfried R.A. Knapp
Vienna, Austria
wilfried.knapp@gmail.com

Abstract: The WDS catalog contains per June 2019 about 148,500 objects. About 50,000 of these come with a magnitude for the primary with single digit precision indicating rather an estimation than a precise measurement and over 16,000 objects are listed with magnitudes in the blue or red band (WDS note codes B/K/R/I) thus in need of a measurement in the V band. After eliminating all objects not suited for resolution with the tools currently available to me (too small separation, too faint, too bright) about 26,000 objects remained as targets of interest for this project. The selection criterion for the objects for a specific report is then at a given point of time simply the currently highest given altitude to eliminate atmospheric effects as far as possible – so this is then a more or less random selection out of the mentioned 26,000 objects. This report covers the first 37 such objects from images taken end of March 2019 with V-filter to allow for visual magnitude measurement by differential photometry. All objects were additionally checked for potential gravitational relationship using GAIA DR2 parallaxes.

Introduction

With few exceptions one single image was taken for all selected WDS objects with iTelescope iT24 with V-filter and 20 seconds exposure time and the imaging conditions were despite several due to bad weather cancelled sessions overall quite favourable. The number of objects in this report is somewhat smaller than planned as in several cases the secondary was too faint to be resolved with 20 seconds exposure time – useful lesson for the next imaging sessions to use for objects expected to be fainter than 15 Vmag longer exposure times.

The images were plate solved with Astrometrica using the URAT1 catalog with reference stars in the Vmag range of 8.5 to 16.5 giving not only RA/Dec coordinates but also photometry results for all reference stars used including an average Vmag error. The objects were then located in the center of the image and astrometry/photometry was then done by the rather comfortable Astrometrica procedure with point and click at the components delivering RA/Dec coordinates and Vmag measurements based on all reference stars used for plate solving.

Results of Photometry and Catalog Checking

The measurement results are given in table 1 below with the following structure:

WDS	=	WDS ID
Disc	=	Discoverer code
C	=	Components (AB if blank)
RA/Dec	=	Positions for primary and secondary in HH:MM:SS.sss/DD.MM.SS.ss format
dRA/dDec	=	Plate solving errors for RA and Dec in arcseconds
Sep	=	Calculated separation in arcseconds
e_Sep	=	Separation error
PA	=	Calculated position angle in degrees
e_PA	=	Position angle error
Mag	=	Vmags for both components measured by differential photometry
e_Mag	=	Magnitude errors
SNR	=	Signal to noise ratio for both components
dVmag	=	Plate solving error in Vmag
Date	=	Julian observation epoch
Notes	=	Additional comments listed below Table 1

(Text continues on page 22)

Double Star Photometry – March 2019

WDS	Disc	C	RA	Dec	dRA	dDec	Sep	e_Sep	PA	e_PA	Mag	e_Mag	SNR	dVmag	Date	Notes
11401+3758	CBL 349		11 40 07.409	37 57 43.20	0.08	0.08	18.92309	0.11314	197.269	0.343	12.240	0.061	93.34	0.06	2019.24395	1)3)
			11 40 06.934	37 57 25.13							16.086	0.112	10.97			
11283+3144	CRB 89		11 28 15.738	31 43 46.94	0.05	0.05	25.30060	0.07071	12.405	0.160	11.356	0.050	186.80	0.05	2019.24104	1)3)
			11 28 16.164	31 44 11.65							16.243	0.098	12.41			
11472+3812	CRB 90		11 47 12.717	38 12 24.78	0.09	0.07	36.55991	0.11402	192.304	0.179	15.974	0.115	10.51	0.06	2019.24394	1)3)
			11 47 12.056	38 11 49.06							16.586	0.180	5.92			
11289+3206	CVR 614		11 28 53.718	32 06 21.27	0.04	0.04	28.12077	0.05657	130.734	0.115	15.850	0.086	13.87	0.04	2019.24110	1)3)
			11 28 55.395	32 06 02.92							16.614	0.297	3.21			
11346+4052	ES 1401		11 34 33.529	40 51 23.13	0.05	0.04	6.39762	0.06403	327.739	0.573	11.955	0.051	141.88	0.05	2019.24382	1)
			11 34 33.228	40 51 28.54							12.538	0.051	105.44			
11318+3513	FMR 101		11 31 49.191	35 13 07.30	0.08	0.09	7.28388	0.12042	145.461	0.947	16.313	0.115	10.03	0.05	2019.24392	1)3)
			11 31 49.528	35 13 01.30							16.342	0.220	4.58			
11460+3149	GIC 102		11 45 56.434	31 49 25.70	0.03	0.03	9.10242	0.04243	271.322	0.267	13.756	0.044	59.09	0.04	2019.24106	1)
			11 45 55.720	31 49 25.91							14.092	0.046	45.65			
11187+3759	GRV 833		11 18 44.768	37 59 28.05	0.10	0.11	33.45107	0.14866	343.599	0.255	11.324	0.051	107.95	0.05	2019.24377	1)
			11 18 43.969	38 00 00.14							11.785	0.051	91.84			
11266+3946	GRV 835		11 26 39.192	39 46 31.01	0.11	0.09	24.52560	0.14213	292.815	0.332	11.687	0.081	96.05	0.08	2019.24384	1)
			11 26 37.231	39 46 40.52							11.836	0.081	81.94			
11500+3612	GRV 842		11 50 01.071	36 12 16.83	0.08	0.08	31.55400	0.11314	357.340	0.205	10.623	0.031	183.84	0.03	2019.24392	1)
			11 50 00.950	36 12 48.35							10.775	0.031	166.02			
11280+3403	HJ 498		11 27 58.447	34 03 40.04	0.05	0.07	21.56549	0.08602	88.725	0.229	11.566	0.050	153.91	0.05	2019.24382	1)
			11 28 00.182	34 03 40.52							12.280	0.051	112.27			
11248+4128	HJ 2570	A	11 24 47.235	41 30 26.40	0.03	0.04	17.50494	0.05000	279.038	0.164	10.677	0.050	182.96	0.05	2019.24113	2)
		B	11 24 45.696	41 30 29.15							13.869	0.056	43.62			
11248+4128	HJ 2570	A	11 24 47.235	41 30 26.40	0.03	0.04	46.08922	0.05000	210.916	0.062	10.677	0.050	182.96	0.05	2019.24113	2)
		C	11 24 45.127	41 29 46.86							12.800	0.052	71.16			
12006+3954	HJ 2593		12 00 38.682	38 54 57.64	0.07	0.07	24.77786	0.09899	333.840	0.229	10.657	0.071	127.90	0.07	2019.24118	1)
			12 00 37.746	38 55 19.88							14.123	0.085	21.64			
11150+3501	KZA 12	A	11 15 02.819	35 01 03.52	0.04	0.04	34.95900	0.05657	20.896	0.093	12.141	0.051	95.82	0.05	2019.24110	2)
		B	11 15 03.834	35 01 36.18							14.661	0.065	25.98			

Table 1: Results for measured WDS objects

Table 1 continues on the next page.

Double Star Photometry – March 2019

WDS	Disc	C	RA	Dec	dRA	dDec	Sep	e_Sep	PA	e_PA	Mag	e_Mag	SNR	dVmag	Date	Notes
11152+3628	KZA 13		11 15 10.809	36 28 11.13	0.09	0.07	22.06597	0.11402	280.444	0.296	13.130	0.093	45.33	0.09	2019.24117	1)3)
			11 15 09.010	36 28 15.13							15.163	0.125	12.10			
11152+3521	KZA 15	A	11 15 26.180	35 20 08.84	0.07	0.05	18.83778	0.08602	138.004	0.262	13.820	0.058	36.86	0.05	2019.24114	1)
		B	11 15 27.210	35 19 54.84							14.212	0.063	28.09			
11152+3521	KZA 15	A	11 15 26.180	35 20 08.84	0.07	0.05	18.91869	0.08602	352.119	0.261	13.820	0.058	36.86	0.05	2019.24114	1)3)
		C	11 15 25.968	35 20 27.58							15.086	0.082	16.32			
12001+4107	LDS5212		12 00 11.131	41 05 27.05	0.05	0.05	7.22402	0.07071	172.989	0.561	14.428	0.066	38.96	0.06	2019.24105	1)3)
			12 00 11.209	41 05 19.88							15.775	0.083	18.27			
11512+3708	NSN 50		11 51 11.989	37 07 49.24	0.13	0.08	4.20700	0.15264	10.979	2.078	11.871	0.050	212.14	0.05	2019.24391	1)3)4)
			11 51 12.056	37 07 53.37							16.458	0.228	4.39			
11507+3312	SKF 8		11 50 42.735	33 12 18.58	0.09	0.15	7.09669	0.17493	108.570	1.412	12.331	0.093	45.17	0.09	2019.24122	1)5)
			11 50 43.271	33 12 16.32							12.208	0.093	47.46			
11478+3648	SKF2577		11 47 47.326	36 47 38.02	0.10	0.09	45.85906	0.13454	283.904	0.168	11.813	0.061	103.31	0.06	2019.24394	2)
			11 47 43.620	36 47 49.04							14.979	0.078	21.41			
11554+3919	SKF2579		11 55 26.264	39 19 19.62	0.14	0.12	6.51689	0.18439	342.059	1.621	12.519	0.072	64.04	0.07	2019.24380	2)
			11 55 26.091	39 19 25.82							12.731	0.073	56.02			
12010+4058	SKF2641		12 00 58.284	40 57 32.21	0.07	0.12	5.36533	0.13892	65.793	1.483	14.027	0.054	51.98	0.05	2019.24104	2)
			12 00 58.716	40 57 34.41							14.997	0.064	26.80			
11498+4024	SKF2692		11 49 50.775	40 24 14.47	0.11	0.09	77.68701	0.14213	27.390	0.105	10.233	0.060	186.54	0.06	2019.24379	2)6)
			11 49 53.904	40 25 23.45							14.301	0.065	45.08			
11527+3937	SKF2693		11 52 44.348	39 36 38.05	0.12	0.13	12.38037	0.17692	4.014	0.819	12.800	0.091	85.35	0.09	2019.24383	2)7)
			11 52 44.423	39 36 50.40							14.714	0.096	33.39			
11141+3926	SLW 580		11 14 03.465	39 25 34.09	0.06	0.06	32.19528	0.08485	50.012	0.151	16.386	0.141	8.35	0.07	2019.24108	1)3)
			11 14 05.594	39 25 54.78							16.514	0.144	8.14			
12069+3921	SLW 684		12 06 52.633	39 20 58.10	0.03	0.04	8.28579	0.05000	19.717	0.346	15.918	0.092	15.10	0.06	2019.24101	1)3)
			12 06 52.874	39 21 05.90							15.945	0.093	14.88			
11246+3752	UC 163		11 24 35.262	37 52 24.92	0.06	0.08	16.22781	0.10000	29.457	0.353	10.778	0.041	159.17	0.04	2019.24389	2)
			11 24 35.936	37 52 39.05							10.810	0.041	157.35			
11390+3253	UC 163		11 38 57.810	32 53 08.64	0.07	0.10	34.16630	0.12207	270.989	0.205	12.549	0.061	93.95	0.06	2019.24376	2)
			11 38 55.098	32 53 09.23							13.717	0.018	59.36			

Table 1 (continued). Results for measured WDS objects

Table 1 concludes on the next page.

WDS	Disc	C	RA	Dec	dRA	dDec	Sep	e_Sep	PA	e_PA	Mag	e_Mag	SNR	dVmag	Date	Notes
11281+3940	UC 2144		11 28 03.377	39 40 21.25	0.05	0.09	25.96301	0.10296	92.252	0.227	10.713	0.091	91.22	0.09	2019.24386	2)
			11 28 05.624	39 40 20.23							13.404	0.093	43.78			
11414+3624	UC 2190		11 41 23.277	36 23 31.45	0.15	0.11	11.02058	0.18601	169.329	0.967	11.761	0.061	84.87	0.06	2019.24396	1)3)
			11 41 23.446	36 23 20.62							14.610	0.091	15.26			
11431+4040	UC 2196		11 43 04.505	40 40 14.94	0.08	0.16	20.25504	0.17889	113.634	0.506	14.393	0.027	40.09	0.05	2019.24384	1)3)
			11 43 06.136	40 40 06.82							16.722	0.162	6.55			
11454+3856	UC 2205		11 45 25.135	38 56 12.46	0.06	0.06	33.13616	0.08485	12.506	0.147	13.997	0.046	46.10	0.04	2019.24393	1)3)
			11 45 25.750	38 56 44.81							15.818	0.083	14.45			
12019+4045	UC 2253		12 01 55.069	40 45 28.89	0.03	0.03	31.20611	0.04243	276.477	0.078	11.029	0.040	227.30	0.04	2019.24103	2)
			12 01 52.340	40 45 32.41							15.714	0.063	21.72			
11150+3501	WNO 35		11 15 02.821	35 01 03.50	0.06	0.06	31.24440	0.08485	165.728	0.156	12.156	0.051	103.61	0.05	2019.24112	1)3)
			11 15 03.448	35 00 33.22							15.551	0.083	15.97			

Table 1 (conclusion). Results for measured WDS objects

Talbe 1 Notes:

1) One image taken with iTelescope T24 with V-filter and 20 seconds exposure time
2) Two images taken with iTelescope T24 with V-filter and 20 seconds exposure time
3) SNR for A or B or both <20: Indicates that the Vmag measurement results might be a bit less precise than desired due to a low SNR value but this is already included in the calculation of the magnitude error range estimation
4) Overlapping star disks: Indicates that the star disks overlap to the degree of an elongation and that the measurement results is probably less precise than with clearly separated star disks
5) B seems to be an optical double, Vmag thus likely too bright
6) A is double itself
7) B is double itself

Object	Comp	PA	e_PA	Sep	e_Sep	Plx1	e_Plx1	Plx2	e_Plx2	Min_D_AU	Med_D_AU	Max_D_AU	LPGR
CBL 349		196.402	0.000	18.55914	0.00008	3.7158	0.0457	3.6504	0.0596	4921	1086968	5804054	9.58
CRB 89		12.503	0.000	25.25153	0.00013	3.3730	0.0755	3.1610	0.1033	7500	4089259	15619502	1.66
CRB 90		193.898	0.000	36.29887	0.00019	1.8739	0.1395	1.9167	0.0605	18056	6085613	58942228	1.79
CVR 614		130.743	0.000	27.91903	0.00010	2.4359	0.0491	2.3833	0.0884	11126	2756750	20310406	4.03
ES 1401		326.757	0.001	6.40594	0.00010	7.0785	0.0571	7.0926	0.0676	897	248338	1715373	41.19
FMR 101		143.896	0.001	7.38382	0.00011	8.1703	0.0774	8.3056	0.0869	892	419687	2039336	23.36
GIC 102		271.738	0.001	9.07326	0.00016	31.9093	0.0473	31.8181	0.1199	284	22454	157008	100.00
GRV 833		343.783	0.000	33.57743	0.00014	4.4512	0.0822	4.5259	0.0714	7288	941913	5823795	11.31
GRV 835		293.900	0.000	24.42271	0.00007	3.6815	0.0411	3.6886	0.0398	6539	590579	3871893	18.12
GRV 842		356.931	0.006	31.76644	0.00311	1.8447	0.8246						
HJ 498		88.363	0.000	21.41405	0.00011	3.5047	0.0627	4.3205	0.1057	3863988	11107893	18294413	0.00
HJ 2570	AB	279.188	0.000	17.61598	0.00006	3.2274	0.0509	0.2019	0.0249	588626193	957060342	1978988952	0.00
HJ 2570	AC	211.069	0.000	45.88431	0.00007	3.2274	0.0509	2.6416	0.0335	8275657	14165474	19917679	0.00
HJ 2593		332.966	0.000	25.03633	0.00006	4.2369	0.0439	0.9070	0.0277	151231586	178708930	216037356	0.00
KZA 12	AB	20.630	0.000	34.91873	0.00007	2.6797	0.0504	1.0246	0.0427	91648787	124296459	169923241	0.00
KZA 12	AC	215.953	0.000	43.76426	0.00007	2.6797	0.0504	1.3338	0.0416	57267221	77652259	106844634	0.00
KZA 13		280.573	0.000	21.96325	0.00009	1.3184	0.0521	1.1586	0.0531	17035	21543491	71113371	0.15
KZA 15	AB	138.168	0.000	18.84457	0.00006	1.9902	0.0415	2.2549	0.0443	385958	12181925	25175618	0.00
KZA 15	AC	352.488	0.000	19.02812	0.00007	1.9902	0.0415	1.2637	0.0591	31623109	59550076	109554970	0.00
LDS5212		171.832	0.000	7.22360	0.00006	7.7240	0.0319	7.6662	0.0494	932	211771	1049347	47.37
NSN 50		10.142	0.001	4.77175	0.00009	7.2536	0.0666	7.1711	0.0935	653	394037	2384315	26.69
SLW 580		50.394	0.000	31.99172	0.00011	3.5263	0.0749	3.4440	0.0806	8784	1638829	10305174	6.34
SLW 684		19.450	0.000	8.34125	0.00007	4.6031	0.0380	4.6768	0.0422	1768	715578	3044818	12.66
UC 163		29.473	0.000	16.27874	0.00008	4.0915	0.0682	3.2223	0.0712	5292104	13597107	20472816	0.00
UC 164		270.989	0.000	34.22015	0.00006	5.6205	0.0372	5.6331	0.0238	6037	201796	1318002	49.61
UC 2144		92.512	0.000	26.05041	0.00006	7.4464	0.0349	7.4163	0.0354	3477	148840	904244	63.66
UC 2190		170.715	0.000	11.34537	0.00006	5.6596	0.0530	5.5420	0.0380	2009	773474	2693529	7.82
UC 2196		112.689	0.000	20.47500	0.00011	2.2147	0.1038	1.8961	0.0502	10544	15642446	35926491	0.06
UC 2205		12.741	0.000	33.09966	0.00008	25.5666	0.0579	25.4984	0.0502	1292	23432	122543	100.00
UC 2253		276.525	0.000	31.19689	0.00006	11.2609	0.0385	11.0959	0.0534	2781	272109	741915	25.39
WNO 35		165.930	0.000	31.36745	0.00008	2.6797	0.0504	0.6600	0.0510	154553143	235644851	382942367	0.00

Table 2: Results for cross-matched objects

Double Star Photometry – March 2019

(Continued from page 17)

Cross-Match with GAIA DR2

All listed objects were additionally cross-matched with GAIA DR2 to check for potential gravitational relationship (PGR) – the results are given in Table 2 with the following structure:

Object	=	Discoverer ID
Comp	=	Components (AB if blank)
PA	=	Position angle in degrees
e_PA	=	Error position angle
Sep	=	Separation in arcseconds
e_Sep	=	Error separation
Plx1	=	Parallax 1 in mas
e_Plx1	=	Error parallax1
Plx2	=	Parallax 2 in mas
e_Plx2	=	Error parallax 2
Min_D_AU	=	Minimum spatial distance in AU between components (see Appen dix)
Med_D_AU	=	Median spatial distance in AU between components (see Ap pendix)
Max_D_AU	=	Maximum spatial distance in AU between components (see Appendix)
LPGR	=	Likelihood of potential gravitational relationship (see Appendix)

To avoid redundant reporting some objects were deleted in Table 2 if already cross-matched with GAIA DR2 in other reports. For the objects UC 2205, UC 2144 and GIC 102 WDS code "T" is suggested for likely physical by common parallaxes. For the objects with LPGR <10 WDS code "U" for likely optical is suggested.

Summary

A good part of the 37 measured objects shows the expected magnitude difference larger than 0.5 compared with the WDS catalog data especially for the secondary but for many objects the given WDS magnitudes were simply confirmed within the given error range. 3 objects have parallaxes and angular separations allowing for a higher than 50% likelihood for a spatial distance between the components of less than 200,000 AU (~1 parsec) suggesting potential gravitational relationship.

Acknowledgements

The following tools and resources have been used for this research:

- Washington Double Star Catalog
- GAIA DR2 catalog
- DSS2 images
- Aladin Sky Atlas v10.0
- iTelescope
    - iT24: 610mm CDK with 3962mm focal length. Resolution 0.625 arcsec/pixel. V-filter. No transformation coefficients available. Located in Auberry, California. Elevation 1405m
- AAVSO VPhot
- Astrometrica v4.10.0.427
- URAT1 catalog
- AstroPlanner v2.2
- MaxIm DL6 v6.08

References

Knapp, Wilfried R. A., 2018, "A New Concept for Counter-Checking of Assumed Binaries", *Journal of Double Star Observations*, **14** (3), 487-491.

Appendix

Description of the PGR assessment procedure

GAIA DR2 data for RA/Dec and Plx are used for a Monte Carlo simulation assuming a normal distribution for these parameters with the given error range as standard deviation. The spatial distance between the components is (according to Knapp 2018) calculated from the inverted simulated parallax data and the simulated angular separation using the law of cosine

$$sep = \sqrt{a^2 - 2ab\cos\gamma + b^2}$$

with a and b = distance vectors for the stars A and B in lightyears calculated as (1000/Plx)*3.261631 and γ = angular separation in degrees calculated as

$$\gamma = \arccos\left[\sin(DE1)\sin(DE2) + \cos(DE1)\cos(DE2)\cos(|RA1 - RA2|)\right]$$

The likelihood for potential gravitational relationship (LPGR) is the percentage of simulation results <200,000 AU (~1 parsec) out of the simulation sample with a size of 120,000

The given smallest, median and largest spatial distance between the components is the smallest, median and largest result out of the simulation sample.

Double Star Photometry – April 2019

Wilfried R.A. Knapp

Vienna, Austria

wilfried.knapp@gmail.com

Abstract: The WDS catalog contains per June 2019 about 148,500 objects. About 50,000 of these come with a magnitude for the primary with single digit precision indicating rather an estimation than a precise measurement and over 16,000 objects are listed with magnitudes in the blue or red band (WDS note codes B/K/R/I) thus in need of a measurement in the V band. After eliminating all objects not suited for resolution with the tools currently available to me (too small angular separation, too faint, too bright) about 26,000 objects remained as targets of interest for this project. The selection criterion for the objects for a specific report is then at a given point of time simply the currently highest given altitude to eliminate atmospheric effects as far as possible – so this is then a more or less random selection out of the mentioned 26,000 objects. This report covers 46 such objects from images taken end of April 2019 with V-filter to allow for visual magnitude measurement by differential photometry. All objects were additionally checked for potential gravitational relationship using GAIA DR2 parallaxes.

1. Introduction

One single image was taken for all selected WDS objects with iTelescope iT24 with V-filter and 20 seconds exposure time and the imaging conditions were overall quite favourable.

The images were plate solved with Astrometrica using the URAT1 catalog with reference stars in the Vmag range of 8.5 to 16.5 giving not only RA/Dec coordinates but also photometry results for all reference stars used including an average Vmag error. The objects were then located in the center of the image and astrometry/photometry was then done by the rather comfortable Astrometrica procedure with point and click at the components delivering RA/Dec coordinates and Vmag measurements based on all reference stars used for plate solving.

2. Results of Photometry and Catalog Checking

The measurement results are given in Table 1 with the following structure:

- WDS = WDS ID
- Disc = Discoverer code
- C = Components (AB if blank)
- RA/Dec = Positions for primary and secondary in HH:MM:SS.sss/DD.MM.SS.ss format
- dRA/dDec = Plate solving errors for RA and Dec in arcseconds
- Sep = Calculated separation in arcseconds
- e_Sep = Separation error
- PA = Calculated position angle in degrees
- e_PA = Position angle error
- Mag = Vmags for both components measured by differential photometry
- e_Mag = Magnitude errors
- SNR = Signal to noise ratio for both components
- dVmag = Plate solving error in Vmag
- Date = Julian observation epoch
- Notes = Additional comments below Table 1

3. Cross-Match with Gaia DR2

All listed objects were additionally cross-matched with Gaia DR2 to check for potential gravitational relationship (PGR) – the results are given in Table 2 with

(Text continues on page 28)

WDS	Disc	C	RA	Dec	dRA	dDec	Sep	Err Sep	PA	Err PA	Mag	Err Mag	SNR	dVmag	Date	Notes
12596+4502	BVD 226		12 59 36.300	45 01 53.01	0.07	0.13	19.11155	0.14765	308.548	0.443	12.526	0.061	128.10	0.06	2019.31764	1)
			12 59 34.890	45 02 04.92							14.537	0.064	47.65			
12359+3758	CBL 596		12 35 56.596	37 58 02.32	0.05	0.09	8.17342	0.10296	178.342	0.722	15.469	0.053	30.61	0.04	2019.31492	1)2)
			12 35 56.616	37 57 54.15							16.296	0.074	17.03			
13064+3042	CRB 93		13 06 22.262	30 41 42.65	0.04	0.03	25.97269	0.05000	107.061	0.110	13.808	0.043	73.11	0.04	2019.31770	1)
			13 06 24.187	30 41 35.03							14.476	0.045	51.05			
13005+2900	CVR 131		13 00 30.056	28 59 39.00	0.08	0.09	35.28610	0.12042	310.208	0.196	15.444	0.073	25.53	0.06	2019.31765	1)2)
			13 00 28.002	29 00 01.78							16.202	0.088	16.42			
13038+3210	CVR 132		13 03 49.959	32 09 59.77	0.06	0.05	9.72754	0.07810	231.917	0.460	15.847	0.076	22.64	0.06	2019.31769	1)2)
			13 03 49.356	32 09 53.77							16.209	0.085	17.64			
12467+3327	DAM 709		12 46 43.687	33 26 49.29	0.03	0.03	5.11083	0.04243	65.985	0.476	15.943	0.060	20.62	0.03	2019.31500	1)2)
			12 46 44.060	33 26 51.37							16.424	0.082	13.69			
12353+3634	ES 2166		12 35 15.841	36 33 30.68	0.09	0.03	4.69447	0.09487	357.499	1.158	12.433	0.041	106.71	0.04	2019.31491	1)
			12 35 15.824	36 33 35.37							12.691	0.041	103.47			
12397+3714	ES 2167		12 39 47.064	37 11 19.54	0.05	0.05	6.19500	0.07071	272.313	0.654	11.555	0.060	191.44	0.06	2019.31495	1)
			12 39 46.546	37 11 19.79							12.485	0.061	132.57			
13065+3240	ES 2471		13 06 32.721	32 40 00.16	0.05	0.08	8.34188	0.09434	39.140	0.648	10.104	0.060	308.25	0.06	2019.31771	1)
			13 06 33.138	32 40 06.63							13.862	0.063	61.51			
13097+3355	GRV 864		13 09 44.701	33 56 09.37	0.08	0.07	24.61192	0.10630	214.389	0.247	11.060	0.060	215.37	0.06	2019.31773	1)
			13 09 43.584	33 55 49.06							11.096	0.060	217.67			
12525+3155	HJ 524		12 52 30.300	31 55 17.71	0.04	0.08	21.78332	0.08944	111.943	0.235	10.224	0.050	279.44	0.05	2019.31761	1)
			12 52 31.887	31 55 09.57							12.299	0.051	136.39			
12319+4034	HJ 2614		12 31 49.680	40 35 01.78	0.05	0.05	25.14680	0.07071	243.882	0.161	11.346	0.050	214.31	0.05	2019.31489	1)
			12 31 47.698	40 34 50.71							12.632	0.051	126.51			
12468+4125	HJ 2620		12 46 48.115	41 25 02.82	0.05	0.05	14.36222	0.07071	293.035	0.282	13.065	0.071	105.05	0.07	2019.31500	1)
			12 46 46.940	41 25 08.44							13.858	0.072	71.05			
12308+3640	J 1023		12 30 46.190	36 39 35.07	0.06	0.05	5.16415	0.07810	172.502	0.866	11.373	0.050	183.29	0.05	2019.31489	1)
			12 30 46.246	36 39 29.95							11.860	0.051	124.31			
18292+1742	J 2912		18 29 17.382	17 41 51.55	0.12	0.13	6.26732	0.17692	142.168	1.617	11.202	0.120	143.64	0.12	2019.31505	1)
			18 29 17.651	17 41 46.60							13.738	0.124	35.87			

Table 1. Results for measured WDS objects

Table 1 continues on the next page.

Double Star Photometry – April 2019

WDS	Disc	C	RA	Dec	dRA	dDec	Sep	Err Sep	PA	Err PA	Mag	Err Mag	SNR	dVmag	Date	Notes
13024+4308	KPP 856		13 02 24.798	43 07 57.42	0.08	0.09	7.12698	0.12042	194.499	0.968	11.871	0.090	152.07	0.09	2019.31766	1)
			13 02 24.635	43 07 50.52							12.339	0.090	115.37			
12548+4105	KPP1796		12 54 46.001	41 05 02.15	0.06	0.17	13.93698	0.18028	237.881	0.741	10.963	0.060	238.49	0.06	2019.31762	1)
			12 54 44.957	41 04 54.74							13.424	0.061	84.04			
12359+3600	KPP2139		12 35 51.410	36 00 19.58	0.06	0.06	17.44376	0.08485	2.991	0.279	11.457	0.070	198.19	0.07	2019.31491	1)
			12 35 51.485	36 00 37.00							14.014	0.072	64.89			
12283+3710	KZA 34		12 28 13.920	37 10 01.17	0.07	0.10	6.46396	0.12207	244.233	1.082	12.750	0.051	100.24	0.05	2019.31487	1)
			12 28 13.433	37 09 58.36							12.541	0.051	118.46			
12285+3722	KZA 35		12 28 27.166	37 22 02.85	0.05	0.06	32.69580	0.07810	27.279	0.137	10.307	0.060	302.40	0.06	2019.31487	1)
			12 28 28.423	37 22 31.91							13.847	0.062	71.43			
12473+2959	LDS4268		12 47 14.513	30 00 19.29	0.08	0.07	6.27032	0.10630	55.960	0.971	11.553	0.100	137.66	0.10	2019.31501	1)
			12 47 14.913	30 00 22.80							11.880	0.100	119.69			
12576+3514	LDS5764		12 57 39.821	35 13 27.47	0.07	0.08	16.03069	0.10630	226.375	0.380	10.607	0.060	279.64	0.06	2019.31764	1)
			12 57 38.874	35 13 16.41							13.270	0.061	94.18			
12523+3836	NI 30		12 52 16.017	38 35 42.37	0.07	0.07	10.70876	0.09899	158.889	0.530	14.644	0.055	44.58	0.05	2019.31761	1)
			12 52 16.346	38 35 32.38							14.463	0.054	51.57			
12556+2933	SKF 490		12 55 34.367	29 32 32.70	0.02	0.02	4.61002	0.02828	179.838	0.352	14.689	0.039	43.57	0.03	2019.31762	1)
			12 55 34.368	29 32 28.09							14.948	0.041	37.85			
13016+2924	SKF 491		13 01 34.415	29 23 48.38	0.02	0.03	8.92912	0.03606	143.959	0.231	13.481	0.032	86.95	0.03	2019.31765	1)
			13 01 34.817	29 23 41.16							14.457	0.036	54.61			
12424+3653	SKF2593		12 42 25.055	36 53 07.37	0.02	0.03	20.95542	0.03606	2.822	0.099	12.382	0.031	149.00	0.03	2019.31499	1)
			12 42 25.141	36 53 28.30							13.956	0.034	70.51			
12463+3341	SKF2594	A	12 46 20.924	33 41 22.04	0.02	0.04	6.83159	0.04472	156.187	0.375	10.400	0.040	268.53	0.04	2019.31499	1)2)
		C	12 46 21.145	33 41 15.79							17.355	0.300	3.17			
12473+3811	SKF2596		12 47 15.102	38 11 06.18	0.02	0.02	6.60055	0.02828	99.593	0.246	12.324	0.061	129.97	0.06	2019.31503	1)
			12 47 15.654	38 11 05.08							14.632	0.065	40.95			
12487+3437	SKF2598		12 48 43.645	34 37 23.30	0.02	0.02	20.54103	0.02828	299.805	0.079	11.990	0.031	146.83	0.03	2019.31503	1)
			12 48 42.201	34 37 33.51							15.033	0.045	31.32			
12382+4212	SKF2652		12 38 09.287	42 12 12.14	0.03	0.04	125.84146	0.05000	125.961	0.023	9.823	0.040	300.96	0.04	2019.31494	1)
			12 38 18.453	42 10 58.25							11.483	0.040	214.61			

Table 1 (continued). Results for measured WDS objects

Table 1 continues on the next page.

Double Star Photometry – April 2019

WDS	Disc	C	RA	Dec	dRA	dDec	Sep	Err Sep	PA	Err PA	Mag	Err Mag	SNR	dVmag	Date	Notes
12568+4029	SKF2656		12 56 49.092	40 29 01.18	0.03	0.03	16.65733	0.04243	113.492	0.146	11.328	0.030	222.81	0.03	2019.31763	1)
			12 56 50.431	40 28 54.54							15.633	0.041	25.99			
12320+3406	SKF2708		12 32 00.310	34 05 30.74	0.05	0.08	24.69309	0.09434	114.067	0.219	11.543	0.050	184.14	0.05	2019.31490	1)
			12 32 02.125	34 05 20.67							12.907	0.051	108.06			
12365+3135	SKF2709		12 36 31.365	31 35 22.22	0.04	0.03	6.12574	0.05000	340.378	0.468	9.767	0.040	341.16	0.04	2019.31493	1)
			12 36 31.204	31 35 27.99							13.437	0.045	54.32			
13029+2935	SLE 908		13 02 56.274	29 34 57.31	0.06	0.06	8.93717	0.08485	234.104	0.544	13.803	0.015	70.28	0.03	2019.31768	1)
			13 02 55.719	29 34 52.07							14.800	0.039	41.92			
13065+2819	SLE 911		13 06 28.633	28 19 23.87	0.08	0.04	6.84299	0.08944	151.787	0.749	12.786	0.051	116.49	0.05	2019.31770	1)
			13 06 28.878	28 19 17.84							14.099	0.053	58.94			
13076+2822	SLE 914		13 07 33.373	28 22 09.95	0.03	0.03	8.56133	0.04243	32.132	0.284	14.539	0.047	44.75	0.04	2019.31772	1)
			13 07 33.718	28 22 17.20							15.081	0.054	29.47			
13086+2920	SLE 915		13 08 35.570	29 19 44.45	0.07	0.07	21.98829	0.09899	151.976	0.258	12.261	0.061	121.70	0.06	2019.31773	1)
			13 08 36.360	29 19 25.04							13.967	0.063	55.01			
12400+4102	SMH 17		12 40 00.643	41 01 31.02	0.04	0.07	12.05396	0.08062	210.274	0.383	13.057	0.051	98.97	0.05	2019.31497	1)
			12 40 00.106	41 01 20.61							13.186	0.051	95.53			
12525+2910	SMH 18		12 52 27.217	29 09 31.01	0.06	0.05	13.49652	0.07810	186.856	0.332	14.083	0.062	63.82	0.06	2019.31761	1)
			12 52 27.094	29 09 17.61							15.908	0.075	24.04			
12406+3444	UC 2383		12 40 35.811	34 44 20.79	0.04	0.05	11.14705	0.06403	103.859	0.329	15.539	0.072	27.27	0.06	2019.31497	1)
			12 40 36.689	34 44 18.12							15.771	0.073	25.25			
12494+4023	UC 2409		12 49 21.736	40 22 33.87	0.09	0.08	17.13774	0.12042	184.704	0.403	15.417	0.082	24.46	0.07	2019.31504	1)
			12 49 21.613	40 22 16.79							15.363	0.080	27.22			
13026+3523	UC 2459		13 02 37.424	35 23 06.93	0.07	0.07	15.40424	0.09899	96.710	0.368	15.631	0.083	24.29	0.07	2019.31766	1) 2)
			13 02 38.675	35 23 05.13							16.154	0.094	16.86			
13032+3944	UC 2461		13 03 09.992	39 44 27.66	0.08	0.09	23.74498	0.12042	29.189	0.291	14.796	0.065	44.29	0.06	2019.31768	1) 2)
			13 03 10.996	39 44 48.39							16.202	0.082	19.09			
13048+3355	UC 2472		13 04 49.713	33 55 20.61	0.13	0.08	8.64258	0.15264	71.377	1.012	16.387	0.087	16.81	0.06	2019.31769	1) 3)
			13 04 50.371	33 55 23.37							16.740	0.104	12.35			
12411+4316	UR 7		12 41 05.007	43 15 30.66	0.04	0.04	5.07058	0.05657	359.136	0.639	12.227	0.051	144.78	0.05	2019.31498	1)
			12 41 05.000	43 15 35.73							12.931	0.051	105.35			
12576+3650	WRS 3		12 57 36.820	36 49 29.43	0.05	0.07	14.85286	0.08602	343.081	0.332	11.655	0.080	184.41	0.08	2019.31763	1)
			12 57 36.460	36 49 43.64							12.446	0.080	136.24			

Table 1 (conclusion). Results for measured WDS objects

Table 1 Notes

1) 1) iT24 1x20s

2) 2) SNR B<20

3) 3) SNR A and B <20

Double Star Photometry – April 2019

Object	Comp	PA	e_PA	Sep	e_Sep	Plx1	e_Plx1	Plx2	e_Plx2	Min_D_AU	Median_AU	Max_D_AU	LPGR	M1_50	M2_50
BVD 226		308.479	0.000	19.09402	0.00003	6.0651	0.0244	6.0947	0.0174	3115	175323	946838	56.43	0.80439	0.60096
CBL 596		178.140	0.000	7.84613	0.00006	5.1038	0.0366	5.2106	0.0507	1519	827186	2847287	8.08	0.60082	0.49982
CRB 93		107.053	0.000	25.93866	0.00003	8.2057	0.0189	8.1676	0.0223	3155	118498	488056	82.24	0.65112	0.64980
CVR 131		310.235	0.000	35.11917	0.00004	5.6245	0.0330	5.6807	0.0425	6159	378847	1889128	26.60	0.54998	0.50078
CVR 132		232.799	0.000	9.81869	0.00005	4.6329	0.0370	4.6946	0.0388	2075	596142	2797625	16.25	0.54875	0.50830
DAM 709		67.435	0.001	5.16618	0.00007	1.8087	0.0424	1.8166	0.0512	2839	2819793	20246472	3.84	0.70024	0.65078
ES 2166		357.490	0.001	4.72871	0.00006	2.1806	0.0428	2.1681	0.0432	2121	1832433	12172445	5.91	1.03544	1.00212
ES 2167		272.261	0.001	6.16502	0.00007	5.8182	0.0494	5.9035	0.0578	1045	521908	2510900	18.79	0.90509	0.79494
ES 2471		39.314	0.000	8.35662	0.00005	6.6569	0.0570	6.7932	0.0205	1233	621848	1852300	6.38	1.05990	0.64987
GRV 864		214.415	0.000	24.59458	0.00004	7.4057	0.0306	7.3710	0.0335	3302	152081	854212	63.03	0.87792	0.88962
HJ 524		111.824	0.003	21.67120	0.00110	3.9984	0.0535	-0.0088	0.9517	56090	326019759	17964918566342	0.00	1.20801	1.11770
HJ 2614		243.519	0.000	25.09931	0.00005	2.3827	0.0382	3.4587	0.0323	19988895	26923986	33807977	0.00	1.26902	0.85352
HJ 2620		292.753	0.000	14.23427	0.00004	4.0367	0.0339	1.0769	0.0221	121037854	140417226	160265566	0.00	0.82209	0.99142
J 1023		172.445	0.004	5.18992	0.00032	6.5976	0.0562	6.5169	0.2763	775	947789	7523756	11.49	0.84511	0.89612
J 2912		142.266	0.005	6.33772	0.00052	0.6996	0.0351	2.8760	0.3994	78054729	222340770	312871510	0.00	1.12132	0.86972
KPP 856		194.191	0.000	7.26244	0.00006	2.2535	0.0252	2.2585	0.0637	3179	1886374	13680208	5.60	1.10955	1.06280
KPP1796		237.865	0.000	13.91535	0.00008	3.3206	0.0387	2.9230	0.0857	50277	8458060	19881063	0.00	1.08782	0.84588
KPP2139		3.067	0.000	17.50379	0.00009	2.6373	0.0546	2.9065	0.0746	7986	7251995	17354752	0.09	1.06736	0.74675
KZA 34		246.636	0.001	6.42455	0.00006	2.0571	0.0461	2.0533	0.0457	3061	2148031	14865770	4.93	1.02680	1.00305
KZA 35		27.259	0.000	32.68862	0.00004	1.3964	0.0351	0.8315	0.0212	68412902	100320981	133323595	0.00	1.12079	1.04994
LDS4268		56.043	0.001	6.26569	0.00006	4.5078	0.0413	4.4827	0.0411	1385	439437	2685588	23.97	0.96707	0.92452
LDS5764		226.712	0.001	16.03564	0.00031	46.8354	0.2763	49.5475	0.1263	115041	240943	360117	7.04	0.60244	0.25947
NI 30		159.322	0.000	10.63970	0.00006	15.3592	0.0441	15.4098	0.0446	689	49917	291424	99.77	0.49838	0.50138
SKF 490		179.649	0.010	4.64087	0.00078	0.7499	0.0343	-1.4745	0.8741	8284	412163369	1777380112183	0.00	1.04534	0.84764
SKF 491		143.751	0.001	8.91217	0.00010	0.5798	0.0751	0.8605	0.1081	14657	115087586	656203586	0.03	1.22050	0.99774
SKF2593		2.878	0.000	20.98699	0.00008	3.1984	0.0763	3.0644	0.0270	6721	2817897	9398334	2.32	0.99372	0.78981
SKF2594	AC	157.003	0.001	6.88694	0.00007	1.0401	0.0431	1.0718	0.0661	6204	10726134	74650190	1.00	1.25635	0.70770
SKF2596		99.145	0.000	6.60536	0.00005	4.4472	0.0357	4.4820	0.0268	1468	412007	2436543	25.40	0.87747	0.64991
SKF2598		299.917	0.000	20.58652	0.00005	0.7061	0.0349	0.9312	0.0316	1005902	70618575	159758728	0.00	1.04020	0.92864
SKF2652		125.985	0.000	125.81510	0.00006	4.5970	0.0403	4.4730	0.0463	27305	1242839	4065941	3.60	1.36481	0.96356
SKF2656		113.542	0.000	16.60596	0.00007	8.0826	0.0309	8.1351	0.0847	2032	225981	1591719	44.93	0.83938	0.54246
SKF2708		114.459	0.000	24.96447	0.00007	2.6064	0.0580	2.6182	0.0487	9276	1566568	10276360	6.99	1.05536	0.91110
SKF2709		340.198	0.000	6.17367	0.00005	3.6443	0.0437	3.7445	0.0323	1658	1512291	4944544	3.70	1.46054	0.78292
SLE 908		235.011	0.000	9.06448	0.00004	2.4739	0.0266	1.9654	0.0334	12912881	21558361	30250084	0.00	0.87912	0.79820
SLE 911		151.330	0.000	6.71560	0.00004	4.3322	0.0354	4.3772	0.0238	1526	509325	2 500 744	19.69	0.77791	0.64890
SLE 914		33.784	0.000	8.48413	0.00004	1.1973	0.0355	0.8983	0.0417	10201064	57293630	123286201	0.00	0.92422	0.90440
SLE 915		152.117	0.000	21.97615	0.00004	0.1222	0.0340	1.1631	0.0249	614182920	1511999042	1383571868948	0.00	0.97943	0.95267
SMH 17		210.840	0.000	12.09272	0.00004	1.1802	0.0347	1.3954	0.0280	4793727	26945460	54319895	0.00	1.15118	1.05843
SMH 18		186.770	0.000	13.55104	0.00006	0.9871	0.0372	0.3064	0.0569	169330402	464713144	4138557157	0.00	0.96279	0.88570
UC 2383		104.323	0.000	11.15556	0.00008	7.1033	0.0512	6.8893	0.0706	1583	903040	2492600	2.66	0.50011	0.50056
UC 2409		185.039	0.000	17.21795	0.00004	6.0951	0.0349	4.9543	0.0340	6208802	7792134	9485998	0.00	0.54975	0.50022
UC 2459		95.958	0.000	15.44458	0.00004	4.7239	0.0269	4.6845	0.0376	3253	406107	2278887	25.55	0.60026	0.54992
UC 2461		30.046	0.000	23.69732	0.00004	3.2548	0.0288	3.2297	0.0389	7191	734503	5249006	14.44	0.67409	0.60002
UC 2472		69.112	0.000	8.53277	0.00006	4.7581	0.0486	4.8578	0.0495	1761	894886	3682680	9.41	0.54669	0.44083
UR 7		359.250	0.002	5.08687	0.00022	8.1240	0.0500	6.2522	0.2159	3406109	7592982	13151359	0.00	0.84082	0.77279
WRS 3		343.375	0.000	14.79647	0.00004	7.2300	0.0381	3.6972	0.0373	24703033	27262263	29970220	0.00	0.87834	0.81560

Table 2: Results for DR2 cross-matched WDS objects

Double Star Photometry – April 2019

(Continued from page 23)

the following structure:

- Object = Discoverer ID
- Comp = Components (AB if blank)
- PA = Position angle in degrees
- e_PA = Error position angle
- Sep = Separation in arcseconds
- e_Sep = Error separation
- Plx1 = Parallax primary in mas
- e_Plx1 = Error parallax primary
- Plx2 = Parallax secondary in mas
- e_Plx2 = Error parallax secondary
- Min_D_AU = Minimum spatial distance in AU between components (see Appendix)
- Med_D_AU = Median spatial distance in AU between components (see Appendix)
- Max_D_AU = Maximum spatial distance in AU between components (see Appendix)
- LPGR = Likelihood of potential gravitational relationship (see Appendix)
- M1_50 = DR2 StarHorse mass50 value primary
- M2_50 = DR2 StarHorse mass50 value secondary

All objects in Table 2 were already cross-matched with Gaia data in other reports, so the values given here on separation and position angle are referenced as input for assessing the likelihood of potential gravitational relationship but are not intended for updating the WDS catalog. For the 4 objects with LPGR > 50 WDS code "T" is suggested for likely physical by common parallaxes. For the objects with LPGR < 10 WDS code "U" for likely optical is suggested.

For objects with LPGR > 50 the minimum and median period of a potential orbit is calculated using the smallest and median spatial distance between the components as estimation for the semi-major axis assuming zero inclination (this assumption ignores the influence of eccentricity, so it is most likely that the observed separation for high eccentricity pairs is near apastron which means that the "real" semi-major axis might in most cases somewhat different) and using the mass50 values from the GAIA DR2 StarHorse catalog sharing the caveats of Anders et al. 2019 for using these data. The results are listed in Table 3 with the following structure:

Object = Discoverer ID
P_min_yr = Minimum period of a potential orbit
P_med_yr = Maximum period of a potential orbit

Object	P_min_yr	P_med_yr
BVD 226	147 496	62 267 755
CRB 93	156 266	35 961 665
GRV 864	143 495	44 856 536
NI 30	18 206	11 215 665

Table 3: Potential orbit periods in years

In all these cases the potential orbit period is far too long to detect any changes in separation and position angle by visual observation over a reasonable time frame.

Summary

A good part of the 46 measured objects shows the expected magnitude difference larger than 0.5 compared with the WDS catalog data especially for the secondary but for many objects the given WDS magnitudes were simply confirmed within the given error range. 4 objects have parallaxes and angular separations allowing for a higher than 50% likelihood for a spatial distance between the components of less than 200,000 AU (~1 parsec) suggesting potential gravitational relationship and 33 objects are most likely opticals.

Acknowledgements

The following tools and resources have been used for this research:

- Washington Double Star Catalog
- GAIA DR2 catalog
- DSS2 images
- Aladin Sky Atlas v10.0
- iTelescope
  - iT24: 610mm CDK with 3962mm focal length. Resolution 0.625 arcsec/pixel. V-filter. No transformation coefficients available. Located in Auberry, California. Elevation 1405 m
- AAVSO VPhot
- Astrometrica v4.10.0.427
- URAT1 catalog
- AstroPlanner v2.2
- MaxIm DL6 v6.08
- GAIA DR2 StarHorse catalog available through the Gaia@AIP services hosted by the Leibniz-Institute for Astrophysics Potsdam using the ADQL query interface at gaia.aip.de

References

Anders, F., Khalatyan, Arman, et al., 2019, “Photo-astrometric distances, extinctions, and astrophysical parameters for Gaia DR2 stars brighter than G = 18”, *Astronomy & Astrophysics*, DOI 10.1051/0004-6361/201935765

Knapp, Wilfried R. A., 2018, “A New Concept for Counter-Checking of Assumed Binaries”, *Journal of Double Star Observations*, **14** (3), 487-491.

Appendix

Description of the PGR assessment procedure

GAIA DR2 data for RA/Dec and Plx are used for a Monte Carlo simulation assuming a normal distribution for these parameters with the given error range as standard deviation. The spatial distance between the components is (according to Knapp 2018) calculated from the inverted simulated parallax data and the simulated angular separation using the law of cosine

$$sep = \sqrt{a^2 - 2ab\cos\gamma + b^2}$$

with *a* and *b* = distance vectors for the stars A and B in lightyears calculated as (1000/Plx)*3.261631 and γ = angular separation in degrees calculated as

$$\gamma = \arccos\left[\sin(DE1)\sin(DE2) + \cos(DE1)\cos(DE2)\cos\left(\left|RA1 - RA2\right|\right)\right]$$

The likelihood for potential gravitational relationship (LPGR) is the percentage of simulation results <200,000 AU (~1 parsec) out of the simulation sample with a size of 120,000

The given smallest, median and largest spatial distance between the components is the smallest, median and largest result out of the simulation sample.

Orbit Determination of Close Binary Systems

F. M. Rica
Editor of News Section, El Observador de Estrellas Dobles (OED) Magazine, Spain
frica0@gmail.com

H. Zirm
Markt Schwaben, Germany
binary71@gmx.de

Abstract: Several years ago we published in IAU circulars the orbital parameters for 6 close binary stars (A 957, HEI 35, A 2833, STF1554, BU 606, I 952). These were the first orbits ever published for those close binaries. The Docobo's method of orbital calculation was used to determine the orbital solutions and it was then improved by using a least square process. A weighting scheme was followed for all astrometric measures (individually for theta and rho). All these orbital solutions are still the most recent published orbits for these binaries.

In this article we publish for the first time, the astrophysical study, the orbit plots and all the astrometric measures with their residuals and ephemerides for these objects.

1. Introduction

In the circular number 174 (June 2011) of IAU G1 Commission, we published the orbital solutions for six close visual binary stars. These orbits were the first calculated for these objects (the literature search produced no evidence of previously computed orbits). These orbital solutions are still the most recent published.

That circular only published the orbital parameters. The orbital plots, the ephemerids for the next few years, the tables with measures, the astrophysical data, etc. are published in this article for the first time. The calculated periods range from 29 to 708 years. The measurements were mostly obtained from the Washington Double Star Catalogue by request from Brian Mason & colleagues.

All the orbits are calculated with the algorithm described in Docobo (1985). The three base points have been chosen carefully from the observational data that seemed most reliable with respect to instrumentation, data density, or critical arc coverage. We also tried to cover as much of the observed arc as possible. Often, we use a parabolic or cubic fit to $\theta(t)$ and $\rho(t)$ to obtain the base points. This may let the area around a single observation represent a base point without additional observational coverage.

Finally, we applied least squares refinement to the preliminary elements by using the formula for differential corrections in polar coordinates (Heintz 1967). The uncertainties of the elements were obtained by the covariance matrix of the normal equations and the sum of the residuals in position angle and separation.

The weights for speckle measures follow the scheme described by Mason (1999). For initial weightings on visual measurements, we choose the algorithm described by Docobo & Ling (2003). The proposal by Heintz (1967, 1978) to reduce the weights for the distances from visual measurements by a factor of 1:4 to 1:5 was used in most cases. Position angles are corrected for precession, Equinox 2000.

The organization of this paper is as follows. In Section 2, we present the general methods for our astrophysical procedures and the data table and figures are published. In Section 3, we include general information for each of the binaries studied.

2. General Information

2.1. Astrophysical procedure

To obtain astrophysical data (spectral type, masses, etc.) of the individual component of close binaries, we used a tool designed by one of us (called Binary_Deblending_Tool) that deblends the combined observed multi-band photometry (Hipparcos, Tycho-2, 2MASS, etc.) into two separate entries corresponding to both stellar components. To create the input table for this tool, we used the CMD 2.7 isochronal to the related photo-metric bands and colors with astrophysical properties. The tool searches in this table for two entries that matches with observational data (multiband photometry, Dmag, reddening and parallax) and selects those which give minimum χ^2.

GAIA-DR2 does not list useful data for these bright and close binary stars.

The reddening in the line of sight was estimated using the maps of Schlegel, Finkbeiner, and Davis (1998) and the more recent of Schlafly and Finkbeiner (2011). The resulting values were scaled to the initial distance using the formula published by Anthony-Twarog, and Twarog (1994).

2.2 Table data and Figures

First, general information about the systems is discussed, followed by important identifications and the calculated orbital elements in Table 3. A comparison of the recalculated Hipparcos parallaxes (van Leeuwen 2007) with the dynamical parallaxes, the resulting masses, absolute magnitudes, and determined spectral types for the individual components can be found in Table 4. The calculation of the dynamical parallaxes and masses follows the Baize-Romani algorithm described by Heintz in 1978. The calculated ephemerids for 2020, 2021, 2022, 2023 and 2024 are available at Table 5. At the appendix we list the astrometric measurements compared with calculated residuals. Finally we show the orbital plots. Tables 6-11 lists the observations for each binary star. The columns are from left to right: the date of the observations, the position angle and angular separation, the number of nights observed, the WDS reference of the publication, the aperture of the telescope (in meters), WDS codes. All these columns are taken directly from WDS. And finally, we list the O-C for θ and ρ. The plots in Figures 1 - 6 came from USNO catalog Sixth Catalog of Orbits of Visual Binary Stars

3. Description of the Close Binary Stars

WDS 02048+6030 = A 957 = ADS 1632

Mag. 8.52 and 10.48. Spectral type F8V.
First measurement: 1905.82
Last measurement: 2011.8569
Used observations: 21

The components are cataloged as HD 12529 and were first resolved by R. G. Aitken in 1905. Since then it has shown relatively consistent visual measurements showing a clear curved arc of about 100 degrees. But the typical scatter in visual measures in regard to the average distance of 0.5 arc seconds makes the calculation of an orbit very difficult. However, our derived orbit is marked as preliminary solution. After the publication of our orbit, two new astrometric points were included in WDS catalog. The residuals for these recent observations suggest that the orbit is opening and that the orbital period is greater than the calculated value (220 years).

This is a system rich in metals (Nordstrom et al. 2004; Casagrande et al. 2011) with an age of 3-4 Gyr and located at 97 pc. The literature shows combined spectral types that ranges from F8V to G2V. Our astrophysical study concludes that this stellar system is composed of F5V and G8V (masses of 1.3 and 0.9 $M_{\odot}$) stars. The astrophysical parameters were corrected by a reddening of E(B-V) ≈ 0.05. Table 1 lists observed photometric data and compares them with the synthetic photometry determined by using our excel tool Binary_Deblending_Tool. Table 2 lists the individual astrophysical properties for both stellar components deter-

(Continued on page 33)

	Observed Photometry	Source	Syntetic Photometry	Difference
U	...	...	...	
B	8.83 ± 0.01	Hipparcos	8.78	0.05
V	8.22 ± 0.01	Hipparcos	8.21	0.01
I	7.54 ± 0.01	Hipparcos	7.57	-0.03
J	7.12 ± 0.02	2MASS	7.15	-0.03
H	6.84 ± 0.02	2MASS	6.94	-0.10
K	6.80 ± 0.02	2MASS	6.87	-0.06
B-V	0.61 ± 0.02	Hipparcos	0.57	0.04
V-I	0.68 ± 0.02	Hipparcos	0.64	0.04
V-K	1.42 ± 0.02		1.35	0.07
J-H	0.28 ± 0.03		0.21	0.07
H-K	0.04 ± 0.02		0.07	-0.03
J-K	0.28 ± 0.03		0.21	0.07

Table 1. Comparison of observed and synthetic data for A 957

	Comp. A	Bomp. B
V	8.30	10.20
(B-V)o	0.48	0.70
Mv	3.40	5.30
Mass [$M_{\odot}$]	1.37	1.08
Teff [°K]	6488	5793
log g	0.6	0.8
SpT	F5V	G8V
Distance [pc]	97	
Age [Gyr]	1.4	

Table 2. Astrophysical Data for the Binary A 957

Orbit Determination of Close Binary Systems

WDS D.D.	HD HIP	ADS other	P^{yr} ±	T ±	e ±	a″ ±	i° ±	ω° ±	$\Omega°_{2000}$ ±
02048+6030	12529	1632	219.97	1870.07	0.462	0.471	125.3	250.1	107.7
A 957	9704		-	-	-	-	-	-	-
04102+1722	285465	-	28.91	2000.53	0.832	0.282	115.7	35.9	165.9
HEI 35	19472		± 1.50	± 0.01	± 0.007	± 0.008	± 0.7	± 1.5	± 0.9
06549+1158	50722	5571	209.09	1987.13	0.927	0.429	43.1	240.7	107.2
A 2833	33240		± 35.98	± 0.19	± 0.010	± 0.040	± 4.6	± 8.3	± 8.9
11361+1251	100797	8230	478.88	1962.44	0.902	0.868	74.8	308.6	84.6
STF1554	56589		± 72.49	± 0.47	± 0.011	± 0.066	± 0.8	± 1.9	± 0.9
12260-1457	108215	8547	707.61	2009.44	0.383	1.441	96.9	123.6	100.1
BU 606	60665		± 36.19	± 6.63	± 0.052	± 0.188	± 3.9	± 4.5	± 6.3
14531-4638	131078	-	99.13	1981.39	0.659	0.521	156.1	268.1	27.1
I 952	72821		± 0.82	± 0.37	± 0.015	± 0.014	± 4.5	± 7.3	± 7.8

Table 3. Identification and orbital elements

WDS D.D.	V_A V_B	Sp.	B-V	π^{mas}_{trig} [1]	$\Sigma M/M^{sol}$	π^{mas}_{dyn}	$M/M_{sol\ A}$ $M/M_{sol\ B}$	$M_{vis\ A}$ $M_{vis\ B}$
02048+6030	8.5	F5V+G8V	0.61	10.28	2.0	9.8	1.4	3.5
A 957	10.5			±1.19			0.9	5.4
04102+1722	9.5	K2V+K6V	1.07	26.98	1.37	28.1	0.72	6.7
HEI 35	10.9			±2.27	±0.37		0.50	8.2
06549+1158	8.3	F2IV+F2IV-V	0.39	7.68	4.0	8.6	1.6	3.0
A 2833	8.8			±1.24	±2.6		1.3	3.9
11361+1251	9.4	G0V+G0/1V	0.58	10.25	2.7	11.1	1.1	4.7
STF1554	9.5			±1.16	±1.3		1.0	4.9
12260-1457	7.4	F4V+G5V	0.51	14.07	2.1	13.3	1.6	3.1
BU 606	9.4			±0.69	±0.9		1.0	5.0
14531-4638	8.5	G5V+K1V	0.70	20.96	1.6	20.6	1.0	5.1
I 952	10.1			±1.06	±0.3		0.7	6.7

Table 4. Astrophysical Data

Remarks: The individual visual magnitudes for each component are calculated from combined visual magnitudes adopted from Hipparcos catalogue and the visual magnitude difference adopted from WDS catalogue. Note 1 is the parallax adopted from Van Leeuwen 2007. Note 2 marks the estimation as main sequence stars.

WDS	2020		2021		2022		2023		2024	
	ϑ_{2000} (°)	ρ (")	ϑ_{2000} (°)	ρ (")	ϑ_{2000} (°)	ρ (")	ϑ_{2000} (°)	ρ (")	ϑ_{2000} (°)	ρ (")
02048+6030	2.1	0.368	0.8	0.368	359.4	0.367	358.0	0.367	356.6	0.367
04102+1722	321.1	0.357	319.1	0.332	316.7	0.303	313.8	0.271	310.1	0.235
06549+1158	142.8	0.481	143.1	0.487	143.5	0.494	143.8	0.500	144.2	0.507
11361+1251	220.2	0.338	220.8	0.344	221.3	0.351	221.8	0.357	222.3	0.363
12260-1457	286.6	0.655	286.3	0.668	286.1	0.681	285.8	0.695	285.6	0.708
14531-4638	311.3	0.766	310.2	0.771	309.0	0.774	307.9	0.778	306.8	0.781

Table 5. Ephemerides

Orbit Determination of Close Binary Systems

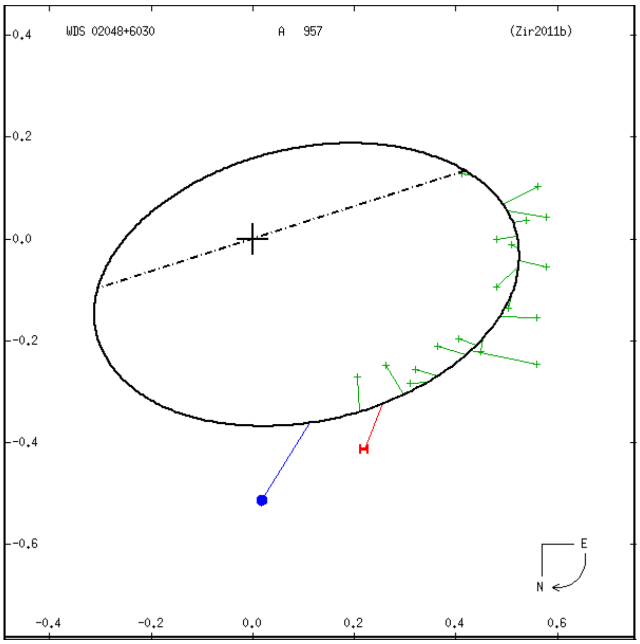

Figure 1. WDS 02048+6030

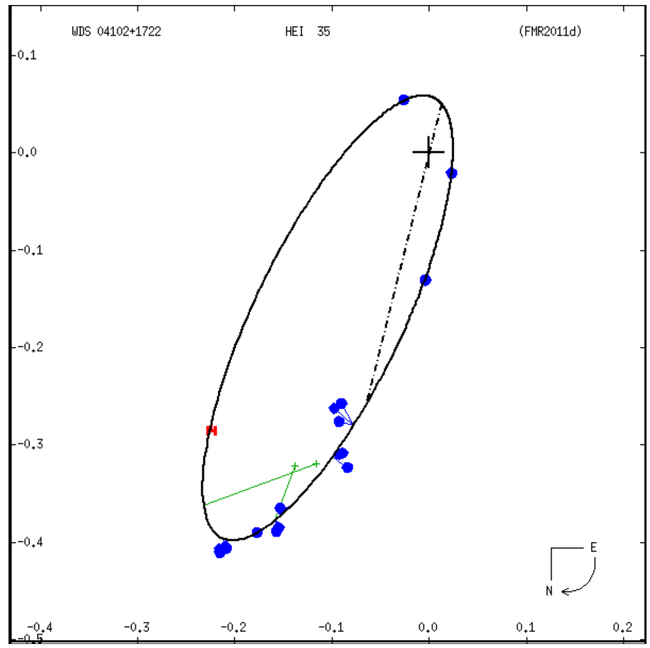

Figure 2. WDS 04102+1722

mined by us using the Excel tool.

The dynamic parallax and dynamic masses are in good agreement with the Hipparcos trigonometric parallax and the expected masses.

The 2012 measure was performed by Francisco Rica using the 1.5-m Carlos Sánchez Telescope and the Fastcam lucky Imaging Camera. It is published here for the first time. For more detail about the instrument used, see Rica et al. (2012).

WDS 04102+1722 = HEI 35

Mag. 9.46 and 10.93; spectral type K5
First measurement: 1979.00
Last measurement: 2016.1338
Used observations: 22

This is a faint system (HD 285465) with high proper motion located in the Hyades open cluster. It was discovered in 1979 by W. D. Heintz and is composed of two stars with a visual brightness difference of 1.5 magnitudes and a medium-K spectrum. It has been measured in 22 occasions, many of them by Elliot Horch. The astrometric measures used for the orbital calculation (up to 2008.69) cover more than one revolution. The work of Y. Y. Balega since 1999 shows a rapid movement nearing a periastron phase. Observations by E. Horch up to now consistently show increasing distances from similar positions nearly 30 years old, observed by Heintz. Since our publication of the orbit in 2011, several astrometric points were published showing small residuals with respect our orbit.

Literature lists combined spectral types of K3 (Bidelman 1985) and K4V (Pickles & Depagne 2010) which is in agreement with our combined spectral type. Our astrophysical study concludes that this stellar system is composed of K2V and K6V stars. The astrophysical parameters were corrected by a reddening of E(B-V) ≈ 0.05. The dynamic parallax and dynamic mass are in good agreement with the Hipparcos trigonometric parallax and the expected masses.

WDS 06549+1158 = A 2833 = ADS 5571

Mag. 8.3 and 9.2; spectral types F5
First measurement: 1914.51
Last measurement: 2008.111
Used observations: 18

This binary system (HD 50722) was discovered by Aitken in 1914, and up to the present day 18 observations have been made. One measurement, obtained by Argue in 1987 via CCD technique, was not used for the calculation. This measurement is listed in the WDS catalog with the comment "... Identification error, position error, or misprint in publication, NOT corrected..." and the calculated theoretical position at this epoch seems to confirm the fact that cannot be the same component. Several tests with different basis points (using Docobo orbital method) showed that the Hipparcos measurement must be assigned a significantly reduced weight (compared to the last speckle measurement).

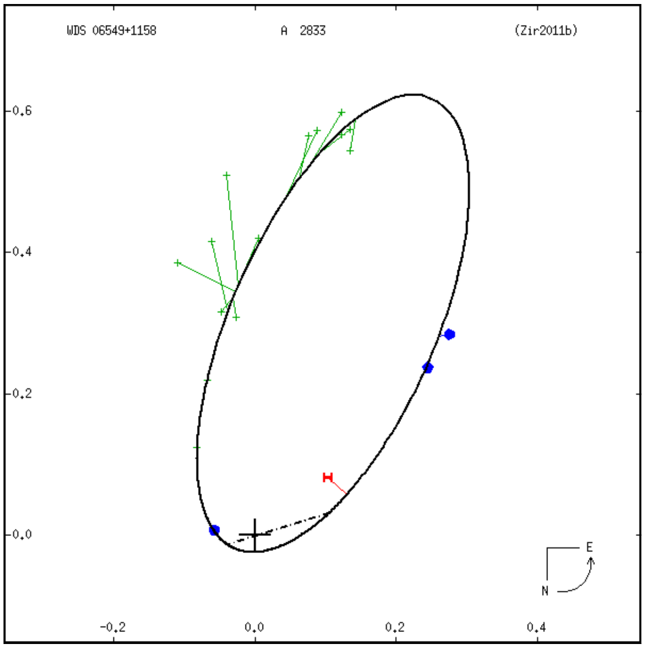

Figure 3. WDS 06549+1158

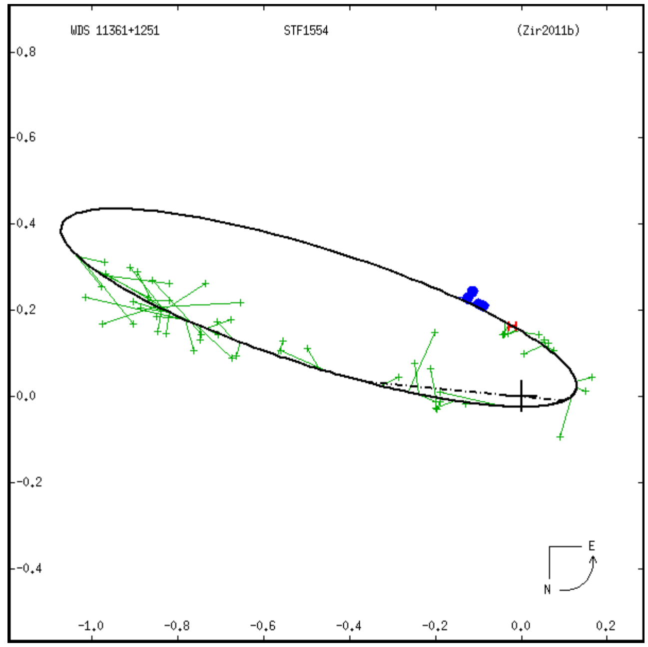

Figure 4. WDS 11361:1251

This binary is listed in the literature as a F5 (ppN catalog) and as a F5IV star by Pickles, Depagne (2010). Fehrenbach, Burnage & Figuiere (1992) catalogued it as a low metallicity star, [Fe/H] = -0.29, with an age of 2.3 Gyr. In this work, we determined the absolute magnitudes from apparent individual components (8.28 and 8.75) and Hipparcos trigonometric parallax. The differential magnitude of Hipparcos has a very significant error and so we don't use its individual photometry. Instead, we use the Hipparcos combined V magnitude and the mean differential magnitude from the WDS historical data. Using evolutionary isochrones for the metallicity listed in the literature and different ages, we determine a stellar age of about 2.2 Gyr (in excellent agreement with the literature) and spectral types of F2IV and F2IV-V. The astrophysical parameters were corrected by a reddening of E(B-V) ≈ 0.02.

Our calculations produced a very eccentric orbit (e = 0.93). The dynamic parallax and dynamic mass are in moderate agreement with the Hipparcos trigonometric parallax and the expected masses.

WDS 11361+1251 = STF1554 = ADS 8230:

Mag. 9.4 and 9.6; spectral types G5
First measurement: 1829.29
Last measurement: 2010.3510
Used observations: 57

This pair (HD 100797) was discovered by Struve in 1829. Nearly 120 years later, there are 57 astrometric measures of its long period orbit. The period is about 480 years and the periastron passage of this eccentric orbit occurred in 1962.

This object has been very poorly studied and no radial velocity and spectral types (except those of Cannon & Pickering 1918) were obtained. Hipparcos determined a distance of 98 pc (GAIA-DR2 does not list this star). Astronomical literature shows combined spectral types of G5 (Cannon & Pickering 1918) and a photometrically determined spectral type of F8V (Pickles & Depagne 2010), in excellent agreement with our results using BVIJHK combined photometry. Therefore, the G5 spectral type listed in Hipparcos catalog must be in error.

Our astrophysical study concludes that this stellar system is composed of G0V and G0/1V stars. The CMD 2.7 isochrone gives two stars with an age of about 3 Gyr. The astrophysical parameters were corrected by a reddening of E(B-V) ≈ 0.01. The dynamic parallax and dynamic mass are in good agreement with the Hipparcos trigonometric parallax and the expected masses.

WDS 12260-1457 = BU 606 = ADS 8547:

Mag. 7.4 and 9.4. Spectral type F6V
First measurement: 1878.3
Last measurement: 2016.3699
Used observations: 24

Orbit Determination of Close Binary Systems

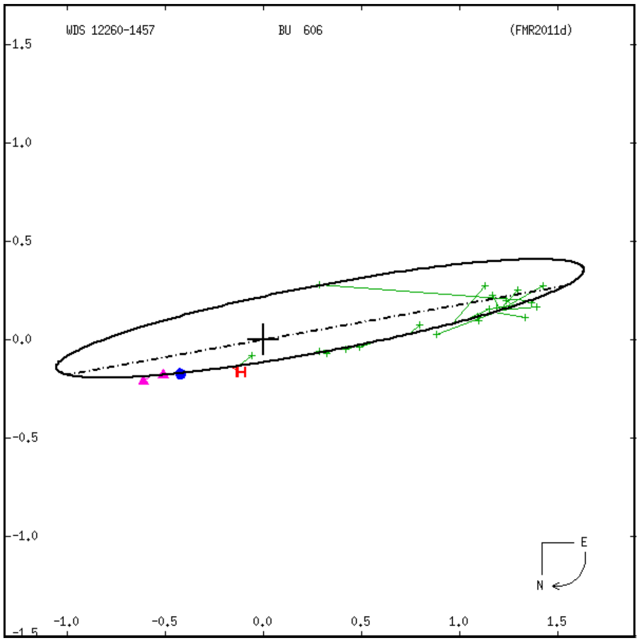

Figure 5. WDS 12260-1457

The components of this binary star (HD 108215) were first resolved by Burnham in 1878. Currently it has 24 measures which are all micrometric except that of Hipparcos satellite. In 138 years, the measures have covered a large, nearly rectilinear arc of about 167 degrees. The older visual measures have significant residuals.

This pair is composed of stars with V magnitudes of 7.32 and 9.26 (Hipparcos magnitudes converted to V band). The Tycho-2 catalog lists a proper motion of -118.3 ± 1.6 mas yr^{-1} in RA and -25.1 ± 1.5 mas yr^{-1} in DEC. The re-reduced (Leeuwen 2007) Hipparcos trigonometric parallax corresponds to a distance of pc. For this distance we calculated a reddening of E(B-V) = 0.02 which was used for our study.

In astronomical literature, BU 606 has been classified as a F6V (Houk & Smith-Moore 1988) or F7V (Abt 1981) star. From combined and differential photometry, we estimated individual spectral types F4V and G5V. Absolute magnitudes +3.1 and +5.1 were calculated using Hipparcos data, which matches the spectral types estimated.

The large linear motion invites the investigation of the nature of the pair of stars. The observed velocity was calculated using the historical measures, with non-zero weights, which covers a time baseline of nearly 128 years (using astrometric data up to 2006). Our result was an apparent motion of -15.42 ± 0.40 mas yr^{-1} in E-W direction and +3.17 ± 0.16 mas yr^{-1} in N-S direction. So, the secondary is moving to the WNW 15.74 ± 0.43 mas yr^{-1} and at the distance of 71.1 pc corresponds to a projected and relative velocity of 5.30 ± 0.15 km s^{-1}. A Monte Carlo simulation shows that the projected observed velocity was less than the escape velocity in 100% of the simulations. We conclude that BU 606 stellar components are gravitationally bound.

Holmberg, Nordström & Andersen (2009) calculated a galactocentric velocity of (U, V, W) = (-33, -20, -16) km s-1 and an age of about 2.6 Gyr. According to this kinematic, this system is a member of the young galactic disk. The calculated fG = 0.18 (Grenon parameter), corresponding to young-middle age thin disk stars of 3-4 Gyr old. This binary is an X-ray emitter whose luminosity in this band suggests that has an age of about 0.1-0.6 Gyr while the projected rotation velocity of 13.5 km/s calculated by Glebocki & Gnacinski (2005) and 15.0 km/s calculated by Nordström (2004) also suggest an age between those of Pleiades and Hyades open clusters. This age is in contradiction with the kinematical age. One possible explanation is that one of the stars is an unresolved and very close binary with synchronized orbital periods.

The derived orbit is very inclined and passed periastron in 2009. The orbital solution presented here is very preliminary. The dynamic parallax and total stellar masses are consistent with Hipparcos trigonometric parallax and with the stellar masses obtained using their spectral types.

A total mass of 2.2 ± 0.4 $M_{\odot}$ was obtained using our orbital parameters and the Hipparcos trigonometric parallax. This value is in good agreement with that calculated using Baize-Romaní method (1.56 + 0.98 = 2.54 $M_{\odot}$) and with that calculated from spectral types (2.27 $M_{\odot}$).

WDS 14531-4638 = I 952:

Mag. 8.5 and 10.1. Spectral type G5V.
First measurement: 1910.6
Last measurement 2013.1276
Used observations: 14

The components of this system were first resolved by Innes in 1910. The last three measures (since 1996) were taken (by Mason and Tokovinin) using speckle technique. The observations span about 103 years, similar to the orbital period, and therefore they cover a complete revolution. The dynamic parallax and total stellar masses are consistent with Hipparcos trigonometric parallax and with the stellar masses obtained using their spectral types. From combined photometric and spec-

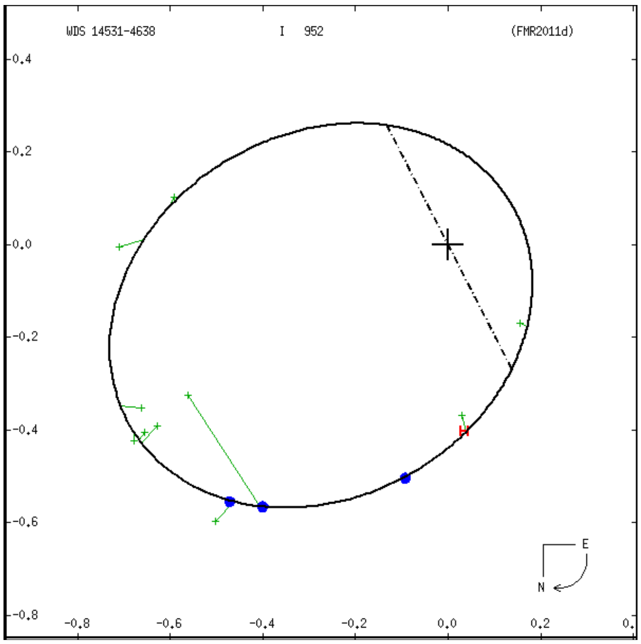

Figure 6. WDS 14531-4638

troscopic data in addition of the differential V magnitude, the individual spectral types of G5V and K1V were determined.

Acknowledgements

This research has made use of the Washington Double Star Catalogue maintained at the U.S. Naval Observatory, the NASA Astrophysics Data System Bibliographic Services and the SIMBAD database (operated at CDS, Strasbourg, France). The authors thank Frank Smith for their respective reviews of this work.

References

Abt, H. A. 1981, *ApJS*, **45**, 437.

Anthony-Twarog B. J., Twarog B. A. 1994, *AJ*, **107**, 1577.

Bidelman, W. P., 1985, *ApJS*, **59**, 197.

Cannon A.J., Pickering E.C. <Harv. Ann. 91-100 (1918-1924)>

Casagrande L. et al., 2011, *A&A*, **530**, 138.

Docobo, J.A., 1985, *CeMec*, **36**, 143.

Docobo, J. A.; Ling, J. F., 2003, *A&A*, **409**, 989.

Fehrenbach, Ch.; Burnage, R.; Figuiere, J., 1992, *A&AS*, **95**, 541.

Glebocki R., Gnacinski P., 2005, *csss*, **13**, 571.

Heintz, W. D., 1978, *Double Stars* (revised edition), Dordrecht, D. Reidel Publishing Co. (*Geophysics and Astrophysics Monographs. Volume 15*), (1978GAM....15.....H).

Heintz, W.D, 1967, *ActaAstr.*, **17**, 311.

Houk N., Smith-Moore M., 1988, Ann Arbor, Dept. of Astronomy, Univ. of Michigan.

Mason, B. D., Douglass, G.G., Hartkopf, W. I., 1999, *AJ*, **117**, 1023.

Nordstrom B. et al., 2004, *A&A*, **418**, 989.

Pickles A., Depagne E., 2010, *PASP*, **122**, 1437.

Rica, F. M., Barrena, R., Vázquez. G., Henríquez, J. A., Hernández, F. et al. 2012, *MNRAS*, **419**, 197R.

Schlafly & Finkbeiner, 2011, *ApJ*, **737**, 103.

Schlegel D.J., Finkbeiner D.P., & Davis M., 1998, *ApJ*, **500**, 525.

van Leeuwen, F., 2007, *Hipparcos, the New Reduction of the Raw Data*, Springer, New York (data obtained from Simbad data base: I/311)

Appendix 1. Observational Data and Residuals

The values in parentheses are the calculated theoretical positions for a given epoch.

Date	ϑ (°)	ρ (")	N	Ref.	Ap	Tec	Cod	O-C ϑ (°)	O-C ρ (")
1905.8200	107.2	0.43	3	A__1906a	0.9	Ma		1.8	-0.02
1915.6400	100.4	0.57	1	A__1929a	0.9	Ma		3.0	0.07
1917.8200	94.2	0.58	2	A__1929a	0.9	Ma		-1.6	0.08
1921.6300	93.9	0.54	2	A__1929a	0.9	Ma		0.9	0.03
1925.8200	89.8	0.48	1	A__1929a	0.9	Ma		-0.3	-0.04
1929.7900	88.8	0.51	2	A__1933d	0.9	Ma		1.3	-0.01
1933.7700	84.6	0.58	2	Kui1961b	0.3	Ma		-0.2	0.05
1935.2600	78.9	0.49	2	VBs1954	1.0	Ma		-4.9	-0.04
1943.7900	74.9	0.52	1	VBs1954	2.1	Mb		-3.2	0.00
1952.4000	74.6	0.58	2	Mrz1956	0.7	Ma		2.5	0.07
1960.0200	63.8	0.50	1	Cou1962a	0.4	Ma		-2.7	0.01
1962.7500	64.1	0.45	4	B__1963b	0.9	Ma		-0.3	-0.04
1965.1500	66.2	0.61	2	Baz1967	0.4	Ma		3.7	0.13
1966.7120	60.0	0.42	4	Wor1971	0.7	Ma		-1.3	-0.06
1975.8800	51.4	0.41	3	Hei1978b	0.6	Ma		-2.1	-0.04
1978.8900	47.7	0.42	3	Hei1980a	0.6	Ma		-3.0	-0.02
1985.7400	46.6	0.36	2	Hei1987a	0.6	Ma		2.6	-0.07
1991.2500	28.0	0.468	1	HIP1997a	0.3	Ht		-10.2	0.056
1997.0400	37.2	0.34	2	Hei1998	0.6	Ma		5.5	-0.06
2008.764	**2.0**	**0.514**	**1**	**Gii2012**	**0.7**	**S**		**-15.2**	**0.136**
2011.8569	**39.4**	**0.3**	**1**	**Gur2018**	**2.1**	**S**		**26.2**	**-0.074**
2012.7263	**356.5**	**0.447**	**1**	**Fmr9999**	**1.5**	**Cl**		**15.5**	**0.074**

Table 6. Measurements of WDS 02048+6030

Date	ϑ (°)	ρ (")	N	Ref.	Ap	Tec	Cod	O-C ϑ (°)	O-C ρ (")
1979.00	336.7	0.35	3	Hei1980a	0.6	Ma		-0.4	-0.06
1986.99	340.0	0.34	3	Hei1987a	0.6	Ma		12.7	-0.09
1991.25	322.0	0.363	1	HIP1997a	0.3	Hh		1.2	0.010
1999.8185	205.6	0.060	1	Bag2004	6.0	S		0.1	0.001
2000.8760	47.6	0.031	1	Bag2006b	6.0	S		0.1	0.000
2001.7585	358.4	0.131	1	Bag2006b	6.0	S	q	0.7	-0.001
2004.1126	340.7	0.273	1	Hor2008	3.5	S		-3.7	-0.018
2004.1126	341.4	0.291	1	Hor2008	3.5	S		-3.0	0.000
2004.1126	339.6	0.280	1	Hor2008	3.5	S		-4.8	-0.011
2004.8241	343.4	0.323	1	Bag2007b	6.0	S		0.8	0.001
2004.9726	345.4	0.334	1	Hor2008	3.5	S		3.1	0.006
2004.9726	343.9	0.321	1	Hor2008	3.5	S		1.6	-0.007
2007.0041	337.2	0.396	1	Hor2010	3.5	S		-1.4	0.006
2007.8178	338.0	0.419	1	Hor2010	3.5	S		0.6	0.011
2007.8204	338.1	0.415	1	Hor2010	3.5	S		0.7	0.007
2008.6900	335.6	0.428	1	Hor2009	3.5	S		-0.6	0.005
2011.6906	**332.1**	**0.4607**	**1**	**Hor2017**	**3.5**	**S**		**0.0**	**0.012**
2011.6906	**332.3**	**0.4636**	**1**	**Hor2017**	**3.5**	**S**		**0.2**	**0.015**
2011.8543	**333.1**	**0.46**	**1**	**Gur2018**	**2.1**	**S**		**0.9**	**0.011**
2012.0949	**332.6**	**0.4557**	**1**	**Hor2017**	**3.5**	**S**		**0.7**	**0.007**
2012.0949	**332.8**	**0.4565**	**1**	**Hor2017**	**3.5**	**S**		**0.9**	**0.008**
2016.1338	**327.3**	**0.4529**	**2**	**Tok2018c**	**4.1**	**St**		**0.3**	**0.026**

Table 7. Measurements of WDS 04102+1722

Date	ϑ (°)	ρ (")	N	Ref.	Ap	Tec	Cod	O-C ϑ (°)	O-C ρ (")
1914.51	166.0	0.56	2	A__1914c	0.9	Ma		0.0	-0.05
1921.89	167.8	0.58	2	A__1932a	0.9	Ma		0.0	0.00
1929.20	166.8	0.59	1	Fur1932	0.7	Ma		-3.0	0.04
1933.22	168.4	0.61	2	Fur1932	0.7	Ma		-2.7	0.08
1938.21	172.4	0.57	3	Baz1942b	0.3	Ma		-0.3	0.06
1942.88	171.2	0.58	3	Vou1955	0.4	Ma		-3.2	0.10
1961.15	184.5	0.51	3	Cou1962a	0.4	Ma		1.0	0.15
1961.85	179.4	0.42	2	Cou1962b	0.9	Mb		-4.6	0.07
1962.25	195.9	0.40	4	Hei1963b	0.3	Ma		11.6	0.05
1963.017	188.5	0.32	4	Wor1967b	0.7	Ma		3.6	-0.02
1963.10	184.9	0.31	4	B__1963b	0.9	Ma		-0.1	-0.03
1965.25	188.3	0.42	4	Hei1967b	0.3	Ma		1.6	0.10
1973.12	197.0	0.23	3	Hei1975a	0.6	Ma		1.5	-0.01
1978.12	213.6	0.15	3	Hei1980a	0.6	Ma		8.2	-0.03
1985.8408	262.6	0.058	1	McA1987b	4.0	Sc	P	-0.4	0.000
1987.03	100.0	0.74	1	Aru1992	1.0	C	T	(327.1)	(0.03)
1991.2500	128.0	0.132	1	HIP1997a	1.4	Hh		13.9	-0.010
2004.2034	134.1	0.341	2	Hrt2008	1.5	Su		-0.7	-0.002
2008.111	**135.9**	**0.396**	**1**	**Gii2012**	**0.7**	**S**		**-1.3**	**0.012**

Table 8. Measurements of WDS 06549+1158

Orbit Determination of Close Binary Systems

Date	ϑ (°)	ρ (")	N	Ref.	Ap	Tec	Cod	O−C ϑ (°)	O−C ρ (")
1829.29	255.4	1.01	3	StF1837	0.3	Ma		3.8	-0.10
1844.30	252.2	1.02	1	Mad1845	0.3	Ma	Q	-0.2	-0.06
1848.35	259.5	0.92	1	Mad1856	0.3	Ma	Q	6.9	-0.15
1856.28	255.2	0.90	1	Se_1860b	0.3	Ma	Q	2.1	-0.15
1866.30	252.2	0.86	3	D__1884	0.2	Ma		-1.5	-0.16
1892.81	254.8	0.85	4	Sp_1909	0.5	Ma		-0.7	-0.05
1896.50	252.0	0.94	4	A__1914d	0.3	Ma		-3.8	0.06
1898.32	260.2	0.99	2	Glp1899	0.2	Ma	Q	4.2	0.12
1899.28	251.5	0.69	1	Bry1899	0.7	Ma		-4.6	-0.18
1899.29	258.6	0.72	1	L__1899	0.7	Ma		2.5	-0.15
1900.33	259.9	0.86	2	Bow1900	0.7	Ma		3.7	0.00
1901.32	250.4	0.78	1	Bry1901	0.7	Ma		-5.9	-0.08
1901.38	251.9	0.96	1	L__1901	0.7	Ma		-4.4	0.10
1903.28	260.0	0.84	1	L__1903	0.7	Ma		3.6	0.00
1903.29	257.0	0.91	3	Bow1903a	0.7	Ma		0.6	0.07
1904.34	256.3	0.93	1	Bow1904a	0.7	Ma		-0.2	0.09
1906.28	253.6	1.01	1	Frm1907	0.2	Ma		-3.1	0.19
1908.32	257.7	0.87	3	Bow1908	0.7	Ma		0.8	0.06
1909.35	257.2	1.04	1	Bow1909	0.7	Ma	Q	0.2	0.24
1909.35	262.0	0.77	1	L__1909	0.7	Ma	Q	5.0	-0.03
1911.12	252.6	0.90	3	Doo1915b	0.5	Ma	Q	-4.6	0.11
1911.57	259.1	0.76	3	Wz_1923	0.5	Ma		1.9	-0.03
1912.25	262.4	0.68	3	Bow1921	0.7	Ma	Q	5.1	-0.10
1914.30	260.1	0.76	2	Rab1923	0.2	Ma		2.6	-0.01
1916.34	255.2	0.70	2	J__1918	0.7	Ma		-2.6	-0.05
1924.19	256.2	0.73	4	B__1925a	0.3	Ma		-2.5	0.05
1925.71	261.9	0.67	3	Fat1928	0.3	Ma		2.9	0.00
1934.37	256.9	0.57	4	Baz1936b	0.3	Ma		-3.5	0.00
1941.97	257.4	0.51	5	Rab1953	0.3	Ma		-4.8	0.04
1943.13	259.3	0.57	3	Vou1955	0.4	Ma		-3.2	0.11
1950.58	261.3	0.29	4	Baz1952b	0.4	Ma	XQ	-4.4	-0.04
1953.39	233.6	0.25	4	Baz1954a	0.4	Ma	Q	(267.8)	(0.26)
1954.24	273.6	0.20	2	Cou1955c	0.4	Ma	X	5.0	-0.04
1954.40	253.1	0.26	1	Mlr1955c	0.5	Mc	Q	-15.7	0.02
1955.83	253.1	0.22	2	Baz1957b	0.4	Ma		-17.6	0.02
1956.18	273.9	0.19	3	Mlr1956a	0.6	Mc		2.6	0.00
1956.27	278.8	0.20	1	Cou1958a	0.4	Ma		7.3	0.01
1957.31	278.0	0.20	1	Cou1958a	0.4	Ma		4.2	0.04
1958.05	277.2	0.13	2	VBs1960	2.1	Mb		1.1	0.00
1960.25	267.0	0.19	1	Cou1962a	0.4	Ma		(297.1)	(0.05)
1960.25			1	Cou1962a	0.4	Ma	S	(297.1)	(0.05)
1960.32		0.25	3	Hei1961	0.3	Ma	S	(298.9)	(0.05)
1961.27			1	Cou1962a	0.4	Ma	X	(0.5)	(0.02)
1962.23			1	B__1963b	0.9	Ma	F	(61.4)	(0.05)
1965.140	43.3	0.13	1	VBs1975	2.1	Mb	Q	(89.7)	(0.12)
1967.32	94.4	0.15	2	Cou1968b	0.5	Ma	Q	-4.1	0.02
1969.231	104.8	0.17	1	Wak1972	1.5	Mb	Q	-0.8	0.04
1971.24		0.16	1	Mlr1976	0.8	Mc	U	(113.0)	(0.13)

Table 9. Measurements of WDS 11361+1251 . Continues on the next page.

Orbit Determination of Close Binary Systems

Date	ϑ (°)	ρ (")	N	Ref.	Ap	Tec	Cod	O-C ϑ (°)	O-C ρ (")
1976.38		0.18	3	Mlr1978b	0.5	Ma	D	(133.2)	(0.13)
1981.65	158.2	0.14	3	Mrl1983	0.7	Ma		3.6	0.01
1982.30	177.0	0.10	2	Hei1983a	0.6	Ma	U	19.8	-0.03
1984.24	152.8	0.14	3	Cou1985a	0.7	Ma		-11.6	0.01
1986.24	144.6	0.13	1	Cou1987b	0.7	Ma		(171.3)	(0.14)
1988.32	163.9	0.15	1	LBu1989	0.5	Ma		-13.8	0.00
1989.36	196.8	0.15	5	LBu1990	0.5	Ma		16.1	0.00
1990.320	191.9	0.15	1	LBu1991	0.5	Ma		8.7	-0.01
1991.2500	187.0	0.163	1	HIP1997a	1.4	Ma		1.4	0.001
1993.21	195.8	0.15	1	LBu1994	0.5	Ma		5.7	-0.02
1994.40	194.8	0.15	1	LBu1996	0.5	Ma		2.2	-0.03
2004.2068	202.8	0.228	1	Hrt2008	1.5	S		-4.7	-0.010
2008.251	**204.9**	**0.269**	**1**	**Gii2012**	**0.7**	**S**		**-6.9**	**0.007**
2008.281	**204.8**	**0.237**	**1**	**Gii2012**	**0.7**	**S**		**-7.0**	**0.026**
2010.3525	**208.7**	**0.26**	**1**	**Orl2015**	**2.1**	**S**		**-4.9**	**-0.016**

Table 9 (conclusion). Measurements of WDS 11361+1251

Date	ϑ (°)	ρ (")	N	Ref.	Ap	Tec	Cod	O-C ϑ (°)	O-C ρ (")
1878.30	97.9	1.38	2	Bu_1879	0.5	Ma		-0.8	-0.02
1882.41	134.5	0.40	2	Sp_1888	0.2	Ma	U	(98.3)	(1.36)
1890.70	97.8	1.20	4	Sp_1909	0.5	Ma		-0.1	-0.10
1891.26	99.1	1.25	3	Bu_1894	0.9	Ma		1.3	-0.04
1898.917	96.8	1.40	3	Doo1901	0.5	Ma		-0.4	0.18
1899.431	101.0	1.19	1	Brs1900b	0.7	Ma		3.8	-0.02
1899.431	100.9	1.45	1	See1900e	0.7	Ma		3.7	0.24
1899.432	101.0	1.32	1	Brs1911	0.7	Ma		3.8	0.11
1900.324	92.0	0.88	2	See1911	0.7	Ma		-5.1	-0.33
1902.423	94.9	1.34	3	Doo1905	0.5	Ma		-2.0	0.16
1909.32	95.2	1.10	1	Ol_1909	0.7	Ma		-1.1	-0.01
1915.648	97.7	1.16	5	Fox1925	0.5	Ma		2.0	0.12
1917.20	96.2	1.10	3	Ol_1920c	0.7	Ma		0.7	0.08
1921.82	103.6	1.16	2	Gcb1934	0.4	Ma		8.7	0.20
1938.10	95.4	0.80	3	Fin1951a	0.7	Ma		3.1	0.06
1949.45	85.6	0.49	4	B__1950c	0.7	Ma		-3.5	-0.08
1952.83	83.5	0.42	4	B__1953a	0.7	Ma		-4.2	-0.10
1955.50			5	Hei1956a	0.2	Ma		(86.4)	(0.47)
1959.17	78.2	0.29	2	B__1959d	0.7	Ma		-6.0	-0.12
1962.30	78.3	0.33	4	B__1962d	0.9	Ma		-3.4	-0.03
1989.39	325.0	0.10	2	Hei1990b	1.0	Mb	Q	8.3	-0.08
1991.25	326.0	0.199	1	HIP1997a	1.4	Ht		15.1	-0.011
2006.1997	292.1	0.456	2	Msn2009	4.0	S		0.0	0.007
2014.244	**289.3**	**0.54**	**1**	**Ant2015**	**0.5**	**Cl**		**0.9**	**-0.033**
2016.3699	**289.3**	**0.646**	**5**	**Hsw2017d**	**0.3**	**Cv**		**1.6**	**0.042**

Table 10. Measurements of WDS 06549+1158

Date	ϑ (°)	ρ (")	N	Ref.	Ap	Tec	Cod	O-C ϑ (°)	O-C ρ (")
1910.60	300.0	0.65	2	I__9999	9	A		-24.7	-0.05
1913.53	319.8	0.78	2	I__1914	9	A		-0.9	0.06
1928.52	301.9	0.74	2	B__1928d	26	A		-1.2	-0.05
1928.95	301.7	0.77	3	Rst1955	27	A		-0.9	-0.02
1930.33	301.9	0.80	4	Vou1932	24	A		0.8	0.01
1934.55	298.1	0.75	4	B__1937b	26	A		1.6	-0.04
1956.41	270.4	0.71	3	B__1957b	26	A		1.2	0.05
1960.50	260.2	0.60	3	B__1961a	26	A		-2.0	-0.01
1985.36	42.5	0.23	2	Hei1987a	36	B	Q	-1.7	-0.02
1991.18	4.6	0.37	2	Hei1992a	40	B	Q	-0.8	-0.04
1991.25	5.0	0.404	1	HIP1997a	54	T		-0.1	-0.003
1996.1815	349.6	0.512	1	Msn1998b	158	S	Q	0.4	0.001
2009.2602	324.7	0.692	1	Tok2009	160	S	Q	-0.1	0.001
2013.1276	**319.6**	**0.7284**	**2**	**Tok2014a**	**4.1**	**St**		**-0.1**	**0.004**

Table 11. Measurements of WDS 14531-4638

The Number of Binaries in the Sky Compared to a Random Distribution of Similar Stars

T. V. Bryant III

Little Tycho Observatory
703 McNeill Road, Silver Spring, Md 20910
NGC7492@gmail.com

Abstract: The likelihood of a pair of stars orbiting one another is investigated using statistics generated from the Gaia DR2 data[1]. Stars brighter than 11, 15, and 18 G band magnitude (Gmag) were searched for pairs with separations less than 60”. The Gaia DR2 stars’ positions were then randomized and again searched. The differences between pairs found in the real sky vs the randomized sky indicate that the likelihood that a pair is physical is inversely proportional to the pairs’ separation.

When two stars are close together in the sky, they are often listed as double stars. Whether a particular pair actually orbit one another or is simply in the same line of sight as seen from the earth has been debated for at least a century. Below is an excerpt from R. Aitken's 1918 book The Binary Stars[2].

> *The data consist of all visual double stars as bright as 0.9 B. D. magnitude which fall within the distance limits set by the following 'working' definition of a double star proposed by me in 1911:*
>
> *(1) Two stars shall be considered to constitute a double star when the apparent distance between them falls within the following limits:*
>
> *1" if the combined magnitude of the components is fainter than 11 .0*
>
> *3" if the combined magnitude of the components is fainter than 9.0 B. D.*
>
> *5" if the combined magnitude of the components lies between 6.0 and 9.0 B. D.*
>
> *10" if the combined magnitude of the components lies between 4.0 and 6.0 B. D.*
>
> *20" if the combined magnitude of the components lies between 2.0 and 4.0 B. D.*
>
> *40" if the combined magnitude of the components is brighter than 2.0 B. D.*
>
> *(2) Pairs which exceed these limits shall be entitled to the name double star only when it has been shown*
>
> *(a) that orbital motion exists;*
>
> *(b) that the two components have a well defined common proper motion, or proper motions of the 61 Cygni type;*
>
> *(c) that the parallax is decidedly greater than the average for stars of corresponding magnitude.*

Our knowledge of this has greatly improved since Aitken's time as the numbers and accuracies of proper motion, parallax, and radial velocity studies have increased significantly. There are, however, other ways to try to analyze this question.

In this paper, a statistical treatment of all of the Gaia DR2 stars brighter than 11.0 Gmag (1,240,319 stars), 15.0 Gmag (35,399,780 stars), and 18.0 Gmag (299,758,720 stars) was done using the programs that can be obtained from the SourceForge site(4). Each of these stars was searched in this way:

The area within a radius of 60” of the given star was searched for the star that was closest to that star and would be selected as the other member of the pair.

The pair found was tested for its commonality of distance, spatial velocity, and orbital velocity. If the parameters were within certain limits (see below), the pair was counted as a binary.

Once a star had been identified as a member of a pair, it was flagged as such and removed from the database of stars being searched.

These searches were then repeated using the same stars, with their positions randomized. Randomization of a star’s position consisted of moving the star an arc minute from its J2000 position in a random direction. The results of the 6 runs that searched for the closest star are shown here, with the number of pairs or binaries found on the vertical axis, and their separation in arcseconds on the horizontal axis. Note that the magenta line represents pairs and binaries found in the real

(Text continues on page 44)

The Number of Binaries in the Sky Compared to a Random Distribution of Similar Stars

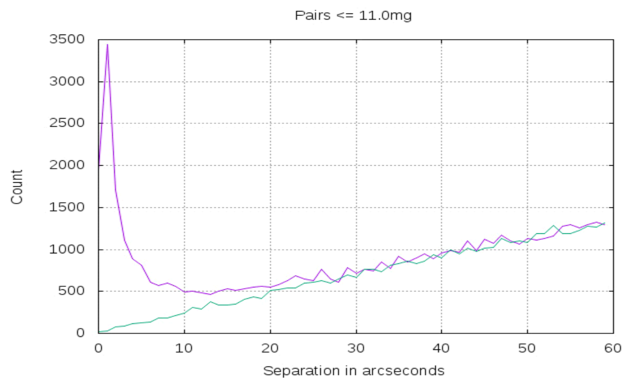

Figure 1

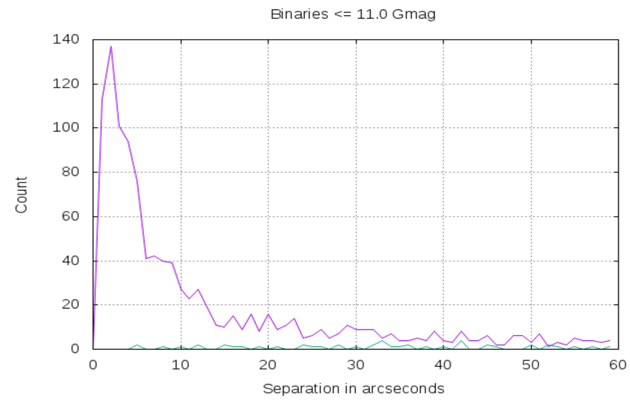

Figure 2

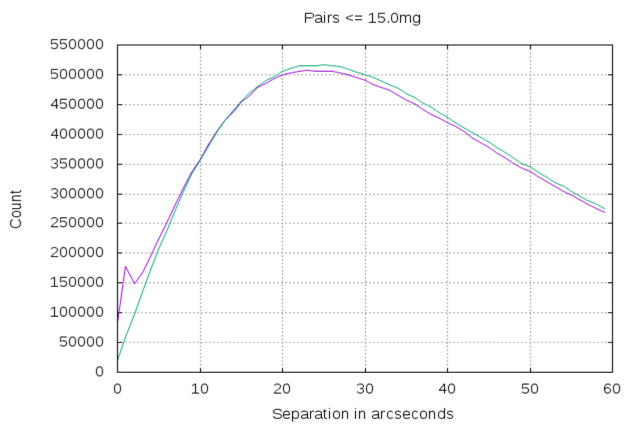

Figure 3

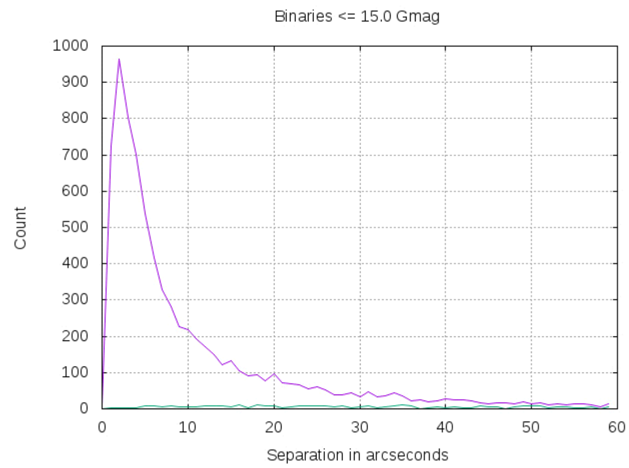

Figure 4

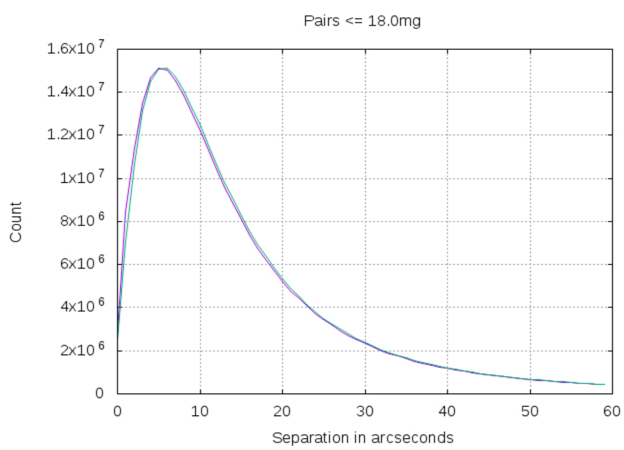

Figure 5

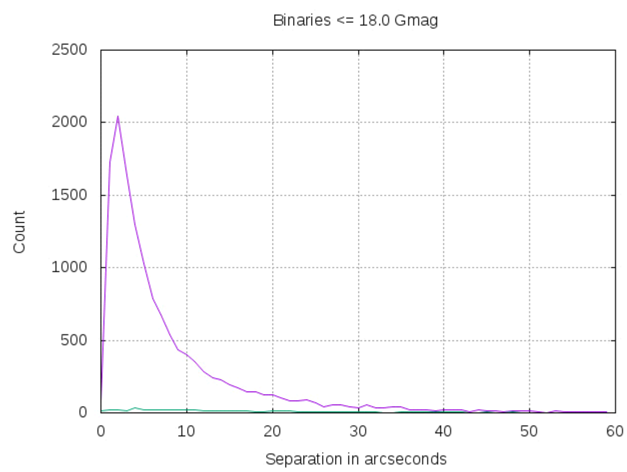

Figure 6

The Number of Binaries in the Sky Compared to a Random Distribution of Similar Stars

(Continued from page 42)

sky, and the green line represents pairs and binaries found in the randomized sky. Comparing the real sky with the randomized sky gives an idea as to the number of actual binaries vs the number of optical pairs in the sky.

Pairs within 2.0 Gmag of One Another.

A majority of the pairs in the WDS were discovered visually. Pairs with a large brightness difference were either ignored or not seen, as the difficulty of resolving a close pair is a function of the difference in brightness of that pair. The Figures 1 - 6 do not consider this fact. Would the results be different if the stars were required to be close in brightness as well as the other criteria? The programs were revised so as to exclude pairs that were more than 2.0 Gmag different in brightness. Figures 7 - 12 are the results for the 11.0 Gmag, 15.0 Gmag, and 18.0 Gmag runs with pairs required to be within 2.0 Gmag of one another. These six plots show the results for the closest pairs found within an arcminute of a given star.

The number of pairs and binaries is much reduced by limiting the brightness differential to 2 Gmag, but the overall shape of the curves is unchanged.

Average Distances of Binaries with Respect to Their Separation.

When the program found that a pair was a possible binary, the distance to the pair, that is the average distance (in light years) of both members from the sun, was computed and saved in its arc second separation bin. When the run ended, the average distance of all binaries found in that separation bin was computed. Please note that Figures 13 - 18 do not show the number of binaries found in each separation bin. Refer to Figures 7 - 12 for that data, although in most cases, the spikes on Figures 13 - 18 only represent one or two stars, so making any statistical trends based on this data inaccurate, with the possible exception of the 18 Gmag data (Figures 17 and 18).

Discussion

The number of pairs less than 1 to 2 arc seconds apart is under counted as it is close to the resolution on the Gaia telescope, especially in a crowded star field.

In order for a pair to be considered for binary membership, both stars needed to have a Gaia DR2 parallax recorded for them. Over 98% of all stars brighter than 18.0 Gmag did.

The chance of a pair of stars being close to one another in the sky is a function of the number of stars in the sky. Note that there are about 30 times more stars brighter than 15 Gmag than 11 Gmag, and about 240 times as many 18 Gmag stars than 11 Gmag. This is reflected in the above plots, which show the ratio of the number of pairs and binaries found in the actual sky compared to those found in the randomized sky decreases as the number of stars searched increases. Note that there are so many pairs found in the 18 Gmag data that most stars are found to be part of a pair, and only when they are checked for binary membership do we see a difference between the real and randomized sky.

The criteria for determining if a pair was mutually orbiting one another were as follows. The ratio of the star's spatial velocities over their estimated orbital velocities needed to be within a factor of 10 of each other and their parallaxes needed to indicate that the stars' distances were within a light year of one another. This distance was chosen as the average distance of stars in the Milky Way is about 5 light years [3]. Two solar mass stars in a circular orbit at this distance take about 6 million years, and after a few orbits, there is a significant chance that the pair will encounter other stars that will disrupt their orbit, so a light year was thought to be a good limit on a stable binaries' orbital diameter.

The stars' orbital velocities were calculated as described by Rica[4]:

$$M = L^{(1/3.5)}$$

$$m = l^{(1/3.5)}$$

$$V = \sqrt{\frac{1.9891 \times 10^{30}\, G\left(M + m\right)}{dr}}$$

Where:

- dr is the average distance to the stars multiplied by their apparent separation in radians.
- L is the first star's luminosity, in solar units.
- l is the second star's luminosity, in solar units.
- M is the mass of the first star.
- m is the mass of the second star.
- V is the orbital velocity, in m/s.
- G is the gravitational constant, 6.67408×10^{-11}.
- The mass of the sun is 1.989×10^{30} kg.

The stars are assumed to be main sequence stars, making the relationship approximately valid.

Note that this simple calculation makes the unlikely assumptions that the orbits are circular, perpendicular to the plane of the sky, with their velocity vectors pointing at the sun. The generous limits of a light year's separation and an order of magnitude between this orbital velocity and the observed spatial velocity are used to

(Text continues on page 47)

The Number of Binaries in the Sky Compared to a Random Distribution of Similar Stars

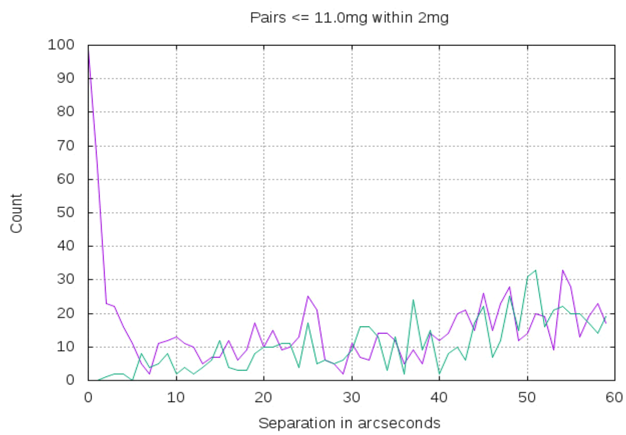

Figure 7.

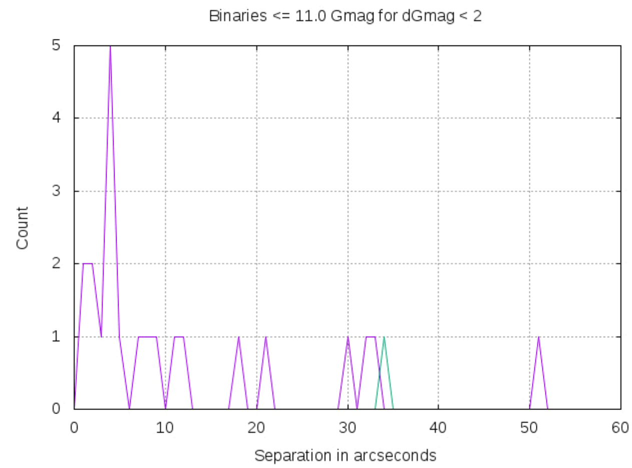

Figure 8.

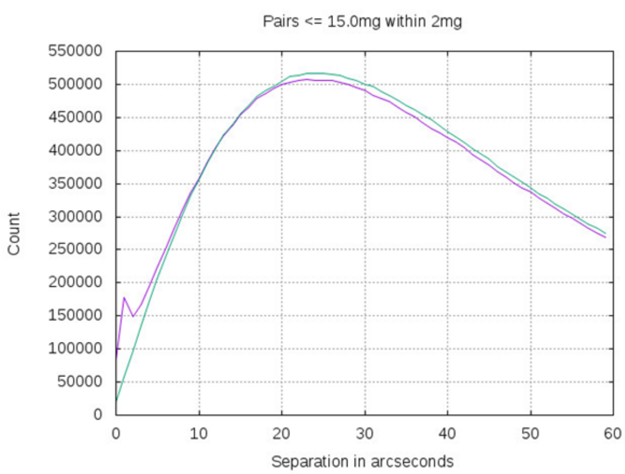

Figure 9.

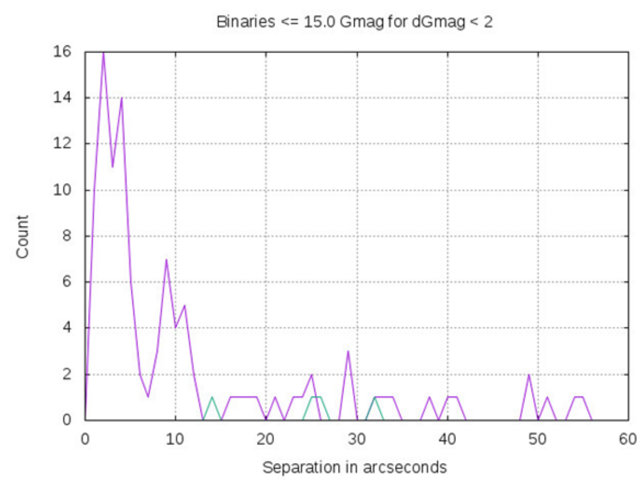

Figure 10.

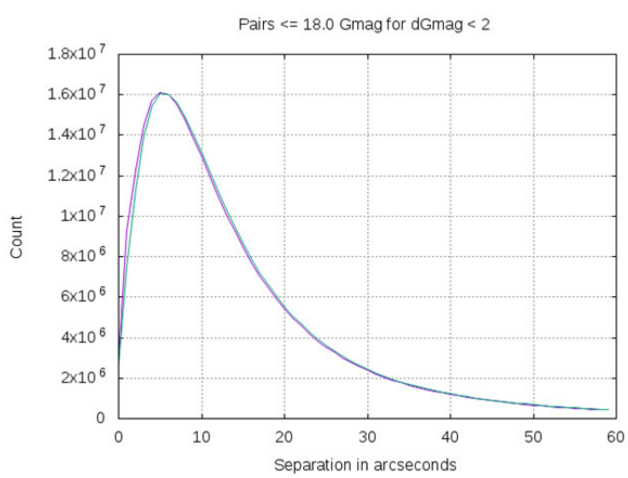

Figure 11.

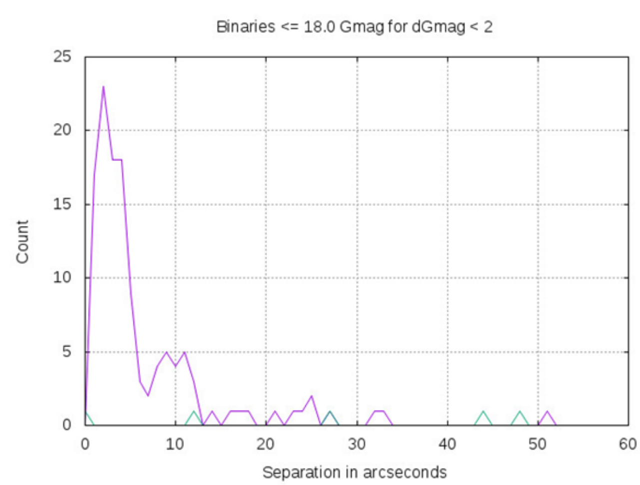

Figure 12.

The Number of Binaries in the Sky Compared to a Random Distribution of Similar Stars

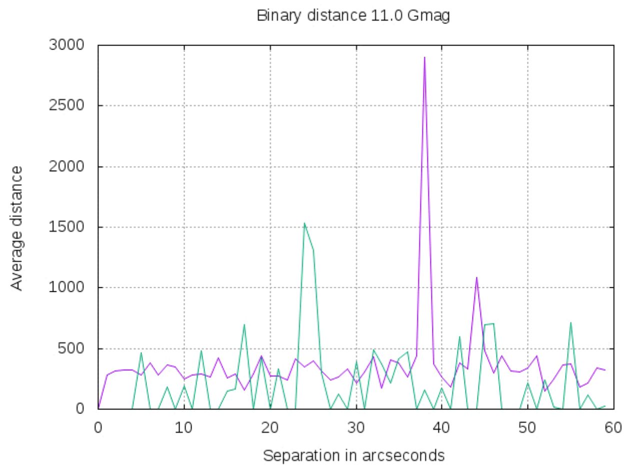

Figure 13.

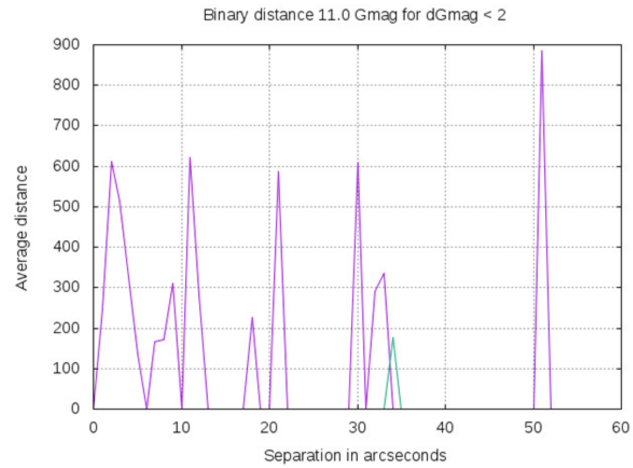

Figure 14.

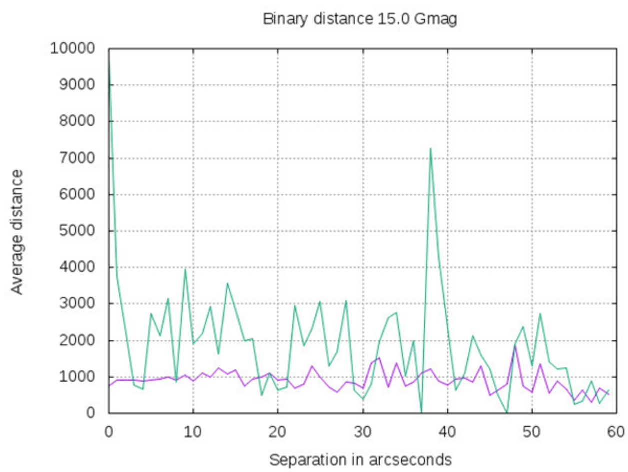

Figure 15.

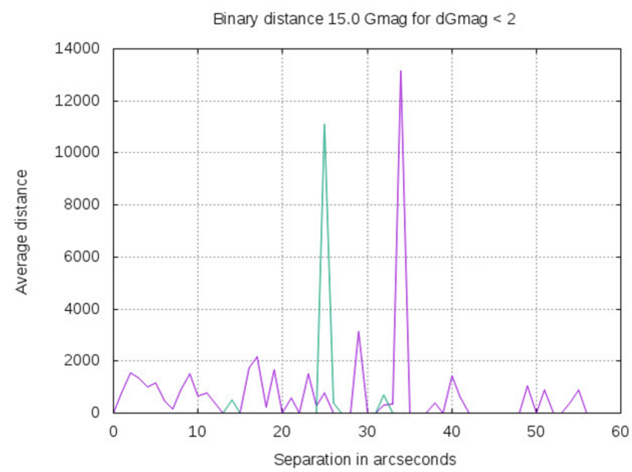

Figure 16.

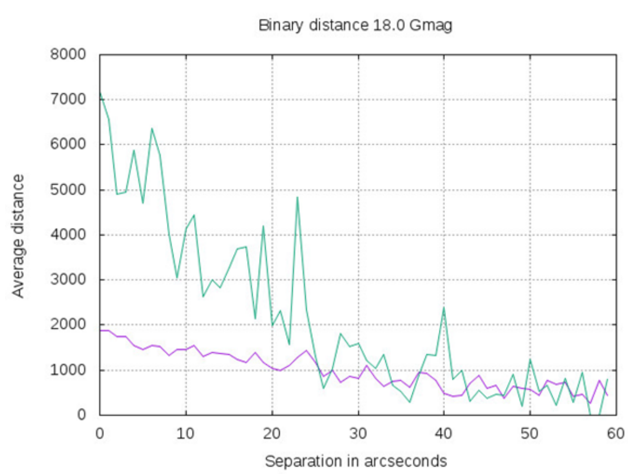

Figure 17.

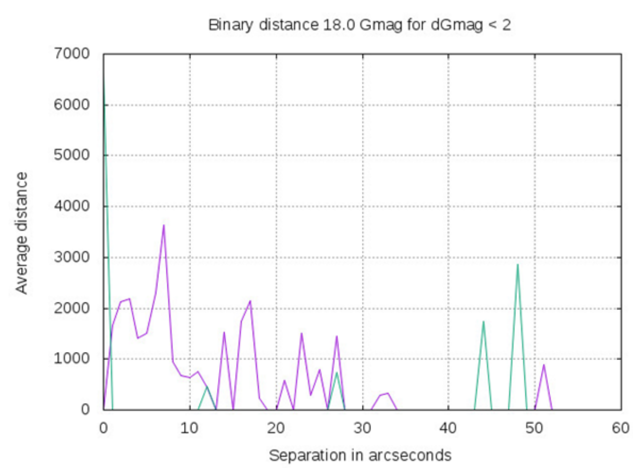

Figure 18.

The Number of Binaries in the Sky Compared to a Random Distribution of Similar Stars

(Continued from page 44)

offset the assumptions made about the orbits. Even with these wide margins, the number of binaries found drops markedly when compared to the number of pairs found.

Initially, it was thought that if the parallax uncertainty limits of the two stars in a pair overlapped, then the pair would be considered to be at approximately the same distance from the sun. This method was abandoned when it was found that over 99% of pairs met this criterion. It was replaced by the requirement that the parallaxes of the two stars needed to indicate that they were within a light year of one another.

The results for the 18.0 Gmag runs simply indicate that virtually all stars have another star 18 Gmag or brighter within an arc minute of them. This was somewhat true of the 15.0 Gmag runs as well. These often optical pairs were minimized in the 11.0 Gmag run. In all runs, however, the above results indicate that the number of binaries found favors the nearer pairs.

Conclusion

Aitken's 1911 guesses were perhaps a bit too conservative, but the basic idea, the closer a given pair, the more likely it is to be a binary, is sound.

While careful measurements over time of the position angle, separation, radial velocities, and parallaxes of a pair are required to determine if the pair is indeed a binary, an initial guess can be made simply from the pair's separation. While using these graphs to determine if a pair is a binary is only a rough estimate of a given pair's binary nature, they might well be useful in selecting which pairs should be chosen for further study, much like Aitken's 1918 criteria were.

Acknowledgements

The grammar and clarity of this paper were greatly enhanced by Tom Corbin's and Kathie Bryant's edits.

This work has made use of data from the European Space Agency (ESA) mission Gaia (https://www.cosmos.esa.int/gaia), processed by the Gaia Data Processing and Analysis Consortium (DPAC, https://www.cosmos.esa.int/web/gaia/dpac/consortium). Funding for the DPAC has been provided by national institutions, in particular the institutions participating in the Gaia Multilateral Agreement.

References

[1]The Gaia DR2 data can be downloaded here: http://cdn.gea.esac.esa.int/Gaia/gdr2/gaia_source/csv/

[2] R. G. Aitken, The Binary Stars, 1918, The University of California.

[3] http://boojum.as.arizona.edu/~jill/EPO/Stars/galaxy.html

[3] F. M. Rica, "Determining the Nature of a Double Star: The Law of Conservation of Energy and the Orbital Velocity", *Journal of Double Star Observations*, **7** (4), 254, 2011.

[4] The C programs used to create, search and randomize the Gaia RD2 data can be downloaded here: http://sourceforge.net/p/realvsrandomdoublestarcount. The plots were created using gnuplot: http://www.gnuplot.info/

Counter-Check of Reported Common Origin Pairs

Wilfried R.A. Knapp

Vienna, Austria
wilfried.knapp@gmail.com

Abstract: All stars are born in molecular clouds most likely together with other stars nearby in the same cloud but most such systems are separated over time by the tidal forces of the galaxy. Kamdar et al. 2019 report the detection of 111 pairs of co-moving stars with similar metallicity assumed to be born together but separated later on.

This report counter-checks this proposition by cross-matching the listed objects with the GAIA DR2 catalog and using the found data to calculate the spatial distance between the components as well as spatial velocity speed and direction. The results confirm with some caveats the data given in the Kamdar et al. 2019 paper but do not necessarily confirm the conclusion that all reported pairs have to be indeed of common origin.

Finally all WDS pairs listed as common proper motion pairs (note code "V") but with spatial separation likely too large for gravitational relationship are checked for common origin.

1. Introduction

Kamdar et al. 2019 report 111 co-moving pairs in the solar neighborhood (which means up to 1kpc distance from the Sun) with distances between the components too large to allow for gravitational relationship but assumed to be of common origin. This report counter-checks this proposition using astrometric data from GAIA DR2 and metallicity data from the GAIA DR2 StarHorse catalog.

2. Cross-Match of WDS FAR Objects with Gaia DR2

The number of KMD objects (for objects reported in Kamdar et al. 2019) is small enough to access the GAIA DR2 data for the counter-check manually by entering the positions of the components directly into Aladin and load the GAIA DR2 data over the default DSS images. The GAIA DR2 data is then copied into a spreadsheet checking for common proper motion and potential gravitational relationship based on Monte Carlo simulation for the distance between the components with a sample size of 120,000 which means a margin of error of 0.37% at 99% confidence. The resulting data is then copied again in another spreadsheet created specifically for this purpose calculating spatial velocity speed and direction. The results are given in table 1 below and confirm the values given in the Kamdar et al. 2019 paper for all objects with a few minor exceptions. The additional information from the LAMOST DR4 catalog suggesting similar metallicities giving additional support for the proposition that these pairs are indeed most likely of common origin are counter-checked by comparison with GAIA DR2 StarHorse metallicity data (Anders et al. 2019).

Table 1 lists the cross-matching results with the following structure:

- Obj = Running object number
- Disc = WDS discoverer code in case of components (mostly A) overlapping with existing WDS objects
- No = Number of additional GAIA DR2 objects with similar values for proper motion, parallax and radial velocity but mostly with spatial velocity not similar enough to be considered also co-moving
- CPMS = Common proper motion score (see Appendix)
- Plx1 = Parallax 1 in mas
- e_Plx1 = Error parallax 1
- Plx2 = Parallax 2 in mas
- e_Plx2 = Error parallax 2
- Min_D_AU = Minimum spatial distance in AU

between components (see Appendix)

- Med_D_AU = Median spatial distance in AU between components (see Appendix)
- Max_D_AU = Maximum spatial distance in AU between components (see Appendix)
- LPGR = Likelihood of potential gravitational relationship (see Appendix)
- V1 = Spatial velocity 1 in km/s
- V2 = Spatial velocity 2 in km/s
- DV1 = Direction of spatial velocity 1 in degrees
- DV2 = Direction of spatial velocity 2 in degrees
- AV1 = Angle between spatial and radial velocity 1 in degrees (<0-45° more radial, >45-90° more tangential)
- AV2 = Angle between spatial and radial velocity 2 in degrees (<0-45° more radial, >45-90° more tangential)

The proper motion vector direction and length for 31 of the listed objects is similar enough to consider these objects as common proper motion pairs.

15 objects have parallax values similar enough to give a likelihood larger than 5% for a spatial distance between the components smaller than 200,000 AU suggesting potential gravitational relationship. The postulated non-existence of a gravitational relationship is therefore not completely ensured for all listed objects.

Four objects have a difference in spatial velocity larger than 10% of the average speed of the components (values given in red type), speaking against common movement. Six objects have differences in the direction of the spatial velocity larger than 10° (values given in red type), also speaking against common movement. Seven objects have a difference in the angle between radial and spatial velocity larger than 5° (values given in red type), also speaking against common movement.

Combining these factors (with the exception of common proper motion) results in 28 objects showing rather not common movement or with a small likelihood potential gravitational relationship.

3. Comparison of LAMOST Effective Temperature and Metallicity Values with data from the Gaia DR2 StarHorse Catalog

As additional information for the listed objects, I selected the median mass values from the Gaia DR2 StarHorse catalog (Anders et al. 2019) as well as the median effective temperature data given there listed in Table 2 below.

- Obj = Running KMD object number
- Source_ID1 = GAIA DR2 source ID
- mass50_1 = Median GAIA DR2 StarHorse Sun mass for the primary
- teff50_1 = Median GAIA DR2 StarHorse effective temperature for the primary
- dTeff_1 = Difference effective temperature between LAMOST and GAIA DR2 StarHorse catalog for the primary
- X-out_1 = LAMOST effective temperature outside percentile 16 to 84 GAIA DR2 StarHorse values for the primary
- Source_ID2 = GAIA DR2 source ID
- mass50_2 = Median GAIA DR2 StarHorse Sun mass for the secondary
- teff50_2 = Median GAIA DR2 StarHorse effective temperature for the secondary
- dTeff_2 = Difference effective temperature between LAMOST and GAIA DR2 StarHorse catalog for the secondary
- X-out_2 = LAMOST effective temperature outside percentile 16 to 84 GAIA DR2 StarHorse values for the secondary
- dmass = Difference in GAIA DR2 StarHorse mass between primary and secondary

Most interesting are the differences between the LAMOST effective temperature values (as given in the Kamdar et al. 2019 report) and the corresponding values in the Gaia DR2 StarHorse catalog with a mean value of 183.512 (which means that the Gaia DR2 StarHorse values are generally somewhat higher) and a standard deviation of 328.036 with a few outliers as for example object 20 and 58. The error range of the given LAMOST values is below 40 while the spread between the 16 and the 84 percentile values is close to 700. Yet about 30% of the LAMOST values are outside of the corresponding 16 and 84 percentile values, but this does not allow for any conclusions as such a percentage is by definition to expect from such percentile values.

On average the median Gaia DR2 StarHorse masses for the 111 pairs are quite similar with an average difference of 0.094 with a standard deviation of 0.117 with a few outliers, especially objects 20, 70 and 85. Same origin should mean same age and same composition, so different mass should account for different effective temperature – this conclusion is not fully confirmed by the listed data as two of the pairs with the largest differences in mass are listed with rather similar effective temperatures.

The comparison of differences in mass with differences in Teff shows. with the exception of a few outliers, a good relationship between the values of the Gaia DR2 StarHorse catalog (see Figure 1).

Completely different impression when compar-

(Text continues on page 56)

Counter-Check of Reported Common Origin Pairs

Obj	Disc	No	CPMS	Plx1	e_Plx1	Plx2	e_Plx2	Min_D_AU	Med_D_AU	Max_D_AU	LPGR	V1	V2	DV1	DV2	AV1	AV2
1		2	4	6.1510	0.0420	6.2039	0.0423	2490518	2562572	3084989	0.00	26.72617	25.95566	119.28	117.61	64.64	63.52
2		2	0	5.9359	0.0418	5.6563	0.0351	1340812	2168992	3584779	0.00	6.41619	7.57869	327.67	301.54	14.17	15.31
3		2	59	6.5862	0.0586	6.6346	0.0483	2255418	2327511	2898098	0.00	34.62374	34.44556	132.68	134.04	69.89	67.52
4		3	5	2.9011	0.0248	2.8558	0.1259	1819541	2950889	18609962	0.00	27.10355	26.32522	170.73	170.68	46.27	43.75
5		5	5	8.7257	0.0486	10.0437	0.0617	3344882	3994724	4599410	0.00	52.92963	52.32685	140.99	140.55	30.02	36.21
6		2	15	7.9693	0.0409	8.0168	0.0565	3174971	3239318	3423317	0.00	21.55138	21.05706	-227.22	-229.32	89.37	87.08
7		2	0	4.7087	0.0529	4.5288	0.0494	2588252	3170787	5566692	0.00	20.12437	19.62902	143.27	149.69	60.49	60.98
8		2	95	2.5524	0.0369	2.5066	0.0351	25185	1601611	8772892	6.40	38.75502	39.67870	101.69	101.41	89.03	87.86
9		2	0	8.0198	0.0834	8.3657	0.0426	3364319	3603404	4173810	0.00	12.45912	12.26464	-248.76	-244.17	40.13	52.69
10	SMA 39	2	62	2.4601	0.0428	2.4956	0.0371	4441	1552725	9550162	6.87	44.63466	45.33590	153.93	154.95	56.28	55.42
11		2	1	2.6953	0.0408	2.6380	0.0395	794142	1932572	8960889	0.00	29.54426	27.46444	141.54	144.34	22.62	23.53
12		2	18	2.5369	0.0431	2.5306	0.0361	2297731	2696252	8745762	0.00	19.56407	20.59840	143.63	140.70	33.78	31.90
13		2	95	2.7248	0.0393	2.7821	0.0411	12630	1637446	8280270	6.12	37.57576	36.72981	-255.92	-255.52	41.68	41.87
14		3	0	1.5758	0.0412	1.5849	0.0435	3242973	4819195	23286169	0.00	21.00581	21.58346	183.80	188.76	55.20	54.38
15		2	0	4.3440	0.0453	4.5413	0.0479	2504468	3286001	5916375	0.00	23.62195	23.87626	236.29	232.53	59.37	56.27
16	BVD 36	2	78	5.9611	0.0352	6.0729	0.0365	6448	635697	1973643	6.46	35.66566	35.09343	175.97	177.70	61.63	61.84
17		3	0	2.5724	0.0429	2.6205	0.0334	3255361	3738475	10439137	0.00	30.23736	30.38125	114.67	123.03	4.55	2.86
18		2	7	5.6230	0.0319	5.7776	0.0389	1216456	1569028	2653799	0.00	39.06484	38.14419	137.89	139.98	47.38	49.07
19		6	1	2.8574	0.0566	2.7725	0.0382	2902826	3749319	9867425	0.00	40.64690	41.62320	136.10	131.98	73.31	75.83
20		2	0	1.1505	0.1346	1.1415	0.0349	3582010	15419254	197262875	0.00	29.79526	30.02603	-328.22	-323.20	15.32	16.44
21	DAM1028	20	78	3.1956	0.0528	3.1507	0.0440	3974	1161257	6686862	9.03	42.50810	42.12051	174.20	174.72	56.49	57.66
22		2	74	1.5443	0.0391	1.5444	0.0438	2773325	4510029	23695340	0.00	76.70089	77.43085	-186.76	-185.11	30.32	30.27
23		47	92	2.1530	0.0408	2.0931	0.0421	2595031	3968481	14661876	0.00	17.42199	16.29870	-173.16	-172.21	39.08	43.95
24		16	4	1.9251	0.0360	1.8903	0.0645	2872334	4389400	23917932	0.00	23.26423	24.04781	-280.27	-281.29	46.48	50.14
25		7	4	4.7728	0.0444	5.0092	0.0419	425854	2081281	4429465	0.00	35.88259	36.73337	101.41	100.24	78.36	77.79
26		8	0	3.9337	0.0366	3.8958	0.0434	2917160	3067307	4700177	0.00	14.59396	15.31586	282.87	286.58	82.61	84.24
27		6	92	1.6805	0.0407	1.6772	0.0516	763969	3359673	22136607	0.00	24.44049	23.99614	-232.58	-231.97	69.52	72.19
28		2	5	1.8477	0.0363	1.8721	0.0356	2512153	3504031	14852686	0.00	16.18745	16.92244	-110.79	-109.88	54.06	56.86
29		5	0	1.4043	0.0401	1.3897	0.0460	3233182	5676292	33276142	0.00	14.87956	14.03716	-250.25	-254.90	60.84	60.52
30		2	74	3.7426	0.0423	3.8179	0.0347	3577907	3843701	5766522	0.00	29.32221	29.10828	131.96	132.51	81.29	81.25
31		3	1	3.0996	0.2180	3.1114	0.0203	2800834	4263671	30062404	0.00	36.81569	37.07512	-153.39	-149.85	29.95	28.99
32		2	1	1.9149	0.0276	1.9350	0.0169	609605	1590269	10711428	0.00	32.97147	33.13897	-175.47	-177.58	37.84	39.34
33		2	56	2.6906	0.0313	2.5880	0.1371	2148113	4220370	26774866	0.00	17.98388	18.26202	-267.91	-266.38	32.48	33.77
34		2	37	3.0828	0.0377	3.2584	0.0371	511230	3635068	8412399	0.00	51.92573	50.85835	271.59	270.87	60.32	59.44
35	A 2135	2	0	3.3147	0.0649	3.4052	0.0498	26470	1698536	8182503	5.73	21.61542	20.54833	202.09	196.13	28.16	28.20
36		2	95	4.4173	0.0470	4.3372	0.0447	18051	877172	3988092	10.65	59.31021	59.97372	-191.38	-191.44	46.55	47.32
37	HJ 91	2	95	1.7665	0.0758	1.7476	0.0529	11063	4263607	31987814	2.49	17.62868	17.59778	223.21	223.01	79.67	82.52
38		2	74	2.6756	0.0425	2.7783	0.0675	1385082	3223549	12327833	0.00	36.31997	35.53158	205.63	205.63	41.36	41.36
39		2	37	3.8017	0.0408	3.6788	0.0509	282998	1842958	6083579	0.00	36.79865	36.55879	209.33	208.92	41.27	42.19
40		2	5	5.4762	0.1673	5.2636	0.0748	1255648	2027303	6789692	0.00	47.99150	47.43376	245.19	244.57	42.07	41.42
41		2	0	8.6380	0.0704	7.6073	0.0402	2624528	3588373	4504860	0.00	65.33412	64.62761	216.99	212.96	52.83	52.28

Table 1: List of Kamdar et al. 2019 objects with spatial movement values derived from GAIA DR2 data

Table continues on the next page.

Counter-Check of Reported Common Origin Pairs

Obj	Disc	No	CPMS	Plx1	e_Plx1	Plx2	e_Plx2	Min_D_AU	Med_D_AU	Max_D_AU	LPGR	V1	V2	DV1	DV2	AV1	AV2
42	GRV 805	2	76	3.0532	0.0484	2.9928	0.0509	11974	1498745	7820905	6.95	34.49595	35.09479	-143.82	-142.72	61.45	61.00
43		2	5	3.1851	0.0616	3.3693	0.0514	1518923	3880802	10761995	0.00	34.53613	35.11742	247.81	248.33	75.29	72.82
44		3	4	3.8092	0.0552	3.9904	0.0487	2895833	3883863	7367667	0.00	37.80677	37.62482	251.15	249.57	88.44	84.68
45		2	0	3.4292	0.0547	3.5960	0.0387	271357	2801455	8364659	0.00	18.94977	17.73630	-293.96	-298.45	3.21	3.12
46		3	1	6.5159	0.0476	6.8929	0.0385	3354390	3784177	4575766	0.00	11.79206	11.51175	-223.40	-229.30	78.87	74.10
47		2	0	9.2591	0.0402	9.3571	0.0501	1497854	1534555	1747949	0.00	33.43232	33.09230	219.67	228.38	37.82	40.18
48		3	1	2.1520	0.0513	2.1954	0.0456	1836787	3122694	16885450	0.00	42.30440	42.43229	197.44	199.52	33.36	35.53
49		2	1	4.9194	0.0448	4.6273	0.0445	2933304	3957858	6049743	0.00	41.58095	42.57121	208.50	211.16	29.29	26.39
50		2	92	3.0131	0.0343	3.0486	0.0372	2673196	2921597	6322768	0.00	28.71449	28.43545	131.91	131.14	77.03	75.26
51	KPP2169	2	1	6.2609	0.0383	5.9648	0.0369	3151730	3543851	4392069	0.00	56.74280	56.35038	-158.12	-154.71	39.31	41.46
52		2	1	6.2478	0.0457	6.5193	0.0388	369384	1419190	2757076	0.00	20.92264	21.85981	-253.24	-255.50	28.62	28.42
53		2	1	3.0357	0.0499	2.9417	0.0486	2062801	3062672	9082849	0.00	26.00852	25.86391	-211.88	-208.90	43.82	43.48
54		2	0	2.8376	0.0363	2.9499	0.0653	2853212	4031268	10739274	0.00	12.75264	11.63919	209.79	215.13	54.53	51.31
55		2	29	2.2583	0.0286	2.2160	0.0579	2945075	3775205	15069757	0.00	17.11587	16.97311	216.91	215.29	77.76	79.82
56		2	0	1.7065	0.0427	1.6929	0.0422	1162845	3212767	19918679	0.00	20.39381	19.79175	-190.34	-199.33	15.80	17.84
57		2	1	3.9322	0.1212	3.9957	0.0508	1346499	1915504	9381293	0.00	14.60067	14.12095	-279.77	-282.79	66.59	67.99
58	DJU 3	2	0	9.1826	0.0468	8.5682	0.0454	3125445	3396053	3861949	0.00	34.57088	33.82232	-301.57	-292.73	39.11	39.94
59		2	4	8.7676	0.0238	8.5874	0.0353	3162403	3226525	3355315	0.00	50.80591	51.12598	-306.43	-307.56	63.37	56.79
60		2	15	4.1098	0.0463	4.2631	0.0322	2776957	3365251	5786600	0.00	65.35614	65.16584	-262.13	-264.33	62.91	60.93
61		2	0	7.4659	0.0503	6.9625	0.0483	2268995	2901133	3879576	0.00	16.74321	16.95336	-154.37	-158.97	34.05	28.93
62	SEI 537	2	97	4.8101	0.0368	4.9042	0.0440	1463	823442	3496196	8.71	68.29955	67.16688	-135.71	-135.45	79.21	79.45
63		2	95	3.0739	0.0272	3.0919	0.0273	29364	630767	4739515	16.83	50.02468	49.87565	-221.63	-221.77	87.78	88.08
64		4	0	5.8600	1.1521	6.2855	0.0270	2038330	4903603	158568938	0.00	32.15929	31.13647	-42.08	-52.11	17.53	21.58
65		2	0	4.0196	0.0231	3.7978	0.0193	1959842	3388930	5018626	0.00	22.54966	23.53348	-261.74	-257.88	35.17	37.25
66		2	5	7.7009	0.0343	7.2244	0.0327	1095145	1817946	2587273	0.00	32.23475	32.78033	-250.40	-251.16	72.16	71.06
67		2	1	1.9542	0.0360	1.9227	0.0295	17560	2147937	13629208	4.98	30.94525	30.40673	254.26	256.45	59.48	58.31
68		2	76	4.3955	0.0246	4.4926	0.0335	18329	1014558	2938270	2.77	21.12998	21.20677	-242.61	-244.25	52.22	50.35
69		2	0	7.4806	0.0259	7.1392	0.0211	2815019	3000490	3293342	0.00	16.84239	16.50907	-347.91	-352.21	79.09	83.37
70		2	37	1.8922	0.0549	1.9337	0.0199	524939	2858863	18321698	0.00	44.42350	45.00879	-343.69	-344.43	67.75	66.31
71		2	59	2.3846	0.0218	2.4707	0.0225	192086	3016066	7528636	0.06	15.52448	15.16066	-346.09	-345.06	39.69	38.34
72	GRV 503	2	97	2.7852	0.0315	2.7492	0.0322	7272	1108984	6511569	9.46	57.20110	58.01430	-224.14	-224.35	72.19	73.36
73		3	0	2.9543	0.0464	2.9732	0.0289	3943691	4197092	8320601	0.00	11.67337	10.50429	-99.51	-103.64	53.38	53.85
74		2	0	3.9800	0.0257	3.7682	0.0307	1270802	3123738	5511708	0.00	15.44167	15.89318	-207.86	-203.25	69.03	67.20
75		2	1	2.7516	0.0334	2.8026	0.0296	1830712	2342581	7312536	0.00	30.88683	31.02633	-59.62	-54.89	70.52	69.83
76		2	59	3.9413	0.0423	3.9043	0.0312	200176	636255	3556104	0.00	38.84212	38.95838	-179.53	-178.14	17.90	18.26
77		2	0	3.2180	0.0206	3.3151	0.0233	2442620	3101555	4986031	0.00	29.51920	29.07355	-39.67	-43.87	9.71	9.06
78		2	0	5.6869	0.0286	5.4580	0.0234	3636326	3915398	4394465	0.00	30.63439	29.64318	-335.49	-2.21	15.62	18.74

Table 1 (continued): List of Kamdar et al. 2019 objects with spatial movement values derived from GAIA DR2 data

Table continues on the next page.

Counter-Check of Reported Common Origin Pairs

Obj	Disc	No	CPMS	Plx1	e_Plx1	Plx2	e_Plx2	Min_D_AU	Med_D_AU	Max_D_AU	LPGR	V1	V2	DV1	DV2	AV1	AV2
79	JKA 38	2	61	4.5741	0.0440	4.4603	0.0248	9115	1151136	3206072	2.64	42.85531	43.28074	223.95	225.09	84.75	85.21
80		2	1	3.7251	0.0642	3.8046	0.0481	25475	1213668	6157484	8.29	11.13034	11.13011	134.95	131.33	65.45	62.46
81		2	92	4.2514	0.0480	4.3513	0.0445	626333	1288527	4498854	0.00	31.34605	30.59609	-75.96	-76.50	23.01	23.14
82		2	4	4.4322	0.0481	4.2183	0.0420	2812066	3708493	6041561	0.00	77.30732	76.74319	-115.35	-116.36	69.65	73.33
83		2	0	10.0574	0.0429	10.6727	0.0500	2677134	2856400	3182981	0.00	9.33643	9.32304	-215.76	-221.82	70.12	69.61
84		2	0	3.3580	0.0391	3.2911	0.0435	123047	1278071	6160050	5.93	25.52551	26.30788	96.55	126.59	3.31	2.46
85		2	74	2.0157	0.0572	2.0255	0.0543	2293818	3664915	19117330	0.00	38.40677	37.65036	-221.13	-222.31	64.69	67.11
86		2	92	1.5416	0.0539	1.5770	0.0447	2070376	5059125	30558049	0.00	55.63124	54.84386	-205.83	-205.32	71.09	70.30
87		2	4	4.7232	0.0389	4.6175	0.0602	3856889	4102796	5648319	0.00	12.52043	12.83181	-112.90	-114.69	69.96	79.36
88		2	0	3.8213	0.4089	3.7524	0.0440	3625316	5540898	42427719	0.00	2.35068	1.89124	-333.29	-341.50	27.25	50.78
89		3	74	1.5286	0.0356	1.5624	0.0510	2498159	4989652	24348508	0.00	47.26016	47.00574	171.63	173.26	48.33	47.91
90		2	1	2.6269	0.0666	2.6303	0.0360	2010175	2590409	11625531	0.00	23.40648	23.99154	240.98	235.68	35.64	34.52
91		2	0	2.7503	0.0334	2.8027	0.0511	726009	1718300	7890262	0.00	30.35580	29.80785	300.87	297.08	17.48	15.93
92		2	29	1.6827	0.0433	1.6928	0.0378	3078837	4350870	20061718	0.00	17.89027	18.28188	256.32	258.14	48.49	48.16
93		2	1	4.3523	0.0448	4.1319	0.0377	2496333	3579762	5869745	0.00	44.43198	45.28878	303.74	305.80	28.95	31.08
94		2	1	3.2720	0.0522	3.1259	0.0392	1939965	3545823	9133646	0.00	30.97192	32.52542	236.90	239.29	16.89	15.14
95		3	4	3.1737	0.0342	3.0038	0.0361	1425574	3949352	8532474	0.00	51.90413	51.57890	270.97	269.03	14.14	12.18
96	BAL1009	2	0	3.0520	0.0377	2.9927	0.0380	2317146	2766935	6930527	0.00	21.30947	21.76326	228.77	232.55	42.81	44.20
97		2	0	2.0420	0.0445	2.0526	0.0339	2891833	3578525	13510016	0.00	52.14251	51.47288	206.56	215.05	11.11	13.38
98		2	29	2.5389	0.0466	2.4340	0.0461	41732	3511901	13306164	1.97	14.89771	15.18480	-56.70	-58.40	76.27	76.08
99		2	92	2.4354	0.0413	2.5142	0.0398	100382	2671292	11465344	2.86	30.89535	29.96532	295.55	296.04	44.76	44.96
100		2	78	6.3615	0.0247	6.2043	0.0223	31501	821115	1610580	0.02	35.38354	36.51072	265.18	265.36	69.13	70.09
101		2	95	3.2150	0.0315	3.1916	0.0366	91998	741831	4663196	12.63	51.51236	51.36674	303.36	303.38	61.69	62.30
102		2	18	5.5254	0.0413	5.5616	0.1643	2886504	3056252	5855040	0.00	31.87713	31.64854	142.86	145.41	89.40	88.50
103	POU1965	3	0	3.6153	0.0424	3.5810	0.0395	3586803	3778767	5663911	0.00	27.81814	28.75788	252.02	257.80	52.44	52.73
104		3	5	3.7680	0.0618	3.9891	0.0797	1374830	3344369	9041317	0.00	45.33209	45.13291	206.30	205.37	29.01	30.48
105		2	0	2.7944	0.0457	2.8621	0.0467	11022	1809283	10737882	5.52	22.35477	22.58473	-299.69	-306.34	30.24	31.44
106		2	15	4.8247	0.0464	4.7717	0.1916	2852472	3215611	9987385	0.00	48.20887	49.10296	-277.99	-275.97	56.72	54.61
107		2	0	8.1079	0.0377	7.8150	0.1058	3427193	3645347	4492516	0.00	42.80824	43.48761	277.18	273.80	73.49	69.01
108		2	0	3.6353	0.0475	3.5082	0.0397	2937821	3647229	7049365	0.00	13.89587	13.21841	-135.11	-124.56	28.04	32.15
109	BAL1482	2	0	4.1091	0.0491	3.8086	0.0488	341875	3971457	7915626	0.00	6.59040	5.40833	-33.85	27.19	88.99	86.98
110		2	5	5.3893	0.0372	5.5387	0.0505	3293697	3494539	4369676	0.00	35.26461	35.38239	-275.91	-276.17	54.73	60.10
111		2	59	1.4992	0.0285	1.5022	0.0338	3369892	4476561	20937110	0.00	80.32007	80.12464	-311.85	-313.20	36.74	37.36

Table 1 (conclusion): List of Kamdar et al. 2019 objects with spatial movement values derived from GAIA DR2 data

Counter-Check of Reported Common Origin Pairs

Obj	Source_ID1	mass50_1	teff50_1	dTeff_1	X-out_1	Source_ID2	mass50_2	teff50_2	dTeff_2	X-out_2	dmass
1	1122704451665024	0.82354641	5498.7480	146.1880	0	3265589567885580928	0.83603233	5604.88818	336.1582	1	0.012
2	7692256363002240	0.84840083	5408.1909	-34.0991	0	20971947349799552	0.85241753	5559.36133	-11.8789	0	0.004
3	16154437152168832	0.79902482	5284.1997	128.2896	0	9880902977577984	0.84556007	5420.12451	84.9746	0	0.047
4	42551825846558592	0.88936770	5797.2202	147.4404	0	42084395964513792	0.91640741	5980.22461	162.9248	0	0.027
5	47857587925189120	0.64921528	4059.8782	158.0081	1	53789109561985664	0.65013093	4077.20435	153.0745	1	0.001
6	111189457686432768	0.82186818	5395.5186	-109.5015	0	64763987951737728	0.85051018	5640.72656	44.3364	0	0.029
7	119917449706594048	0.93315661	5864.3799	85.1597	0	167938413891896320	0.96537900	6005.25098	267.4912	0	0.032
8	123121907625515264	1.26741958	6491.2031	99.0132	0	123122109487531392	1.24347806	6853.45947	390.8696	0	0.024
9	125696203647091968	0.98452550	6015.6221	76.4819	0	130090337447459456	0.96829951	5948.62891	91.6890	0	0.016
10	169924131895224576	1.28370500	6755.4702	-26.2397	0	169924338053653888	1.16347039	6437.42139	-196.8584	0	0.120
11	170420595752139136	1.04931045	6444.7534	274.9937	0	218583323918729344	1.01199782	6374.47900	313.9390	1	0.037
12	218585080564110720	1.04612553	6005.7607	309.0010	0	219558079636107904	0.96354043	5711.76318	93.7334	0	0.083
13	219306463271848960	1.05499613	6258.9482	12.6782	0	219306669430278528	0.99368417	6164.08740	105.5674	0	0.061
14	231950159800091136	1.33756506	7054.1221	453.0620	0	227143507276539776	1.71516764	6390.08984	-224.0200	0	0.378
15	232399379018288000	0.97196430	6011.7480	495.8979	1	243874294680919040	0.98462313	5817.71680	259.0269	1	0.013
16	238163534366737792	1.16875386	6421.9092	440.0693	1	238164255921243776	1.06772888	6172.66309	225.8433	0	0.101
17	246940626453544448	0.95937753	6067.3677	41.1675	0	247256285068674688	1.04637659	6385.91016	248.0503	0	0.087
18	441835346009033984	0.88860452	5651.0308	122.6509	0	249672122574436096	0.91421098	5921.97021	213.1802	0	0.026
19	250841487549136384	1.09061027	6330.7832	25.5132	0	251596813379978752	1.06547701	6300.90723	151.0771	0	0.025
20	251334240556370688	2.30334878	10220.6240	2644.8643	0	443759220778884224	1.77058589	7417.18799	-161.9619	0	0.533
21	261380718817244160	1.03973842	6310.4351	-90.9351	0	261380718817241088	1.03881931	6374.73389	131.6240	0	0.001
22	324809272581952000	1.41529906	6508.9897	238.0298	0	324514710840745856	1.31336868	6583.26660	119.8267	0	0.102
23	341881492706662144	1.03255880	6162.2339	-371.4561	0	341622798236732544	1.19063318	6680.63037	91.4902	0	0.158
24	454947949883907584	1.03670335	6178.4028	-220.7974	0	359930701929480576	1.15079343	6465.92969	-40.6401	0	0.114
25	375862311879284608	1.08074927	6232.2070	-85.0332	0	375470099761825152	1.07294464	6282.23291	-36.3770	0	0.008
26	378396823620082176	0.94099438	6020.3726	436.8325	1	2863674156188051968	0.91534865	5677.97119	182.8911	0	0.026
27	391987680693489152	1.15636611	6586.3306	106.4604	0	392030252409329152	1.22869611	6651.58447	28.3442	0	0.072
28	393820124202543744	1.23344064	6665.6909	-388.7593	0	393318025340738304	1.21399820	6684.61377	-568.1265	1	0.019
29	404970954514021248	1.48430407	6280.6831	302.7930	0	410369144287662848	1.21617508	6302.15381	308.1440	0	0.268
30	435642209326124672	0.94299531	6133.8262	257.5859	1	443414833121045376	0.97542882	6002.25684	138.7769	0	0.032
31	447513503231078400	0.94598198	5827.5762	109.3662	0	449590205816652416	0.92190880	5734.71973	89.9600	0	0.024
32	448952656574582912	1.38989246	6607.0918	116.6519	0	448597243738258176	1.28586125	6382.28662	63.4365	0	0.104
33	454335594920988288	1.25482953	6569.2393	193.8193	0	454131631217853312	1.09048426	6290.67480	-221.4053	0	0.164
34	584181183652059520	0.93888760	5719.1206	38.3804	0	584164828416571264	0.86158121	5671.30811	40.8682	0	0.077
35	636738934675606784	1.59599984	6871.2813	419.4414	0	636739179489212032	1.51452315	6928.14258	381.5127	0	0.081
36	646124645103549312	1.33366895	6781.7344	713.8545	1	646125297938578944	1.40570605	6345.96826	374.5581	0	0.072
37	649308177943887744	1.28194988	6899.8096	189.4697	0	649308177943888256	1.41994059	7520.42529	811.9053	1	0.138
38	649872875947754368	0.96449602	5945.3491	145.4990	0	649658509835641984	1.07643330	6166.14893	355.1890	1	0.112
39	681387387460651392	0.98258853	6012.6191	211.1489	0	681308634941086592	1.01606786	6052.39746	381.5474	1	0.033
40	694859604653048320	0.84657586	5395.4961	202.0361	1	698203249576119424	0.85109192	5306.54736	-60.4028	0	0.005

Table 2. List of Kamdar et al. 2019 objects with masses and comparison of effective temperature values

Table 2 continues on the next page.

Counter-Check of Reported Common Origin Pairs

Obj	Source_ID1	mass50_1	teff50_1	dTeff_1	X-out_1	Source_ID2	mass50_2	teff50_2	dTeff_2	X-out_2	dmass
41	700628394269760384	0.64959866	4521.0425	58.2227	0	712157155941158528	0.71526599	4770.91699	162.7471	1	0.066
42	743956681482125696	1.35093105	7145.5308	492.9507	0	743944930451603584	1.28289664	6508.82422	-37.8960	0	0.068
43	759993226077119744	0.92548752	5661.4824	117.1826	0	757566711288894336	0.93561995	5696.64600	-17.2842	0	0.010
44	772021200385350656	0.94391233	5885.9219	-32.8979	0	771335483086516608	0.96646762	5955.19873	81.3989	0	0.023
45	809876320578914560	1.00969779	6152.6660	-66.9941	0	809892916332505344	1.08645821	6430.24365	86.2036	0	0.077
46	1013151556420133760	0.83115226	5402.2441	25.8843	0	824940179634765184	0.88349777	5802.80078	263.2910	1	0.052
47	893835131555196928	0.85144681	5394.0493	134.2896	0	881823826013408384	0.84755492	5226.06641	43.5264	0	0.004
48	887350001520664320	1.20806801	6746.3696	584.7896	1	887785476843657216	1.15230465	6536.98242	208.5625	0	0.056
49	888398321434606336	0.82226795	5353.3774	312.4175	1	3384590875297070336	0.83390433	5264.92578	33.2856	0	0.012
50	895244705461615360	0.95762074	6122.1138	49.6538	0	892704932384262016	1.01139796	6248.44238	210.2822	0	0.054
51	905618632028815488	0.69929254	4690.4795	260.2393	1	903078893312116992	0.69810742	4732.06543	181.3057	1	0.001
52	946471222781159040	0.86123198	5442.1948	473.0249	1	946435007617437056	0.72477883	4874.40039	-26.6694	0	0.136
53	951384665369338496	1.12926197	6488.9829	22.1230	0	953385505948551424	1.35763168	6965.49268	310.9727	0	0.228
54	964632547829087104	1.58103168	7173.2129	500.7930	0	951885909527428608	1.19650888	6701.50928	132.5293	0	0.385
55	990900426075527552	0.96854061	6052.1865	12.0967	0	966619154885685632	0.99235028	6185.04346	49.8232	0	0.024
56	984419320425738368	1.32092071	6754.4351	253.7949	0	985206124075128832	1.29392290	6448.38721	-41.2529	0	0.027
57	1001366818996615808	0.93009263	5673.2266	649.2266	1	1000361659209075584	0.86338896	5387.76367	251.0737	1	0.067
58	1168180153315910016	0.90105122	5431.5835	1068.2734	1	1154953573894521856	0.70068246	4587.10938	411.7495	1	0.200
59	1224871213362969088	0.99256539	6029.8086	321.9087	1	1206701371397064320	0.92105979	5934.45117	341.0713	1	0.072
60	1257207742959979776	0.89396465	5688.6553	116.6055	0	1259706146911669376	1.07587135	6237.99756	562.0874	1	0.182
61	1281094087612638976	0.85173374	5623.3350	234.4048	1	1286716440326271616	0.87724942	5394.81543	-71.8848	0	0.026
62	1283252566380133888	1.03986490	6129.4985	348.1587	1	1283252566380134016	0.94234687	5829.38037	170.2305	0	0.098
63	1291119606434912384	1.07280505	6159.2847	170.4448	0	1291120362349158016	1.16432071	6317.44287	359.1631	0	0.092
64	1304112397900299648	0.90432316	5936.0337	268.3335	0	1301234048257809664	0.88407356	5664.48730	6.5674	0	0.020
65	1312512490643339264	0.97247839	6060.1050	153.4448	0	1312257786198974208	0.94912940	6049.83057	275.2808	1	0.023
66	1536912922562394880	0.70140457	4537.9131	299.4429	1	1537081560158538240	0.69993162	4644.82275	337.4028	1	0.001
67	1541225138449580928	1.22434998	6302.2651	1.3452	0	1541225310245728640	1.41579914	6200.96045	-116.6597	0	0.191
68	1574123282265128576	0.95434684	5973.5825	23.6123	0	1574123454063820928	0.93853801	6068.65332	169.0034	0	0.016
69	1586864388649398656	0.80125594	5315.1611	63.4312	0	1589711432272952448	0.78449023	5184.50781	113.3677	0	0.017
70	1588873265111172992	1.36576605	6336.8926	202.9224	0	1589069356138116608	0.97696918	6270.41016	40.2002	0	0.389
71	1594637248661284864	1.10911000	6627.0273	353.5674	1	1594612952030474496	1.00242877	6135.75049	-141.3794	0	0.107
72	1897440689367972096	1.20438313	6194.0449	18.4751	0	1897440689367972736	1.18771827	6351.32617	140.3560	0	0.017
73	1935112912675231360	1.24469006	6474.5093	275.2495	0	1924718984440067584	1.03835642	6198.70264	128.4824	0	0.206
74	1931948690008232960	0.97435808	6004.8057	-19.1143	0	1935115386576401152	1.03344274	6228.21582	123.1060	0	0.059
75	1998564659266179840	1.05144942	6141.1816	-17.1182	0	1997199585521495808	1.14105678	6298.01709	134.4170	0	0.090
76	2052491723180057856	1.26357603	6604.1338	728.7339	1	2076462137513753600	0.97298032	6050.66162	241.1118	1	0.291
77	2080536931908027392	1.20488608	6633.3350	98.9048	0	2128080536248155776	1.26988995	7061.06836	485.2886	0	0.065
78	2130506398193844352	0.79537481	5315.3970	63.9067	0	2128941861868381952	0.78793889	5170.17480	15.2646	0	0.007
79	2130775885920987520	0.92900294	5973.7861	51.5264	0	2130775782841768192	0.98768097	6097.32520	66.9951	0	0.059
80	2663390691484861440	1.02303529	6195.1787	-52.2515	0	2663390485326432000	1.40682697	6382.39063	133.0806	0	0.384

Table 2 (continued). List of Kamdar et al. 2019 objects with masses and comparison of effective temperature values

Table 2 concludes on the next page.

Counter-Check of Reported Common Origin Pairs

Obj	Source_ID1	mass50_1	teff50_1	dTeff_1	X-out_1	Source_ID2	mass50_2	teff50_2	dTeff_2	X-out_2	dmass
81	2735779131148531840	0.83648479	5244.3921	154.3320	0	2735476215694707072	0.88949895	5489.33643	287.7563	1	0.053
82	2810800188196233344	0.85231125	5375.4116	323.9214	1	2762037775217685888	0.85252297	5382.29736	232.8071	1	0.000
83	2803106080703163264	0.73399782	4961.4956	182.1558	1	2783778556072274432	0.74062973	5241.76709	400.8770	1	0.007
84	2785776059462243200	0.83328438	5540.5679	36.9678	0	2784261344756137984	0.85572886	5721.98486	123.0947	0	0.022
85	2807938777904465792	1.03713477	6369.8535	56.1235	0	2807428329631314048	1.66207433	6449.70801	33.9380	0	0.625
86	2837284227854578432	1.23242128	6226.0879	268.9277	0	2825213239449531008	1.23556089	6550.00684	403.7769	1	0.003
87	2878471795992127232	0.96573788	5989.6182	-22.0918	0	2861383426791456640	0.96537614	6192.89355	270.4136	1	0.000
88	3007597685645337472	0.77373809	5442.5234	-210.8467	0	3019102494281388288	1.30822289	6043.48047	304.4307	0	0.534
89	3021022993201243264	1.06230366	6274.8755	-33.8745	0	3021430087381710464	1.14204693	6505.12793	62.9180	0	0.080
90	3021426342170234624	0.93413943	5867.9731	55.0029	0	3024359809129971584	0.96781063	6036.91113	132.9912	0	0.034
91	3022721326349517696	0.94521022	6139.9404	211.5503	0	3022981567008196864	0.92936379	6177.56445	384.9243	1	0.016
92	3109969433741698560	1.28052187	6743.5186	-530.3613	1	3061624869539761664	1.37799323	7044.90381	-121.7261	0	0.097
93	3080846875411001728	1.29392874	7131.1445	728.8545	1	3068202869648745472	1.18023348	6685.26563	133.8154	0	0.114
94	3082939177319324160	1.03866470	6166.2568	344.2070	1	3081181470543888128	0.92971134	5934.84961	118.5098	0	0.109
95	3095492782609237376	0.89617717	5561.5698	-65.8403	0	3143607686319804544	1.18344760	6440.63379	647.0937	1	0.287
96	3124167496106659584	1.09877348	6461.3291	86.6489	0	3120372630506706432	1.03270340	6174.51709	-162.3428	0	0.066
97	3124120350247568000	1.15627027	6534.2935	173.9033	0	3130078745494663680	1.01909208	6223.10791	8.4678	0	0.137
98	3130844997721522944	1.38587451	6861.1143	330.5044	0	3130845723576534016	1.41342878	6912.54248	330.6924	0	0.028
99	3132274672076250624	1.07736921	6378.1455	9.5957	0	3132273508145500032	0.99969578	6289.34033	-84.9697	0	0.078
100	3133697444423385984	0.64873683	4368.1567	15.3667	0	3133697444423388288	0.73728192	5267.02051	1090.2905	1	0.089
101	3210885119193585536	1.12358272	6467.6489	69.3091	0	3210886042610196480	1.16674078	6493.28027	174.4204	0	0.043
102	3366175910957358080	0.89170694	5734.9111	145.4409	0	3367337441911377920	0.92681462	6058.41797	472.3481	1	0.035
103	3385798109000950144	1.06518805	6082.3159	169.1357	0	3379735706825164544	0.91416997	5829.45508	72.8853	0	0.151
104	3385278383597632896	1.48119915	7691.0225	416.0127	0	3386349479721943040	1.68937874	7654.55762	469.3975	0	0.208
105	3413324584462632576	1.03972507	6285.7153	-96.1846	0	3413324657478444160	1.04975462	6355.91650	-84.7334	0	0.010
106	3672044382058159488	0.80100942	5099.9419	329.8818	1	3661316962501936512	0.77204216	5242.91650	323.8867	1	0.029
107	3795747411642295168	0.69937313	4158.0396	219.3896	1	3813985006717191936	0.76842570	5167.81104	1152.3911	1	0.069
108	3992114209767880960	1.03982913	6267.6538	21.8638	0	3994508877374172160	0.96582818	5924.03271	-165.6973	0	0.074
109	4381826932186259712	1.06430030	6330.2222	177.1821	0	4381843046903618688	1.21808851	6369.93994	164.9800	0	0.154
110	4403568262795516032	0.92257452	5780.6030	163.4331	0	4417843806373635840	1.01630294	6132.86914	336.4990	1	0.094
111	4444214630694301696	1.09055841	4855.4824	3.2524	0	4444406254955951488	1.11599422	4630.28662	-172.0034	1	0.025
	Mean value	183.5117							164.6727		0.094
	Standard deviation	328.0360							237.0024		0.117
	Maximum value	2644.8643							1152.3911		0.625

Table 2 (conclusion). List of Kamdar et al. 2019 objects with masses and comparison of effective temperature values

Counter-Check of Reported Common Origin Pairs

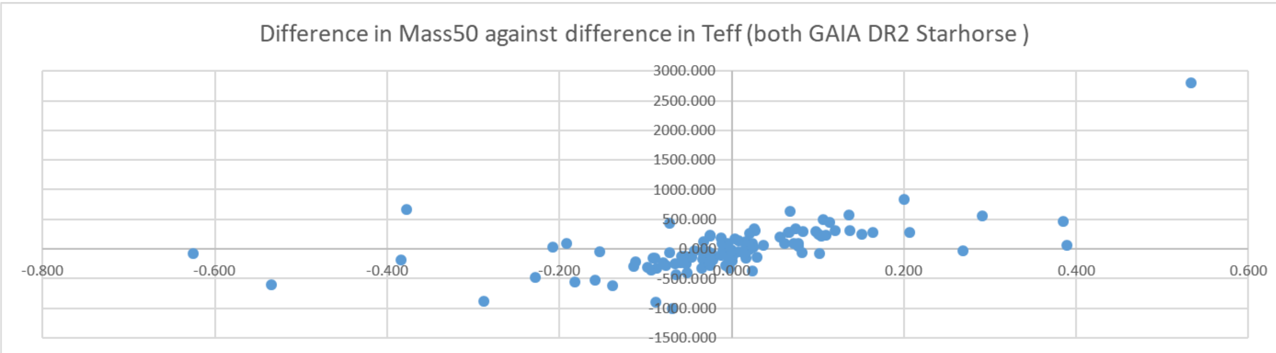

Figure 1: Relationship difference Mass50/Teff for GAIA DR2 StarHorse

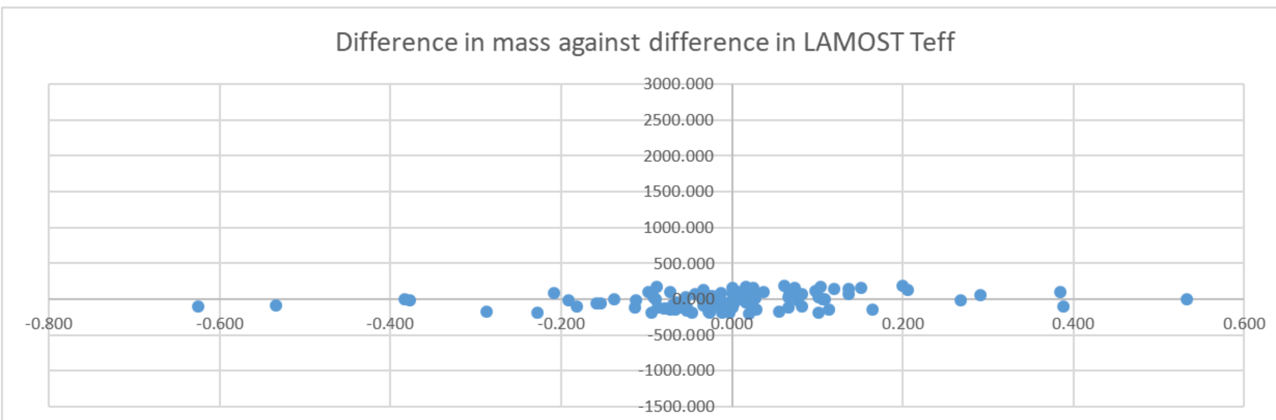

Figure 2: Relationship difference GAIA DR2 StarHorse Mass50/LAMOST Teff

(Continued from page 49)

ing GAIA DR2 StarHorse Mass50 differences to LAMOST Teff differences (see Figure 2) – no relationship between MASS50 and Teff to be explained by the dTeff<200 cut applied by Kamdar et al. 2019.

GAIA DR2 StarHorse provides also metallicity data – this time the relationship with LAMOST data is somewhat different as 48% of the LAMOST values are outside the StarHorse 16 and 84 percentile values which can no longer to be explained by statistical means. Table 3 gives the GAIA DR2 StarHorse metallicity values with the LAMOST metallicity values for comparison:

Content description:

- Obj = KMD object number
- met16_1 = GAIA DR2 StarHorse percentile 16 metallicity value primary
- met50_1 = GAIA DR2 StarHorse percentile 50 metallicity value primary
- met84_1 = GAIA DR2 StarHorse percentile 84 metallicity value primary
- [Fe/H]_1 = LAMOST metallicity value primary
- e_[Fe/H]_1 = LAMOST metallicity value error primary
- met16_2 = GAIA DR2 StarHorse percentile 16 metallicity value secondary
- met50_2 = GAIA DR2 StarHorse percentile 50 metallicity value secondary
- met84_2 =
- GAIA DR2 StarHorse percentile 84 metallicity value secondary
- [Fe/H]_2 = LAMOST metallicity value secondary
- e_[Fe/H]_2 = LAMOST metallicity value error secondary

With few exceptions the LAMOST [Fe/H] are rather high near the StarHorse met84 values indicating a regular pattern towards higher metallicity values.

(Text continues on page 60)

Obj	met16_1	met50_1	met84_1	[Fe/H]_1	e_[Fe/H]_1	met16_2	met50_2	met84_2	[Fe/H]_2	e_[Fe/H]_2
1	-0.504730	-0.214799	0.018472	0.174	0.024	-0.533411	-0.287828	-0.026535	0.135	0.027
2	-0.329780	-0.072325	0.127610	0.068	0.027	-0.419454	-0.170029	0.090333	-0.058	0.026
3	-0.336304	-0.158173	0.037918	0.212	0.036	-0.339459	-0.116237	0.117755	0.141	0.029
4	-0.486111	-0.218653	0.024346	0.112	0.032	-0.617031	-0.254580	0.031695	0.012	0.033
5	-0.034633	0.111280	0.238216	-0.255	0.064	-0.015918	0.109144	0.220651	-0.099	0.055
6	-0.411372	-0.189868	0.032739	-0.159	0.026	-0.491621	-0.236863	-0.005390	-0.100	0.017
7	-0.465934	-0.170349	0.050404	0.172	0.016	-0.543610	-0.257203	0.000011	0.110	0.026
8	-0.478800	-0.245652	0.029777	-0.264	0.013	-0.591997	-0.303373	-0.021739	-0.350	0.011
9	-0.538603	-0.213167	0.067907	0.115	0.019	-0.497312	-0.145970	0.123018	0.028	0.019
10	-0.571332	-0.263635	0.009952	0.016	0.013	-0.461071	-0.172921	0.108874	0.045	0.063
11	-0.684599	-0.375784	-0.149648	-0.017	0.018	-0.705887	-0.410444	-0.146290	0.096	0.027
12	-0.604344	-0.310685	-0.009425	0.140	0.024	-0.735991	-0.394119	-0.045994	0.142	0.025
13	-0.478824	-0.221713	0.021298	0.006	0.015	-0.554977	-0.251318	-0.014994	0.035	0.019
14	-0.486413	-0.235910	0.000006	-0.056	0.036	-0.220633	0.054005	0.296181	0.031	0.032
15	-0.454740	-0.127553	0.103158	0.173	0.026	-0.223838	0.082330	0.282742	0.291	0.029
16	-0.490128	-0.185930	0.080898	0.186	0.012	-0.444843	-0.162316	0.136129	0.108	0.009
17	-0.567472	-0.274933	-0.010450	-0.168	0.033	-0.678518	-0.344229	-0.070892	-0.467	0.048
18	-0.373046	-0.129227	0.080382	0.113	0.017	-0.520404	-0.217929	0.036367	0.249	0.021
19	-0.552573	-0.229601	0.032306	-0.058	0.015	-0.553500	-0.251073	0.011146	0.188	0.063
20	-0.445734	-0.176862	0.100036	-0.124	0.084	-0.475487	-0.190004	0.140063	-0.075	0.032
21	-0.591864	-0.298452	-0.023195	-0.017	0.030	-0.668509	-0.338875	-0.095745	-0.038	0.037
22	-0.460254	-0.190557	0.058184	0.107	0.014	-0.536076	-0.126156	0.117013	0.087	0.016
23	-0.492197	-0.236133	0.012984	-0.013	0.021	-0.580382	-0.295423	-0.035518	-0.044	0.011
24	-0.417558	-0.182820	0.092814	0.089	0.025	-0.496123	-0.192172	0.060389	0.006	0.012
25	-0.411062	-0.132018	0.170217	0.204	0.015	-0.504694	-0.200349	0.065168	0.076	0.014
26	-0.528237	-0.259098	-0.001440	0.152	0.027	-0.336341	-0.056597	0.168923	0.287	0.042
27	-0.571472	-0.263488	-0.000101	-0.111	0.044	-0.494434	-0.193868	0.023416	-0.047	0.019
28	-0.545967	-0.225304	0.003052	-0.112	0.011	-0.631137	-0.283507	-0.027862	-0.144	0.023
29	-0.446516	-0.131022	0.131600	-0.300	0.084	-0.420453	-0.162598	0.092312	0.135	0.021
30	-0.654620	-0.356302	-0.108279	0.095	0.028	-0.522167	-0.228267	0.030653	0.121	0.034
31	-0.394132	-0.108565	0.116114	-0.138	0.088	-0.317991	-0.041902	0.167132	0.182	0.046
32	-0.347239	-0.034190	0.273158	0.043	0.029	-0.269190	0.046649	0.363325	0.090	0.079
33	-0.464321	-0.135290	0.105043	-0.007	0.020	-0.462254	-0.177135	0.073527	-0.048	0.046
34	-0.316906	-0.030815	0.206894	0.069	0.038	-0.504110	-0.252154	-0.020714	-0.073	0.017
35	-0.516252	-0.210490	0.014526	-0.148	0.011	-0.520692	-0.238573	0.079828	-0.280	0.009
36	-0.417207	-0.126166	0.144058	0.331	0.034	-0.323733	-0.074603	0.218316	0.316	0.035
37	-0.603742	-0.284685	0.027087	-0.169	0.012	-0.686952	-0.333572	-0.026532	-0.139	0.010
38	-0.392878	-0.162378	0.102092	0.142	0.072	-0.420150	-0.128506	0.191816	0.101	0.014
39	-0.467818	-0.167664	0.074249	0.164	0.023	-0.416215	-0.113584	0.130606	0.251	0.025
40	-0.291330	-0.044508	0.152809	0.007	0.025	-0.188218	0.008024	0.234578	0.090	0.035

Table 3: Comparison metallicity values GAIA DR2 StarHorse and LAMOST index

Table 3 continues on the next page.

Counter-Check of Reported Common Origin Pairs

Obj	met16_1	met50_1	met84_1	[Fe/H]_1	e_[Fe/H]_1	met16_2	met50_2	met84_2	[Fe/H]_2	e_[Fe/H]_2
41	-0.467962	-0.310881	-0.149665	-0.490	0.024	-0.326669	-0.110265	0.023105	-0.530	0.037
42	-0.576009	-0.223598	-0.004569	-0.173	0.009	-0.530385	-0.234885	0.048425	-0.157	0.014
43	-0.156943	0.019955	0.228716	0.241	0.057	-0.317150	-0.034048	0.188641	0.207	0.032
44	-0.426928	-0.115645	0.118799	-0.009	0.013	-0.442575	-0.156124	0.118844	0.368	0.026
45	-0.482139	-0.168969	0.099184	-0.116	0.016	-0.590733	-0.303078	-0.012615	0.034	0.012
46	-0.403086	-0.174252	0.037731	0.080	0.025	-0.610894	-0.323304	-0.072447	0.013	0.020
47	-0.311652	-0.074635	0.173896	0.344	0.039	-0.161045	0.027214	0.251074	0.403	0.090
48	-0.576217	-0.269161	-0.023067	0.009	0.054	-0.574138	-0.254205	0.033766	0.257	0.016
49	-0.337515	-0.154410	0.075029	0.092	0.088	-0.283678	-0.025871	0.190184	0.222	0.030
50	-0.539819	-0.297980	-0.016171	-0.645	0.015	-0.627590	-0.314466	-0.064572	-0.493	0.045
51	-0.351187	-0.162341	0.083178	-0.158	0.036	-0.411089	-0.250350	-0.051253	-0.477	0.042
52	-0.285749	-0.019436	0.192397	0.397	0.056	-0.327668	-0.174744	-0.012329	-0.233	0.265
53	-0.558527	-0.265057	-0.011548	-0.045	0.019	-0.418650	-0.162158	0.072589	0.006	0.016
54	-0.405367	-0.131515	0.128203	-0.251	0.009	-0.580979	-0.254307	-0.022309	-0.056	0.030
55	-0.597362	-0.273575	-0.004613	0.066	0.046	-0.613184	-0.317751	-0.029745	-0.131	0.032
56	-0.488602	-0.144363	0.132350	0.061	0.013	-0.474647	-0.177635	0.108953	0.073	0.012
57	-0.203543	0.033767	0.279636	0.079	0.137	-0.252783	-0.023820	0.210767	0.257	0.074
58	-0.033633	0.203981	0.348046	-0.205	0.032	-0.244737	-0.025005	0.242549	-0.149	0.050
59	-0.467855	-0.161181	0.103636	0.198	0.021	-0.574943	-0.269228	-0.011852	0.189	0.028
60	-0.397423	-0.134122	0.060205	0.158	0.031	-0.427342	-0.128383	0.134354	0.408	0.021
61	-0.494288	-0.248751	-0.007749	0.109	0.020	-0.227273	0.010158	0.272978	0.172	0.018
62	-0.464254	-0.137565	0.143238	-0.069	0.024	-0.382538	-0.070400	0.158991	-0.071	0.031
63	-0.426165	-0.124629	0.170746	0.183	0.024	-0.461149	-0.136512	0.149124	0.306	0.020
64	-0.653075	-0.323214	-0.060079	0.466	0.022	-0.431629	-0.210161	0.040055	-0.002	0.126
65	-0.517179	-0.217378	0.069149	0.062	0.014	-0.620444	-0.314410	-0.029756	0.236	0.019
66	-0.105293	0.071622	0.275868	-0.072	0.044	-0.332103	-0.106805	0.169103	-0.093	0.052
67	-0.500502	-0.211273	0.055008	-0.181	0.015	-0.495982	-0.161934	0.070655	-0.223	0.009
68	-0.544916	-0.209462	0.032198	-0.089	0.019	-0.598782	-0.318575	-0.051733	-0.030	0.017
69	-0.411865	-0.195246	-0.003980	-0.030	0.024	-0.407800	-0.211744	-0.017349	-0.062	0.102
70	-0.556978	-0.254612	0.043373	-0.038	0.014	-0.744829	-0.368586	-0.125936	-0.630	0.144
71	-0.847239	-0.435922	-0.103198	-0.053	0.011	-0.514046	-0.178073	0.086689	-0.123	0.169
72	-0.393255	-0.106633	0.192288	0.158	0.011	-0.403667	-0.096065	0.126546	0.098	0.011
73	-0.427884	-0.105269	0.157445	-0.006	0.021	-0.598389	-0.247903	0.026764	0.028	0.075
74	-0.446517	-0.114970	0.126011	-0.100	0.266	-0.519610	-0.251212	0.029192	-0.344	0.191
75	-0.385577	-0.089389	0.164477	0.072	0.016	-0.406135	-0.139310	0.111336	0.034	0.025
76	-0.417588	-0.114350	0.145133	-0.041	0.013	-0.476157	-0.191820	0.009347	-0.013	0.016
77	-0.517962	-0.206479	0.027314	0.156	0.012	-0.619084	-0.324270	-0.124792	-0.043	0.007
78	-0.455724	-0.207887	-0.022782	0.147	0.028	-0.347699	-0.161017	0.028828	0.104	0.039
79	-0.597275	-0.287297	-0.023274	-0.401	0.015	-0.582232	-0.287810	-0.013766	-0.362	0.010
80	-0.516644	-0.232680	0.013543	-0.115	0.020	-0.497026	-0.163418	0.105706	-0.101	0.012

Table 3: Comparison metallicity values GAIA DR2 StarHorse and LAMOST index

Table 3 concludes on the next page.

Obj	met16_1	met50_1	met84_1	[Fe/H]_1	e_[Fe/H]_1	met16_2	met50_2	met84_2	[Fe/H]_2	e_[Fe/H]_2
81	-0.245099	-0.025589	0.182754	0.200	0.038	-0.274318	-0.052505	0.204684	0.289	0.030
82	-0.255055	-0.047360	0.178653	0.045	0.098	-0.250551	-0.028803	0.210143	0.069	0.026
83	-0.415291	-0.221541	-0.049659	-0.097	0.031	-0.585354	-0.360555	-0.161202	-0.008	0.040
84	-0.539896	-0.302899	-0.074394	-0.139	0.052	-0.560185	-0.302825	-0.038305	-0.104	0.036
85	-0.661037	-0.357688	-0.063986	-0.150	0.050	-0.293320	0.013868	0.266422	0.139	0.065
86	-0.472739	-0.113192	0.196950	-0.114	0.014	-0.495787	-0.235061	0.079860	-0.051	0.017
87	-0.491012	-0.194485	0.076004	-0.048	0.012	-0.710104	-0.386832	-0.151339	0.072	0.014
88	-0.745131	-0.381134	-0.115921	0.414	0.034	-0.428539	-0.170137	0.144898	0.026	0.014
89	-0.620113	-0.321608	-0.035361	-0.157	0.020	-0.574907	-0.236641	0.011743	-0.175	0.088
90	-0.508143	-0.181210	0.033789	0.119	0.046	-0.513228	-0.234314	-0.013196	0.109	0.017
91	-0.675210	-0.348837	-0.053654	0.005	0.029	-0.695992	-0.451026	-0.187099	0.209	0.039
92	-0.513469	-0.229146	0.026655	-0.049	0.012	-0.546004	-0.231167	0.047707	-0.052	0.014
93	-0.722804	-0.384410	-0.099262	0.103	0.010	-0.624944	-0.336379	-0.071526	-0.183	0.163
94	-0.438684	-0.191086	0.085585	0.120	0.035	-0.544101	-0.278767	-0.005878	0.157	0.051
95	-0.324121	-0.087987	0.146839	0.256	0.096	-0.400773	-0.133940	0.161750	0.272	0.036
96	-0.579761	-0.314241	-0.033525	0.107	0.019	-0.490528	-0.190337	0.091962	-0.120	0.012
97	-0.508968	-0.246256	0.019071	0.131	0.073	-0.612042	-0.301296	-0.022261	-0.042	0.052
98	-0.421883	-0.178091	0.124905	-0.112	0.019	-0.498384	-0.193039	0.097248	-0.118	0.016
99	-0.576596	-0.299978	-0.010733	-0.219	0.024	-0.613788	-0.328775	-0.082957	-0.211	0.028
100	-0.415308	-0.186204	-0.030741	-0.485	0.148	-0.657282	-0.416836	-0.235046	-0.656	0.176
101	-0.565219	-0.262246	-0.003038	-0.348	0.011	-0.539020	-0.216841	0.029790	-0.328	0.010
102	-0.461958	-0.213569	0.016547	-0.063	0.035	-0.603614	-0.312158	-0.029837	0.179	0.015
103	-0.417991	-0.149785	0.102371	-0.137	0.016	-0.471003	-0.210515	0.032888	0.086	0.030
104	-0.551161	-0.244398	0.020161	-0.285	0.009	-0.487894	-0.149511	0.123009	0.594	0.024
105	-0.610076	-0.316874	-0.027733	-0.585	0.017	-0.601856	-0.312392	-0.053280	-0.595	0.018
106	-0.207767	0.002264	0.233144	0.180	0.051	-0.467373	-0.268151	-0.033045	0.118	0.072
107	-0.075377	0.299468	0.457746	-0.099	0.152	-0.401706	-0.243814	-0.028263	-0.017	0.043
108	-0.615981	-0.264281	0.014048	-0.053	0.031	-0.411049	-0.121928	0.115080	-0.046	0.215
109	-0.628613	-0.284778	0.011912	-0.061	0.090	-0.504638	-0.186563	0.100059	0.017	0.072
110	-0.388020	-0.093996	0.170338	0.188	0.054	-0.430975	-0.143925	0.115032	-0.001	0.015
111	-0.417117	-0.176035	0.106590	-0.146	0.023	-0.278125	-0.030774	0.211766	-0.363	0.015

Table 3 (conclusion) Comparison metallicity values GAIA DR2 StarHorse and LAMOST index

Counter-Check of Reported Common Origin Pairs

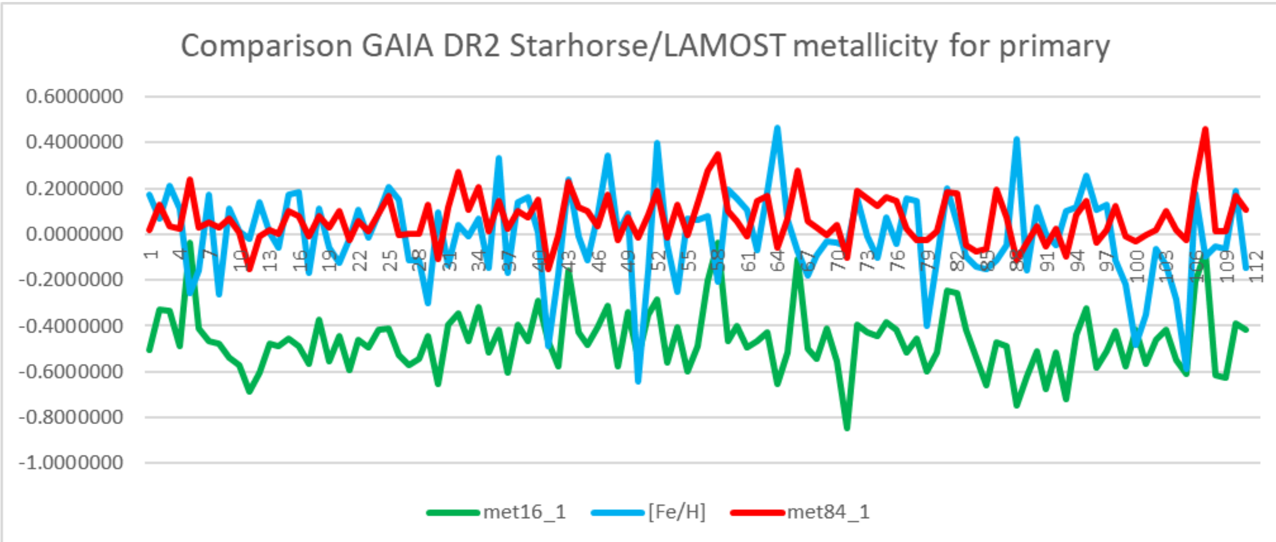

Graph 3: Comparison GAIA DR2 StarHorse metallicity (met16 and met84) with LAMOST [Fe/H] for the primary

(Continued from page 56)

These noticeable differences between GAIA DR2 StarHorse and LAMOST metallicity values remain in this context without explanation but comparing the StarHorse met50 values for primary and secondary shows in ~67% a difference of less than 0.1 indicating similar metallicity also with StarHorse catalog values.

4. Discussion

The question how stars are born and how they move over time is certainly fascinating. A star with a moderate fast spatial velocity of 20km/s needs only 150 million years to change is position relative to our Solar system by ~10 lightyears. Taking the age of the Sun with ~4.6 billion years this makes then about 300 lightyears or nearly 100 parsecs. As the speed and direction of the movement of stars is quite diverse this means that the neighborhood of a star might change significantly over its lifetime.

This report basically confirms with some caveats the data given in the Kamdar et al. 2019 paper but does not necessarily confirm the conclusion that the reported pairs have to be indeed of common origin due to the following reasons:

- Several seemingly co-moving pairs are despite very similar data values for parallax, proper motion and radial as well as spatial velolicty moving in directions different enough to question the "co-moving" property (see comments below Table 1). With a bit more restrictive thresholds for the direction of the spatial velocity even most of the listed KMD objects would not be assessed as co-moving
- Several KMD objects might if with a small likelihood be very well bound by gravitation according to a Monte Carlo simulation with a sample size of 120,000 using GAIA DR2 data for RA/Dec and Plx with the given error range used as standard deviation
- The KMD objects are listed as pairs and with few exceptions most are confirmed as such as no other objects with similar parameters are to be found in GAIA DR2. In a few cases such additional objects were found but could not be identified as co-moving members. This confirms the proposition that the listed pairs are most likely no longer part of a cluster – on the other side it seems a bit surprising that the "common origin" property should be restricted to pairs
- More or less all KMD objects come with parallax error values larger than 0.5% which means that at least for this parameter the data quality for the selected objects might be questionable. As the derived values like the spatial velocity are directly depending on the parallax data this casts a shadow at the final assessment of these objects
- With distances between the components of in average 40 light years the tidal forces of the Galaxy are no longer identical and such differences would over time counter-act against co-movement questioning the overall setup of the Kamdar et al. 2019 paper

- The total number of GAIA DR2 objects with parallax >1 and existing radial velocity data is 3,129,408 suggesting some likelidhood for pairs to have by chance similar values for parallax, proper motion and radial velocity – so it seems possible that the presented pairs are just random even if the additional criteria "metallicity" is considered
- Several KMD objects are already known double stars listed in the WDS catalog rendering these WDS pairs as likely opticals.

5. Common Origin/Common Movement Pairs in the WDS

The WDS catalog contains per June 2019 about 25,000 objects with code "V" for common proper motion. These objects offer a good chance to detect stars born together without being close enough for gravitational relationship by differentiating three szenarios:

- Doubles with a high likelihood for a spatial distance between components smaller than 1 parsec allowing for potential gravitational relationship - binaries
- Doubles with proper motion values by chance similar but with parallaxes and radial velocities and as a result spatial velocity far too different to be born together - opticals
- Doubles with all parameters similar enough to be considered to be born together but with parallaxes different enough make potential gravitational relationship rather unlikely either from the very beginning or by splitting up wide binaries later on – common origin.

After eliminating all pairs with separation less than 0.4" or more than 9999.9" plus the objects with insufficient RA/Dec data 24,635 objects remained for cross matching with GAIA DR2. The first X-match run with 5" radius around the primary position yielded 33,232 matches. The second X-match run with calculated J2000 positions for these objects and again 5" search radius yielded 55,882 objects with the unavoidable self matches and double matches for doubles with a separation smaller than 5". After eliminating all self-matches and likely wrong matches with delta in separation larger than 20%, delta in position angle larger than 15°, delta in M1 and M2 larger than 4 and eliminating the remaining multiple matches due to dense star fields 23,476 objects remained considered as likely correct cross-matches.

To be able to calculate spatial velocity all objects with missing parallax data or values below 1 mas or missing radial velocity values were eliminated as well reducing the object count drastically to 2,654. From these 2,203 objects have similar spatial movement (spatial velocity delta below 10% of the mean spatial velocity of both components and less than 10° delta in spatial movement direction – this allows for a few pairs a larger delta in spatial velocity than the 1.5km/s cut used by Kamdar et al. 2019 but the additional cut with the direction of the spatial velocity should overcompensate this generosity) and from these 1,030 have a spatial distance between the components (calculated with the given parallax values and the angular separation) of less than 1 parsec considered as threshold for potential gravitational relationship. From the remaining 1,173 objects a few with a spatial distance larger than 100 lightyears as threshold for the diameter of star forming molecular clouds had to be eliminated leaving 1,137 objects.

This selection of WDS objects is based only on the available astrometric data. An attempt to check the aspect of similar metallicity with LAMOST was not very successful due to the limited LAMOST DR4 coverage – only 32 pairs have [Fe/H] values for both components with 25 of them up to a delta of 0.1 meeting the cut applied by Kamdar et al. 2019.

The GAIA DR2 StarHorse catalog offers ~98% coverage but the spread of the given metallicity values indicated by the percentile 16 and 84 data is significantly larger than the spread of the [Fe/H] values in LAMOST. With a doubled cut value of 0.2 applied on the GAIA DR2 StarHorse median metallicity value 904 of the listed WDS code "V" objects qualify for similar metallicity and 233 pairs are despite common movement most likely not of common origin due to different metallicities including some outliers with large differences up to 1.96.

This means that out from the sample of V-coded WDS objects with data available for assessment 44% show common spatial movement and 34% have additionally similar metallicity suggesting common origin. It might make sense to add an additional WDS notes code for such objects – for example "G" for "proper motion, parallax and radial velocity suggest common origin and common movement".

Table 4 lists 20 such objects as stub with the full table available as flat text file "WDS V common origin and movement" for download.

- WDS = WDS ID
- Disc = Discoverer ID
- *C = Components (AB if blank, in Table 2 all AB)
- PA = Position angle from GAIA DR2 positions
- *e_PA = Error position angle

(Text continues on page 63)

WDS	Disc	C	PA	Sep	Plx1	pmra1	pmdec1	rV1	Plx2	pmra2	pmdec2	rV2	V1	V1D	V2	V2D	D_1-2
00013+0504	UC 304		53.647	15.33981	8.2162	-56.863	-23.221	12.43	8.3387	-57.641	-28.541	14.57	37.55	247.79	39.36	243.66	5.832
00061+2649	GRV 4		19.102	7.27753	2.6503	18.946	-8.057	-51.42	2.6719	19.038	-8.275	-44.36	63.24	113.04	57.65	113.49	9.949
00093+2517	GIC 2	AB	237.130	29.61193	24.8900	175.348	-158.970	0.67	22.4794	171.422	-145.634	4.71	45.08	132.20	47.66	130.35	14.052
00094-3321	TDS1322		277.574	9.46621	7.0201	167.998	-20.353	2.82	7.1058	167.660	-21.768	3.42	114.30	96.91	112.83	97.40	5.604
00102+0417	GRV 12		174.406	45.84872	4.7830	42.249	-25.818	-0.02	4.5758	42.832	-26.555	-1.77	49.07	121.43	52.23	121.80	30.879
00110-6309	UC 331		311.131	35.11078	3.7097	51.032	20.737	-25.51	3.7404	51.617	21.094	-25.32	74.86	67.89	75.06	67.77	7.218
00141-0602	KPP 52		196.820	3.50176	2.4400	2.805	-14.824	-57.53	2.4279	3.351	-14.913	-59.73	64.57	169.29	66.77	167.34	6.662
00159+1706	GRV 18		359.979	16.09166	4.2445	25.805	-30.356	-38.99	4.2743	25.842	-30.438	-37.03	59.16	139.63	57.72	139.67	5.358
00174+0221	STF 21		51.638	7.65779	5.6454	12.511	51.421	-61.17	5.6817	13.230	50.902	-60.20	75.61	13.67	74.49	14.57	3.691
00175-6142	KPP1737		130.295	13.40715	3.0868	40.117	7.579	-1.60	3.0467	40.374	7.870	-1.78	62.71	79.30	64.02	78.97	13.907
00185-3005	KPP1566		335.377	11.81386	2.6561	-9.674	-31.869	-2.41	2.6430	-8.606	-31.498	-3.69	59.48	196.89	58.68	195.28	6.087
00185-5325	UC 351		223.453	28.96995	7.4621	47.531	-24.364	-10.30	7.5238	46.284	-22.534	-11.19	35.46	117.14	34.31	115.96	3.585
00196+6457	CBL 568		12.476	24.68793	4.6139	73.984	19.281	-14.47	4.6375	73.907	18.312	-12.28	79.87	75.39	78.79	76.08	3.598
00211+5447	CBL 3		332.118	18.03992	5.7191	75.425	8.714	8.82	5.6807	75.713	8.555	10.43	63.54	83.41	64.43	83.55	3.855
00215-6744	HJ 3361	AB	293.406	5.06627	4.4129	-53.342	-20.102	17.27	4.3495	-52.848	-21.031	16.94	63.62	249.35	64.26	248.30	10.774
00248+5030	KPP1866		211.506	14.46339	3.4277	40.495	-16.087	1.67	3.4742	40.499	-16.434	1.16	60.28	111.67	59.64	112.09	12.736
00250-5904	SPM 2		3.943	24.51298	5.8662	82.091	66.293	17.47	5.9561	82.592	67.876	20.27	87.03	51.08	87.46	50.59	8.392
00276+1616	GWP 52		73.467	19.52921	2.5648	50.140	-4.752	-0.67	2.6465	50.352	-4.498	0.32	93.08	95.41	90.54	95.10	39.258
00280-3051	UC 375		335.925	39.77174	4.4577	-30.718	-44.846	-3.77	4.5852	-28.046	-44.646	-3.86	57.92	214.41	54.64	212.14	20.346
00298+0727	LOC 1		77.057	9.27217	3.4029	-15.519	-30.537	-7.81	3.4884	-16.535	-31.076	-7.98	48.35	206.94	48.49	208.02	23.492

Table 4. WDS pairs assumed to be of common origin

Counter-Check of Reported Common Origin Pairs

(Continued from page 61)

- Sep = Separation from GAIA DR2 positions in arcseconds
- *e_Sep = Error separation
- *Vest1 = Vmag1 estiamted from GAIA DR2 G/B/R-mags
- *Vest2 = Vmag2 estiamted from GAIA DR2 G/B/R-mags
- Plx1 = Parallax 1 in mas
- pmra1 = Proper motion RA 1 in mas/yr
- pmdec1 = Proper motion Dec 1 in mas/yr
- rV1 = Radial velocity 1 in km/s
- Plx2 = Parallax 2 in mas
- pmra2 = Proper motion RA 2 in mas/yr
- pmdec2 = Proper motion Dec 2 in mas/yr
- rV2 = Radial velocity 2 in km/s
- *Vt1 = Transverse velocity 1 in km/s
- V1 = Spatial velocity 1 in km/s
- V1D = Velocity 1 direction
- *Vt2 = Transverse velocity 2 in km/s
- V2 = Spatial velocity 2 in km/s
- V2D = Velocity 2 direction
- D_1-2 = Spatial Distance between the components in lightyears calculated by inverting the given parallaxes
- *met50_1 = GAIA DR2 StarHorse median metallicity 1 in dex
- *met50_2 = GAIA DR2 StarHorse median metallicity 2 in dex
- *dmet50 = Metallicity difference between the components

* = Data given only in download file

A side result of this matching process is that WDS objects BPM 489/490/491/492/493/494 have an identical primary.

6. Acknowledgements

The following tools and resources have been used for this research:

- DSS2 images
- Aladin Sky Atlas v10.0
- GAIA DR2 catalog
- LAMOST DR4 catalog
- GAIA DR2 StarHorse catalog
- Washington Double Star Catalog
- CDS VizieR
- GAIA Archive (ADQL Search)
- Gaia@AIP Services hosted by the Leibniz-Institute for Astrophysics Potsdam (AIP)

7. References

Anders, F., et al., 2019, “Photo-astrometric distances, extinctions, and astrophysical parameters for Gaia DR2 stars brighter than G = 18”, *Astronomy & Astrophysics*, 10.1051/0004-6361/201935765.

Harshil Kamdar, et al., 2019, “Stars that Move Together Were Born Together”, arXiv:1904.02159 [astro-ph.GA]. Submitted to ApJL

Knapp, Wilfried R. A., 2018, “A New Concept for Counter-Checking of Assumed Binaries”, *Journal of Double Star Observations*, **14** (3), 487.

Appendix

Description of the PGR assessment procedure (according to Knapp 2018)

GAIA DR2 data for RA/Dec and Plx are used for a Monte Carlo simulation assuming a normal distribution for these parameters with the given error range as standard deviation. The distance between the components is calculated from the inverted simulated parallax data and the simulated angular separation using the law of cosines

$$\sqrt{a^2 - 2ab\cos\gamma + b^2}$$

with a and b = distance vectors for the stars A and B in lightyears calculated as (1000/Plx)*3.261631 and γ = angular separation in degrees calculated as

$$\gamma = \arccos\left[\sin(DE1)\sin(DE2) + \cos(DE1)\cos(DE2)\cos(|RA1 - RA2|)\right]$$

The likelihood for potential gravitational relationship (LPGR) is the percentage of simulation results <200,000 AU (~1 parsec) out of the simulation sample with a size of 120,000 corresponding with the likelihood that the real distance is smaller than 200,000 AU with an margin of error of 0.37% at 99% confidence.

The smallest, median and largest distance is the smallest, median and largest result of the simulation sample.

TYC 2036-1173-1: An Optical Triple Star System in Corona Borealis?

Trygve Prestgard
trygvep@hotmail.fr

Abstract: TYC 2036-1173-1 is a V= 12.4 mag star in Corona Borealis, neighboured by two fainter stars of V= 15.7 mag and V=17.1 mag. While their colours and comparable proper motion might be suggestive of a true visual triple star system, astrometric data from Gaia DR2 and UCAC5 indicate that they may potentially be unrelated.

Introduction

While hunting for uncataloged multiple stars in SDSS images, I came across an interesting group of three stars that give the appearance of a visual triple star system in survey imagery (see figure 1). The system is composed of TYC 2036-1173-1 (V= 12.36), UCAC4 579-051312 (V=15.65) and UCAC4 579-051311 (V= 17.13), which I have decided to label A, B and C respectively throughout the rest of this paper. The group appears to be absent from the SIMBAD, Stelle Doppie and Vizier database.

In the case of A, the Visual Magnitude and the B-V colour index were extracted from the APASS (Henden, 2016) catalogue. However, due to the fainter nature of B and C, their B-V indices and Visual magnitude could only be determined from GSC2.3 (STScI, 2006) data.

The B-V and the Gaia Bp-Br colour indices (Gaia Collaboration, 2018) of these stars indicate that they have the following spectral types: G9.5V or K1V (A), K4V or K6.5V (B), and K6.5Vor M1.5V (C). These colours reflect the appearance of the stars in survey imagery (e.g. figure 1), as well as those of a potentially true trinary system. Based on the absolute magnitude of the Gaia G filter (MG) and the Bp-Br colours (Gaia Collaboration, 2018) it appears that A and B are of the main sequence (Gaia Collaboration, 2018b). The lack of Gaia DR2 parallax data for the faintest component (see Table 3) makes it impossible to calculate its MG. However, the object's faint Mid-IR response in WISE suggests that it is most likely a main-sequence star rather than a K or M-type giant. The photometric properties of these stars are summarized in Table 1.

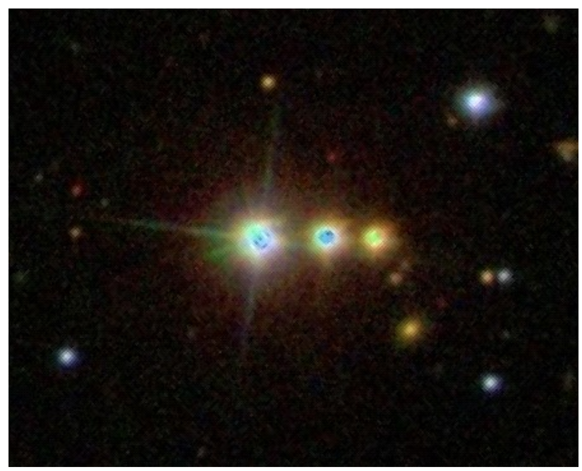

__Figure 1:__ Discovery SDSS image extract showing the group of three stars. Their visual appearance in this image is much like that of a triple star system. From left to right: TYC 2036-1173-1 (A), UCAC4 579-051312 (B) and UCAC4 579-051311 (C). The image was taken on B2003.4818.

Star	Mag	MG	G	Bp	B-V	Bp-Br
A	12.4	3.5	12.3	12.7	0.83	0.96
B	14.0	7.3	14.0	14.6	1.62	1.32
C	16.0	--	15.4	16.2	2.17	1.69

Table 1. Photometry (APASS, Gaia DR2 and GSC2.3)

TYC 2036-1173-1: An Optical Triple Star System in Corona Borealis?

Star	UCAC5 PM (RA)	UCAC5 PM (DEC)	URAT1 PM (RA)	URAT1 PM (DEC)
A	-9.3	12.3	-6.4	17.7
B	-7.4	13.8	-5.5	21.6
C	-13.8	7.0	-5.1	17.2

Table 2: Proper Motion (UCAC5 and URAT1)

Astrometry

In regards to the astrometric properties of this system, the URAT1 (Zacharias, 2015) catalogue indicates that all three stars have a relatively similar proper motion, especially A and C (see Table 2), very much like a true common proper motion triplet. UCAC5 (Zacharias, 2017) shows comparable proper motion values to URAT1, but indicates that A and B are significantly more similar in terms of their proper motion than C (see Table 2).

Interestingly, astrometric data from Gaia DR2 shows that A and B are likely unrelated based on their parallax. Indeed, B appears to be significantly closer than A (~950 ly and ~1860 ly respectively), even when including the measurement uncertainties . Gaia DR2 measurements were also used to calculate the apparent separation (Sep) and the Position angle (PA). The Gaia DR2 astrometry measurements for these stars are summarized in Table 3. Note that the UCAC5 measurements are significantly more similar to Gaia DR2 in comparison to URAT1.

Unfortunately, Gaia DR2 does not list any astrometric data for C, with the exception of positional data. Hence, it is not possible to rule out the possibility of C being at a similar distance to A or B. Indeed, the apparent separation is such that C could theoretically be gravitationally bound to either A or B, based on the parallax measurements of the latter two. More specifically, assuming C is at the same distance as A, the physical distance would be ~2.5 ly. In comparison, the separation would be ~0.5 ly if at the same distance (bound) to B. However, due to the differences in the proper motion measured by UCAC5, it is possible that C may be unrelated to A and B.

Conclusion

While the colors and the relatively similar proper motion of TYC 2036-1173-1, UCAC4 579-051312 and UCAC4 579-051311 are indicative of a trinary star system (especially according to URAT1 astrometry), Gaia DR2 shows that the two brightest members are likely unrelated based on their parallax. Furthermore, UCAC5 astrometry indicates that the faintest member differs significantly in its proper motion from the two others (despite being relatively similar), hence indicating that this star may perhaps be unrelated to the two others. Further study may be needed to assess the true nature of this system, especially in the case of UCAC4 579-051311 in relation to the two others.

Acknowledgments

This work has also made use of data from the European Space Agency (ESA) mission Gaia (https://www.cosmos.esa.int/gaia), processed by the Gaia Data Processing and Analysis Consortium (DPAC, https://www.cosmos.esa.int/web/gaia/dpac/consortium). Funding for the DPAC has been provided by national institutions, in particular the institutions participating in the Gaia Multilateral Agreement.

References

Evans et al., 2018, “Gaia Data Release 2: Photometric content and validation”, ArXiv e-prints

Gaia Collaboration, 2016, “The Gaia mission”, *A & A* **595**, A1.

Gaia Collaboration, 2018, “Gaia Data Release 2: Summary of the contents and survey properties”. ArXiv e-prints.

Gaia Collaboration, 2018b, “Observational Hertzsprung -Russell diagrams”, *A & A*, **616**, A10.

Henden, A., et al., 2016, “VizieR Online Data Catalog: AAVSO Photometric All Sky Survey (APASS) DR9”

Lindegren, L., et al., 2018, “Gaia Data Release 2: The astrometric solution”, ArXiv e-prints.

Luri, X., et al., 2018, “Gaia Data Release 2: using Gaia parallaxes”, ArXiv e-prints.

Star	Coordinates (RA+DEC)	PM (RA)	PM (DEC)	Plx (mas)	Sep	PA
A	154525.06+253740.2	-9.25	11.81	1.75	--	--
B	154524.29+253740.3	-7.50	14.29	3.44	10.6″	271°
C	154523.74+253740.3	--	--	--	17.8″	270°

Table 3: Gaia DR2 Astrometry

STScI., 2006, “The Guide Star Catalogue, Version 2.3.2”.

Riello, M. et al., 2018, “Gaia Data Release 2: processing of the photometric data”, ArXiv e-prints.

Zacharias, N., et al., 2015, “VizieR Online Data Catalog: URAT1 Catalogue”

Zacharias, N., et al., 2017, “VizieR Online Data Catalog: UCAC5 Catalogue”

Measurement of Rasalgethi with a DSLR Camera

Blake Nancarrow

Bradford, Ontario, Canada
RASC Carr Astronomical Observatory, Blue Mountains, Ontario, Canada
astronomy@computer-ease.com

Abstract: In an effort to apply new methods learned, digital images were acquired of Rasalgethi aka STF 2140 AB and nearby calibration stars with a DSLR affixed to a C14 to determine the position angle and separation. On analysing the images in REDUC software, a position angle of 103.3 degrees and separation of 4.90 arc-seconds was calculated.

Introduction

While I learned to visually measure doubles with the Celestron Micro Guide, I was inclined to use a DSLR camera. Ernõ Berkó helped me understand the equipment I would need and process that I should use.

I chose Rasalgethi or Alpha Herculis, WDS ID 17146+1423 (STF2140AB), to practice my data gathering workflow. I prepared a list of calibration stars in the vicinity using the SkyTools planning software.

My observations were made at Carr Astronomical Observatory. I used a Canon 40D (unmodified) camera body on an unguided Celestron 14-inch f/11 SCT with Optec TCF-S temperature-controller focuser. The 'scope was permanently mounted atop a Paramount ME controlled by TheSky6. The OTA primary mirror was not locked. The camera was controlled remotely with the EOS Utility software running on a small netbook computer. The camera was set to use ISO 1000 and capture in RAW format (3888x2592 pixels). The focal length of the C14 is approximately 3.9 metres; no further magnification (i.e. Barlow) was used.

In all the included images, north is up and east is left.

Methods

My observations were made on 15 July 2015 (2015.53) between 12:30 AM and 3:30 AM Eastern Standard Time. Work was conducted at this time to avoid a meridian flip with the equatorial mount. Approximately 100 digital images in total were captured. The altitude of the target stars ranged from +62° through +33 during the session.

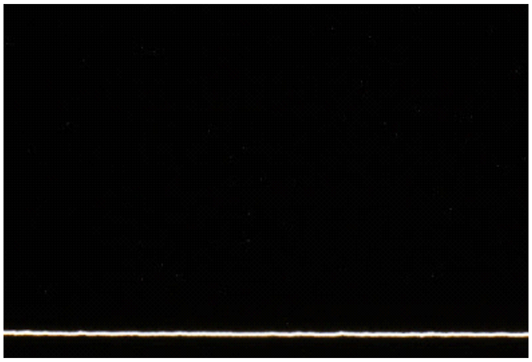

Figure 1. Image captured during drifting process showing alignment to the declination axis.

Using the camera Live View, I focused on the star Unukalhai aka Alpha Serpentis initially moving the C14 primary, then using the Optec hand paddle.

I rotated the camera in the focuser to align the long edge of the frame with the declination axis and captured a couple of long exposure images, drifting Unukalhai with the mount tracking off, to refine the alignment. The camera was not touched after this time. I then slewed Unukalhai to the bottom edge of the frame from centre so to ease verification (Figure 1). I programmed a dozen shots to record the camera orientation, repositioning Unukalhai at the east edge of the field before each exposure.

Measurement of Rasalgethi with a DSLR Camera

Figure 2. Calibration star HD 159481 aka Σ2185 exposed at 30 seconds.

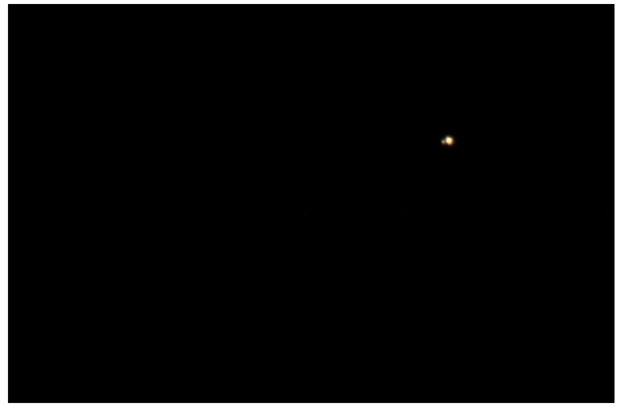

Figure 3. Image of Rasalgethi aka Σ2140 captured at 1/15th of a second.

The mount was then slewed to previously selected calibration stars. Several images were captured for each star. Various exposures were taken to ensure the dimmest element remained visible while avoiding over-exposing the bright stars. For each calibration star 3 to 8 images were captured. Exposure times ranged from 30 seconds to 1/125th of a second. The digital image of HD 159481 (STF 2185) in Ophiuchus revealed a multi-star system with over 8 elements (Figure 2).

The altitude of Rasalgethi was approximately +36° when imaged. Over 15 digital images were captured for Rasalgethi, again at various exposures. The exposure of Alpha Her at 1/15th of a second reveals the delicate companion B aside the bright primary (Figure 3).

After the session, the drift alignment, calibration star, and target star shots were processed and converted to JPG format using the Canon Digital Photo Professional software. The evening's proceedings with a selection of images were documented on my astronomy blog.

Analysis

All images were converted at full size from Canon CR2 RAW format to Windows BMP with IrfanView 4.51 .

REDUC 5 software by Florent Losse was used with Automatic Centering enabled.

A total of 16 drift images were captured for declination analysis (Table 1). The Δ or image inclination in relation to the celestial equator was measured for each image. The average was calculated at -0.20 with a standard deviation of 0.04.

The calibration images were visually assessed. The best ones selected showed good exposure and little or no vibration. Similarly, the best exposure (file IMG_5171) of Rasalgethi was selected for final analysis.

In September 2015, the first pass at calculating the image scale or E value of the calibration star images was performed using separation values from the SkyTools 3 Professional software. From the 12 images, an average value of 0.56 was obtained. When the inclination and scale average values were applied a single image of Rasalgethi, the position angle of 103 and separation of 4.8 were derived. These compared well to the values shown in SkyTools for alpha Her: 103 and 4.6.

A later pass was conducted using the separation values as found at the time in the WDS. The scale average value 0.56 was obtained. When calculations were performed for the target star, REDUC yielded the values 102 and 5.3.

image file	Δ	notes
IMG_5105	-1.16	different position
IMG_5106	-0.15	
IMG_5107	-0.17	
IMG_5108	-0.18	
IMG_5109	-0.25	
IMG_5110	-0.23	
IMG_5111	-0.28	
IMG_5112	-0.19	
IMG_5113	-0.21	
IMG_5114	-0.21	
IMG_5115	-0.18	
IMG_5116	-0.22	
IMG_5117	-0.20	
IMG_5118	-0.19	
IMG_5119	-0.14	windy
IMG_5120	-0.21	

Table 1. Image files for drift analysis with inclination values from REDUC.

Measurement of Rasalgethi with a DSLR Camera

Another attempt was made in July 2018 again drawing the reference separation values for the calibration stars from the WDS (Table 2). It was noted a couple of the entries had reports post-dating the period when the image data was captured. Nevertheless, E was computed to be 0.28 with a standard deviation of 0.00. The inclination and scale averages were applied to the Rasalgethi image yielding theta 103.3 and rho 4.90. The published values for 17146+1423 [STF2140AB] from 2017 were 104 and 4.8.

image file	WDS ID	last	ρ	E
IMG_5151	16315+0818 SHJ 233	2015	59.2	0.28
IMG_5158	16435+2043 STTA149	2011	97.7	0.28
IMG_5135	16442+2331 STF2094AC	2013	24.7	0.28
IMG_5191	17249+1320 STF2159	2015	26.4	0.28
IMG_5197	17348+0601 PWS 16AH	2001	187.3	0.28
IMG_5200	17433+1741 STH 4	2010	15.5	0.28
IMG_5156	16354+1703 WEB 6	2015	155.5	0.28
IMG_5168	17037+1336 STFA 33AB	2014	304.9	0.28
IMG_5203	18057+1200 STF2276AC	*2016*	63.8	0.28
IMG_5129	16081+1703 STF2010AB	*2017*	27.0	0.28
IMG_5142	17150+2450 STF3127AD	2009	191.6	0.28
IMG_5192	17016+1457 H 4 122	2014	18.9	0.28

Table 2. WDS separation values for the calibration stars with scale E values from REDUC.

Conclusions

I set out to practice digital imaging a double star to be measured and calibration stars for determining the image scale.

The double star STF 2140AB was measured with a DSLR. The separation was found to be 4.9 arc seconds and the position angle was determined to be 103.3 degrees (Table 3).

Acknowledgements

I am grateful for Geoff Gaherty's support while at the early stages of my fascination with double stars. I thank Ernõ Berkó for helping me understand how to capture doubles with a DSLR. I found Jolyon Johnson's video and the text in Bob Argyle's book very helpful in preparing a paper. I thank Dr Roberto Abraham for his guidance in writing a scientific paper. I appreciate the access to the research-grade telescope and mount equipment at the CAO offered through my RASC Toronto Centre membership. And thanks for Florent Losse for providing the REDUC software.

References

The Baader Micro Guide is equivalent to the Celestron Micro Guide. https://www.baader-planetarium.com/en/micro-guide-eyepiece-with-log-pot-illuminator.

SkyTools 3 Professional planning software. https://www.skyhound.com/skytools.html

REDUC software. http://www.astrosurf.com/hfosaf/uk/tdownload.htm

IrfanView software, https://www.irfanview.com/

Author blog post noting local weather conditions with Clear Sky Chart 3 hours prior to session. http://blog.lumpydarkness.com/2015/07/the-sun-through-clear-band.html.

Author blog post with a fast exposure colour image of Rasalgethi showing the B companion. http://blog.lumpydarkness.com/2015/07/shot-rasalgethi.html

Author blog post featuring detailed report of imaging run with drift and all calibration star images. http://blog.lumpydarkness.com/2015/07/performed-full-double-star-imaging-run.html

Washington Double Star catalog. http://www.astro.gsu.edu/wds

How to Write a Double Star Research Paper. Jolyon Johnson YouTube video, 2015, https://www.youtube.com/watch?v=akF3T4on0mA

Observing and Measuring Visual Double Stars, 2/e, Bob Argyle, Ed, 2012. Springer, New York.

"Observing Double stars for Fun and Science", Ronald Tanguay, *Sky and Telescope*, Feb 1999, https://www.skyandtelescope.com/observing/celestial-objects-to-watch/observing-double-stars-for-fun-and-science/

Name	RA+Dec	PA	Sep	Date	N	Note
STF2140AB	17146+1423	103.3	4.90	2015.53	1	1

1. Canon 40D (unmodified) camera and Celestron 14 inch f/11 SCT.

Table 3. Final calculated separation and position values for Rasalgethi.

"Double-Star Measurement Made Easy", Thomas Teague, *Sky and Telescope*, pg 112, July 2000.

"Double Star Measures Using a DSLR Camera", Ernõ Berkó, *JDSO*, **4**(4), 144, 2008.

"Double Star Measurements in the Pleiades Cluster Using a DSLR Camera", Michel Michaud, *JDSO*, **8** (4), 249, 2012.

Blake Nancarrow has observed double stars as a young amateur astronomer. His first log entry of a double was made in June 1991. He learned and practiced the Celestron steps, Ronald Tanguay's techniques, and Tom Teague's method, developing his own refined workflow. On reading Ernõ Berkó's 2008 and Michel Michaud 2012 JDSO papers on using a DSLR to capture double star data, he decided to go the digital imaging route.

The Carr Astronomical Observatory on Blue Mountains in south-western Ontario is owned and operated by the Royal Astronomical Society of Canada - Toronto Centre. Nancarrow is one of the site supervisors.

CCD and Gaia Measurements Indicate that WSD 12095 + 3356 is a Physical System

Alexa Brammer [1], Jessica Padron-Loredo [1], Charmain Brammer [1], and Cameron Pace [2]

1. SUCCESS Academy
2. Southern Utah University

Abstract: The Double Star System WSD 12095 + 3356 was observed using the Great Basin Observatory telescope. The images were plate solved and calibrated, and then position angle and separation were measured using AstroImageJ. Our measurements (θ = 324.131° and ρ = 63.490”) were compared to historical observations. Parallax and proper motion data from the Gaia database indicate that the stars in this system are physically associated.

Introduction

The goal of this project was to provide additional measurements of the separation and position angle to determine if WSD 12095 + 3356 is a binary system. WSD 12095 + 3356 is recorded as a double star with components A and B. It was first observed in 1998 and most recently in 2015, with a total of six observations. This system was selected because it could be viewed with the Great Basin Observatory (GBO) Telescope. This research was done by high school students from SUCCESS Academy (an early college high school) in collaboration with Southern Utah University.

Figure 1. The Great Basin Observatory and the control room (Anselmo et al. 2018).

Methods

This research was conducted using the telescope at the Great Basin Observatory in Great Basin National Park (Figure 1). The GBO is the first research grade telescope in a national park. It is managed by the Great Basin National Park and the Great Basin National Park Foundation, in collaboration with Concordia University, Southern Utah University, University of Nevada-Reno, and Western Nevada College. The telescope has an aperture of 27 inches (Anselmo et al. 2018).

The images of WSD 12095 + 3356 (Figure 2) were acquired remotely on February 22, 2018. A total of 26 images were taken with an exposure time of 180 seconds with the V filter. The exposure time was chosen so the target stars would not be over-exposed. The images were binned 1x1. Images were plate solved using astrometry.net and then the images were calibrated by applying dark, bias, and flats using AstroImageJ version 3.2.27 (Collins et. al 2017). Position angle (θ) and separation (ρ) were measured through AstroImageJ.

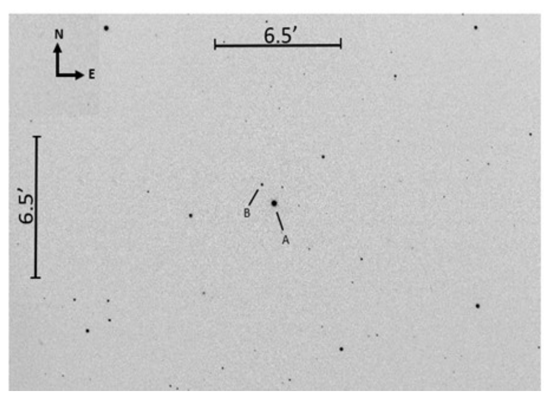

Figure 2. Image of A and B components of WSD 12095 + 3356. Plate scaled at 0.4 arcsec/pixel.

CCD and Gaia Measurements Indicate that WSD 12095 + 3356 is a Physical System

WDS No.	ID	Nights	Date	Observations		θ°	ρ″
12095 + 3356	GRV 853	1	JD2458172 Feb.22,2018	26	Mean	324.131	63.490
					Std. Dev.	0.028	0.230
					Std. Error	0.056	0.005

Table 1. Observations from the data collected. θ, ρ, mean, standard deviation, and standard error.

The centroid feature was used to improve accuracy by measuring from the center of each star. All data was exported into Excel to calculate the mean, standard deviation, and standard error for θ and ρ.

Results

The mean, standard deviation, and standard error were measured for the star system, and the results are shown in Table 1.

Discussion

Table 2 shows the historical data for WSD 12095 + 3356. The measurements cover 1998 to 2015 with six observations in total. In Figure 3, the measurements are shown, with the primary star at (0,0). All of the data is in the same range, but there are two possible outliers. As seen in Figure 4, either the original observation in 1998 or the 2004 data could be an outlier. Stars do not move several arcseconds away then return to their previous positions. This could mean that the data from 2004 is be spurious, as Figure 4 shows that with the exception of the 2004 data point, the other observations suggest a more linear form for the motion of the B component.

To further determine if the stars are physically associated, we retrieved data from the Gaia database (Gaia Collaboration, 2018) for the parallax and proper

Epoch	θ°	ρ″
1998.19	324.0	63.770
2000	324.0	63.600
2002.04	324.0	63.568
2004.205	324.500	63.395
2010.5	324.100	63.560
2015	324.064	63.581
2018.17	324.131	63.490

Table 2. Historical Data for WSD 12095 + 3356.

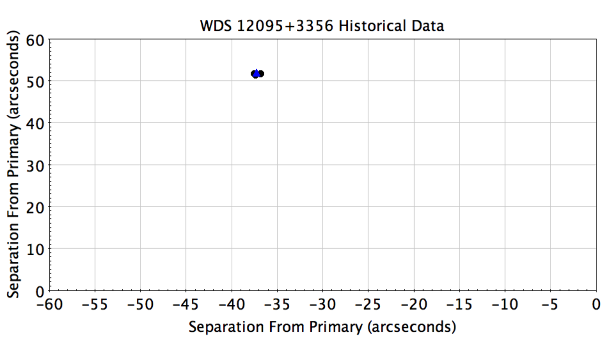

Figure 3. This graph shows our measurements (orange triangle) along with historical measurements (blue circles) around the primary star. The measurements are in arcseconds. In this graph, the primary star is located at the origin.

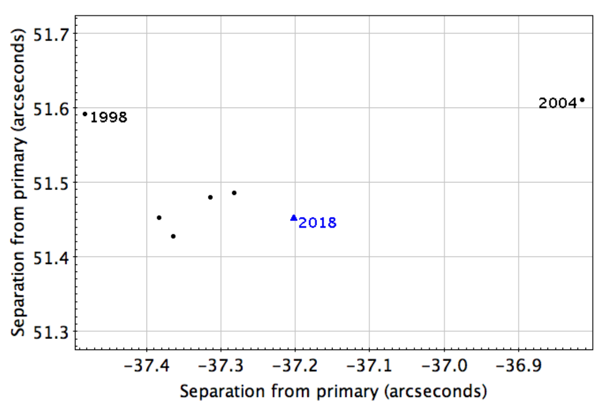

Figure 4. A closer look at the historical data (blue circles) and collected data (orange triangle). The data points suggest the secondary star is orbiting the primary star, but there is one discrepant data point, which is the 2004 measurement.

Component	Right Ascension	Declination	Parallax [mas]	Parallax Error [mas]	Proper Motion RA	Proper Motion DE
A	182.391	33.944	5.847	0.077	-59.935	12.358
B	182.379	33.958	5.840	0.045	-59.319	12.661

Table 3. Data obtained from the ESA Gaia telescope (Gaia Collaboration, 2018). Both the parallax and proper motion data indicate that the stars are indeed a binary.

motion of each star. The coordinates of the stars are given in the second and third column of Table 3. The parallax is the measurement of how far away the stars are from Earth. When the parallax is converted to parsecs we find that both stars are at a similar distance (171 parsecs). However, since Gaia's accuracy begins to drop off around 5 mas, we can only conclude that the stars in this system are physically associated. Table 3 shows that both stars have similar proper motion in declination and right ascension, which further suggests they are physical stars. The distance data agrees with the proper motion data; both stars are at a similar distance and moving the same way, which indicates that the system is physical. To determine if this pair forms a binary system, an orbit would need to be computed.

Acknowledgments

This project was made possible by the collaboration with Southern Utah University and the Great Basin Observatory (GBO). We would like to thank those who operate the GBO. This research made use of AstroImageJ, Astrometry.net, and the Washington Double Star Catalog maintained by the U.S. Naval Observatory. This work has made use of data from the European Space Agency (ESA) mission Gaia (https://www.cosmos.esa.int/gaia), processed by the Gaia Data Processing and Analysis Consortium (DPAC, https://www.cosmos.esa.int/web/gaia/dpac/consortium). Funding for the DPAC has been provided by national institutions, in particular the institutions participating in the Gaia Multilateral Agreement.

References

Anselmo, Dallas, et al., 2018, "CCD Measurements of AB and AC Components of WDS 20420+2452", *Journal of Double Star Observations*, **14** (3). http://www.jdso.org/volume14/number3/Anselmo_492_495.pdf

Collins, K. A., Kielkopf, J. F., Stassun, K. G., & Hessman, F. V., 2017, *The Astronomical Journal*, **153** (2), 77.

Gaia Collaboration Brown, A. G. A. Vallenari, A. Prusti, T. de

Bruijne, J. H. J. et al., 2018, "Gaia Data Release 2. Summary of the contents and survey properties." *Astronomy & Astrophysics*, **616**, A1.

Great Basin Observatory, 2016, retrieved Feb. 22,2018, from http://planewave.com/great-basinobservatory/

Mason, Brian D, 2019, The Washington Double Star Catalog, Astronomy Department, U.S. Naval Observatory.

Astrometric Measurement of WDS 12459-7511 HJ 4545

Isabel Zheng[1], Yael Brynjegard-Bialik[1], Jackie Roche[1], Pat Boyce[2], and Grady Boyce[2]

1 West Ranch High School, Stevenson Ranch, California, USA
2 Boyce Research Initiatives and Education Foundation, San Diego, California, USA

Abstract: This paper reports the astrometric measurements of the double star system WDS 12459-7511 HJ4545 using the Las Cumbres Observatory. We found the relative position of the AB pair to have a separation of 9.15" and position angle of 192.6° for epoch 2019.294. Additionally, the relative position of the AC pair was also measured to have a separation of 36.9" and position angle of 238.0° at for epoch 2019.294. When combined with GAIA parallax and proper motion data, the results strongly suggest that the AB pair is gravitationally bound and the AC pair is optical.

Introduction

The binary star HJ 4545 was selected because it met the following requirements:

- Observable from the Southern Hemisphere in the spring
- Angular separation of at least 5 arcseconds
- Difference in magnitude of no more than 3

HJ 4545, Figure 1, was first observed by John Herschel in 1835. Since the initial measurement, HJ 4545AB has been observed 22 times with the latest measurement in 2000 (Sordiglioni, G.).

The primary star has a spectral type of A5V (Mason and Hartkopf, 2015), and is a main sequence star. According to data from Tycho in the visible band, the A star has a magnitude of 9.1, the B star has a magnitude of 9.25, and the C star has a magnitude of 11.17. The initial and most recent measurements for each pair are outlined in Table 1. These measurements do not include those reported in this paper.

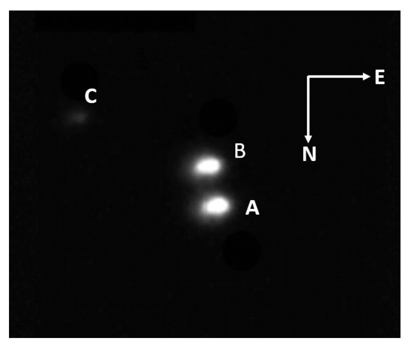

Figure 1. Image of WDS 12459-7511 cropped to show target stars.

Pair	Epoch	Theta	Rho
AB	1835 (Initial)	189.0°	12.000"
	2000 (Most recent)	192.0°	9.100"
AC	1895 (Initial)	235.9°	36.262"
	2000 (Most recent)	237.9°	36.930"

Table 1. Initial and most recent measurements of each star pair, excluding the measurements in this paper.

Materials and Methods

The images of HJ 4545 were taken in Sutherland, South Africa by an SBIG 6303 camera on a 0.4-meter Meade telescope, part of the Los Cumbres Observatory (LCO) system. A total of 7 images were measured and

Astrometric Measurement of WDS 12459-7511 HJ 4545

Epoch 2019.294	Postion Angle (θ)	Separation (ρ)
Mean	192.6	9.15
Standard Deviation	0.264	0.023
Standard Deviation of the Mean	0.1	0.009

Table 2. Results of Mira Pro astrometric measurements of WDS 12459-7511 for AB.

Epoch 2019.294	Postion Angle (θ)	Separation (ρ)
Mean	236.5	36.3
Standard Deviation	1.081	1.111
Standard Deviation of the Mean	0.120	0.123

Table 3. Results of Mira Pro astrometric measurements of WDS 12459-7511 for AC.

taken on 2019.294 with an exposure time of 15 seconds using a Bessell B filter.

The images were calibrated by Our Solar Siblings (OSS) data pipeline (Fitzgerald 2018). The software, MiraPro x64, was used to measure the position angle (θ) and separation (ρ). These separation and position angle measurements were then entered into Google Sheets for calculations of the mean, standard deviation, and standard deviation of the mean for θ and ρ.

Results

A total of seven images were measured for the separation and position angle as shown in Table 2 and Table 3 for AB and AC, respectively.

Discussion

Astrometry, derived from these current results, are plotted together with historical data from the WDS, Figure 2. There is no apparent trend in the positions of the B or C star in relation to A over the period from first observation to our 2019 observation. The only points outside the tight patterns for both are the first two for B and could well be measurement error.

We found that Stelle Doppie (Stelle Doppie Web) has classified the AC pair as physical and the AB pair as uncertain. In Richard Harshaw's analysis of the WDS data merged with the Gaia DR2 data, he classified the AC pair as "unknown" largely because the Gaia DR2 data was missing from his merged database. He classified the AB pair as very likely to be physical. These opposing classifications arise from the differences in proper motions for the stars between the WDS and Gaia DR2, Table 3. The proper motions in RA for all three components are comparable between WDS and the more accurate Gaia DR2 data. The proper motions in DEC for the A and B stars are substantially different in the WDS but almost identical in Gaia DR2. Thus, Stelle Doppie's reliance on the WDS proper motions could have led to the conclusion that AC is physical and AB is not. Conversely, when the more accurate Gaia DR2 is applied, as in Harshaw, the nearly identical proper motions for the A and B stars yield a compelling case for their being physical and possibly weaken the case for AC to be physical. Figure 3 depicts the proper

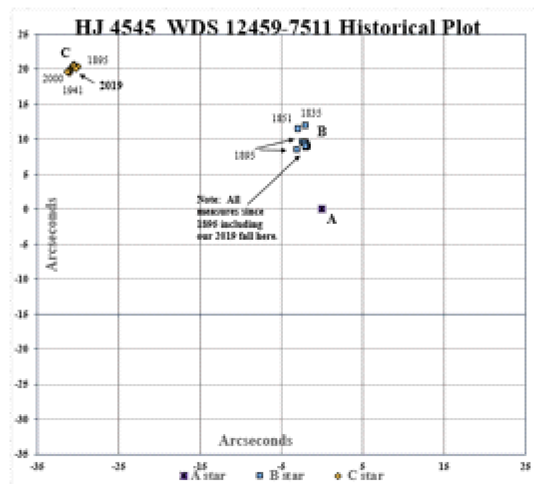

Figure 2. Historical positions of HJ4545 B and C compared to A at the origin.

Star	Proper Motion Data	RA	DEC
A	WDS	-028	+007
	Gaia DR2	-28.239	2.368
B	WDS	-030	-006
	Gaia DR2	-28.231	2.26
C	WDS	-038	+007
	Gaia DR2	-38.924	7.32

Table 3. Comparison of WDS and Gaia DR2 data for HJ 4545

Astrometric Measurement of WDS 12459-7511 HJ 4545

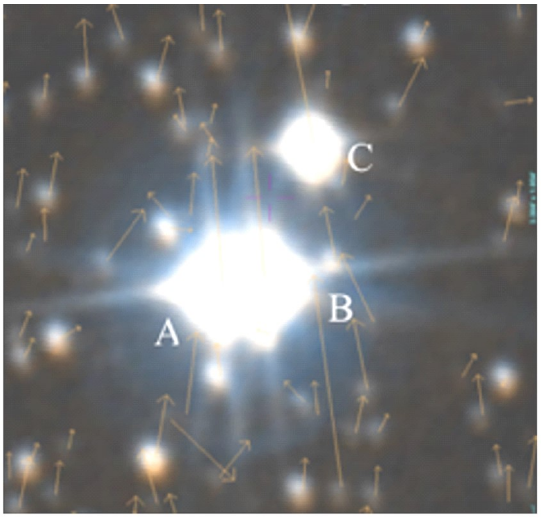

Figure 3. Image from Aladin 10 showing proper motion vectors for HJ4545

motion vectors of the system using ALADIN with GAIA data displayed.

Gaia DR2 parallax of the A star yields a distance of 789.29 light years and that of the B star yields a distance of 785.07 light years. Thus, with nearly identical proper motions and distances, this suggests the possibility that these two stars may be gravitationally bound.

The C star of the system has a parallax measure from Gaia DR2 that yields a much greater distance than the A and B at 1106.59 light years. The C star is likely to be optical as its proper motion vectors are different and its distance is distinct from the A star and B star. The parallax for the A star is 1.2669×10^{-3} arcseconds and the parallax for the B star is 1.2738×10^{-3} arcseconds while the parallax for C is drastically different at 9.0368×10^{-4} arcseconds.

Conclusion

After using the 0.4m telescope at LCO's South African observatory, we were able to provide additional astrometric data of the double star system WDS 12459-7511 HJ 4545. By applying data from Gaia DR2, we able to strongly suggest that s the AB pair is likely to be gravitationally bound and noted as a T in the WDS. The AC pair appears to be an optical double only and noted as an S in the WDS classification system.

Acknowledgments

The authors thank the United States Naval Observatory for providing historical measurement data and LCO for the use of their service, and we appreciate the ability to have Simbad and Gaia access from the CDS Strasbourg Database. We also thank Boyce Research Initiatives and Education Foundation (B.R.I.E.F.). Additionally, we thank Jerry Hilburn for his guidance and effort to the research team. Appreciation is extended to Christine Hirst for providing us the opportunity to participate in this project and supporting our team. Measurements were made using Mira Prox64, which provided accurate astrometric measurements for our double star system.

References

Fitzgerald, M.T. (2018, accepted), "The Our Solar Siblings Pipeline: Tackling the data issues of the scaling problem for robotic telescope based astronomy education projects.", *Robotic Telescopes, Student Research and Education Proceedings*

Mason, B. and Hartkopf, W. The Washington Double Star Catalog, October 2015. Astrometry Department, U.S. Naval Observatory. https://ad.usno.navy.mil/wds/Webtextfiles/wdsnewframe3.html

O'Connor, J J, and E F Robertson. "John Frederick William Herschel." John Herschel (1792-1871), July 1999, www-history.mcs.st-andrews.ac.uk/Biographies/Herschel.html.

Stelle Doppie Web: Sordiglioni, Gianluca Stella Doppie, Double Star Catalog. https://www.stelledoppie.it/index2.php?iddoppia=54877 (Accessed Sept 15, 2019)

Astrometric Measurements of OSO 51 AB

Shreya Goel[1,2], Shabdika Gubba[1,2], Pat Boyce[3], Grady Boyce[3]

1. BE WiSE
2. Thurgood Marshall Middle School
3. Boyce Research Initiatives and Education Foundation (BRIEF)

Abstract: The double star system WDS 13111+1220 OSO 51 AB was studied by a team of students using the Las Cumbres Observatory (LCO) to analyze the nature of the double star. Images were measured for position angle (Theta) and separation distance (Rho) through image analysis software AstroImageJ. The position angle was measured to be 299.33° and the angular separation was measured to be 11.467" arcseconds. It was determined through measurements and Gaia parallax data that the double is most likely an optical double and not a physical binary.

Introduction

The objective of this research was to observe and measure double star system WDS 13111+1220 OSO 51 AB. OSO 51 AB was discovered by Maria Rosa Zapatero Osorio in 1994 (Stelle Doppie Web) and has been observed 7 times from 1994 to 2001.

A primary factor considered in the selection of OSO 51 included choosing a double star system with the necessary Right Ascension (RA) for observation, between 08-14 hours, as observations were taken in spring. The difference in magnitude was also taken into consideration with the magnitudes for the A and B stars of 14.22 and 15.50 respectively, resulting in a delta magnitude of 1.28, low enough for neither star to obscure the other from view in a CCD image. The third star, C, of OSO 51 AC, with a magnitude of 19.1, was too dim to be seen in an image even with a high exposure time and could not be studied with the resources available.

The nature of OSO 51 as an optical double star system or as a binary system was to be reviewed by these observations. Proper motion and parallax are often used to determine the nature of double stars. The team used Aladin10 to find proper motion vectors for the two stars, Figure 1. Parallax is the angle subtended by the star on opposite sides of the Earth's orbit. This can be used to find the distance of the star from Earth. Stars which are very different distances from Earth, and therefore far from each other, are usually not gravitationally bound.

After requesting historical WDS data for the system, it was noted there are 7 historical measurements with the first in 1994 and the latest, before this paper, in 2001. These measurements are plotted in Figure 2. Then, a linear trendline was compared to a polynomial trendline, Figure 3 and Figure 4, for the data, and there seemed to be some sort of non-linear trend that might indicate an orbit.

Methods and Materials

The Las Cumbres Observatory (LCO) telescope network was used to acquire images. Images were captured by a 0.4-m Meade 6303 telescope, Figure 5, with an SBIG CCD camera resulting in a pixel size of 0.571" binned 1x1. The images had a field of view of 29'x19' and were taken at Haleakala Observatory, Hawaii, at 10,000 feet above sea level. Due to the dim nature of both stars in the system, no filter was used while ob-

(Text continues on page 80)

Astrometric Measurements of OSO 51 AB

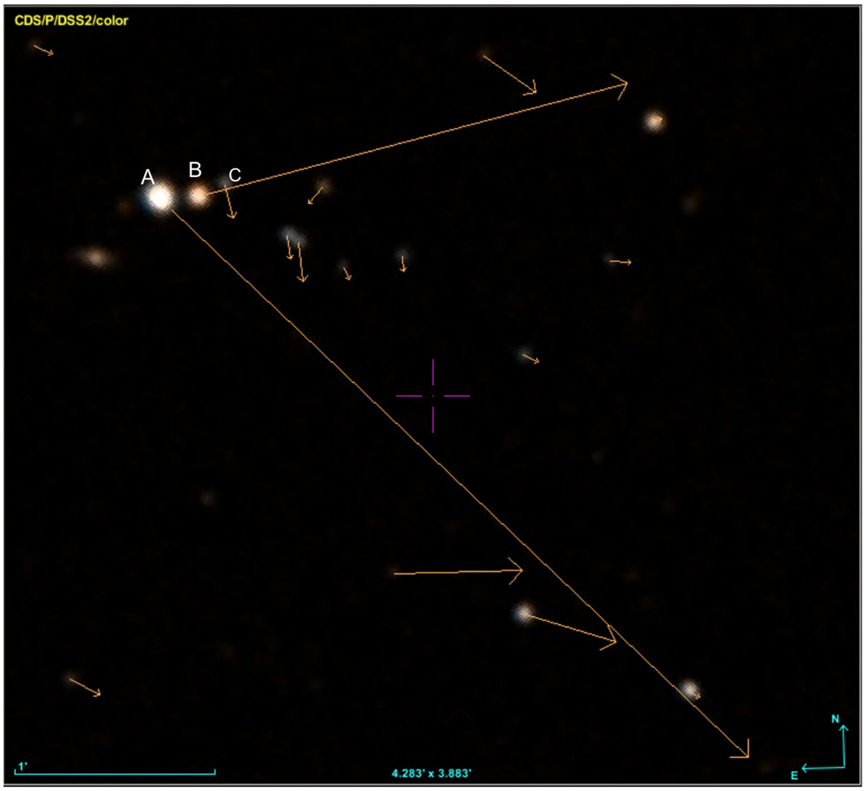

Figure 1. WDS 13111+1220 as shown on Aladin 10 with proper motion vectors.

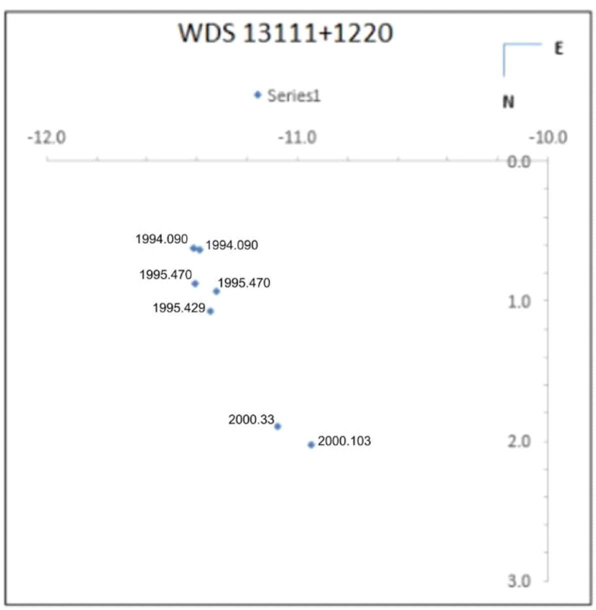

Figure 2. Graph of historical data.

Astrometric Measurements of OSO 51 AB

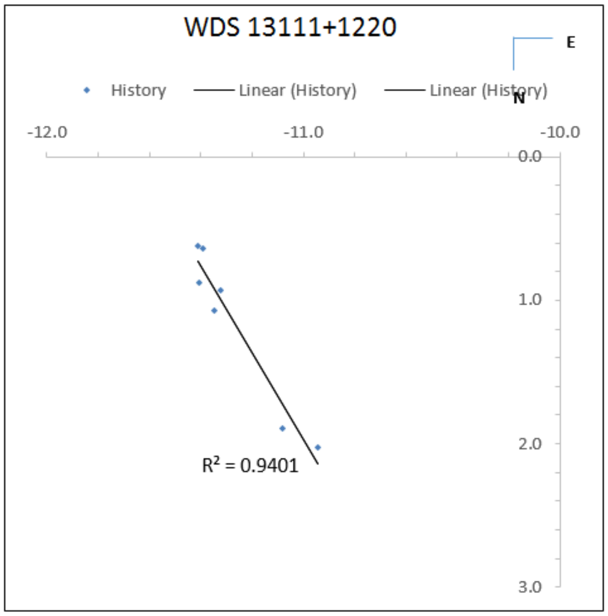

Figure 3. Graph of historical data with linear trendline

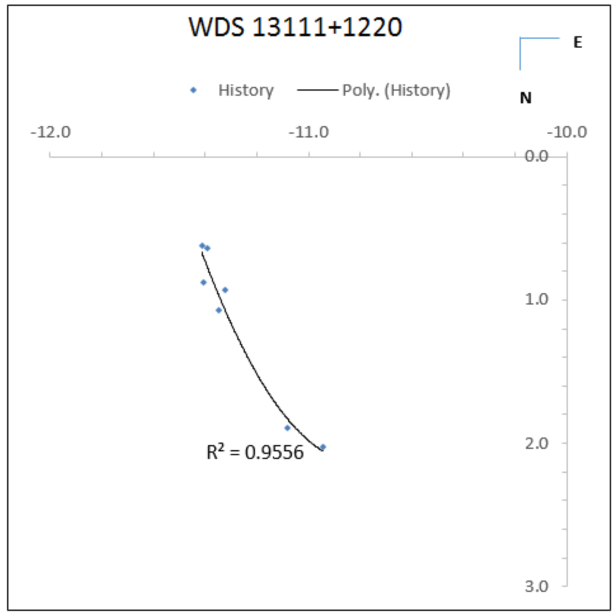

Figure 4. Graph of historical data with polynomial trendline

#	Theta (°)	Rho (")
1	299.51	11.393
2	296.84	11.923
3	301.96	11.337
4	299.05	11.551
5	299.29	11.510
6	300.14	11.000
7	298.25	11.523
8	298.86	11.530
9	299.02	11.529
10	299.22	11.572
11	299.83	11.344
12	299.11	11.373
13	299.18	11.430
14	299.96	11.515
15	299.78	11.473
Avg	299.33	11.467

Table 1. Measurements from new observations with final average. All measurements were made on Besselian date 2019.284, JD 2458588.

taining images with an exposure time of 300 seconds. 15 images were taken on 2458588.291667 (BJD).

Images were processed through the Our Solar Siblings (OSS) pipeline (Fitzgerald 2018) to ensure image quality and ease for measurement, by embedding World Coordinate System (WCS) coordinates, calibration, and photometry. AstroImageJ was used to measure separation distance and position angle.

Data and Results

Two team members independently took measurements which were then averaged to ensure greatest accuracy. Measurements of Theta and Rho are provided, Table 1. The mean position angle was calculated to be 299.33°, and the mean separation was 11.467", Table 2. The standard deviation of position angle was 1.079 and the standard deviation of separation was 0.191, indicating the data was fairly consistent, Table 2. A combination of the historical measurements with Theta and Rho from this paper are provided, Table 3. The average of all measurements is plotted in Figure 6. The data was graphed, showing how it made sense and seemed rea-

(Text continues on page 82)

Epoch	# of obs.	Mean PA	Std. Dev.	Mean Sep.	Std. Dev.
2019.284 JD2458588	15	299.3	1.1	11.47	0.19

Table 2. Mean Position Angle (Theta) and Angular Separation (Rho) with related statistics.

Astrometric Measurements of OSO 51 AB

Figure 5. 0.4-m Meade telescope provided by LCO.

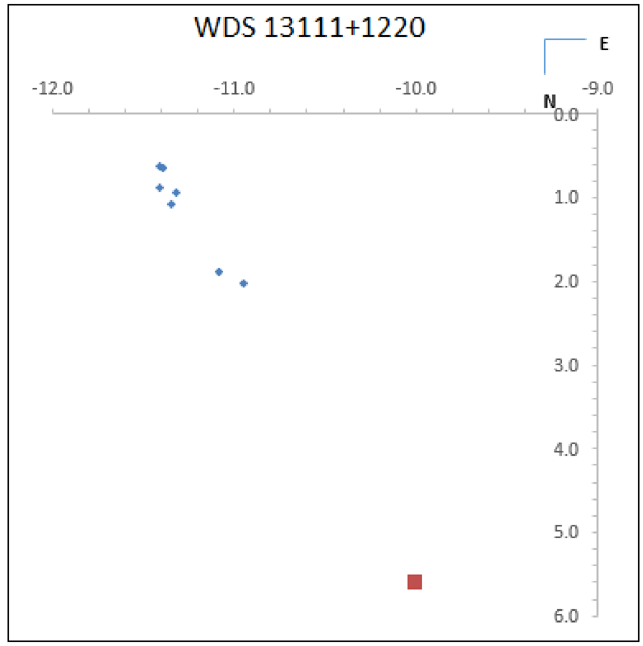

Figure 6. Historical data graphed alongside the average of the measurements presented in this paper. The gap between current and historic measurements is expected for the time passage.

Epoch	PA	Sep
1994.109	273.1	11.43
1994.09	273.2	11.41
1995.429	375.4	11.4
1995.47	374.4	11.44
1995.47	274.7	11.36
2000.33	279.7	11.24
2001.103	280.5	11.13
2019.284	299.3	11.5

Table 3. Historical measurements for OSO 51 AB with Theta and Rho from this paper.

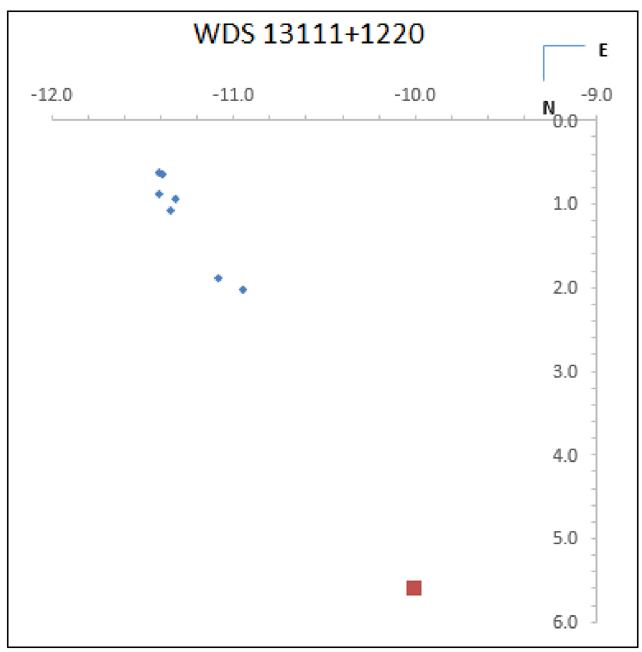

Figure 6. Historical data graphed alongside the average of the measurements presented in this paper. The gap between current and historic measurements is expected for the time passage.

Astrometric Measurements of OSO 51 AB

(Continued from page 80)
sonable as the average of the group's data lined up well with historical data, Figure 6.

Discussion

With the historical and current data sets combined, a seeming linear trend was observed, Figure 7. Figure 8 was used as a comparison between a polynomial trend and a linear trend. After comparing a linear trend and a polynomial trend, the polynomial trend had a slightly lower error by 0.0018, but the difference between the linear and polynomial trends was so minimal, that it was decided that, it is likely a linear trend, or possibly a nonlinear trend that we do not have enough data to see. With current measurements, it was observed that the system most likely was not a binary system. In the 2019 measurement, the position angle, Theta, increased, relative to historical data, Table 3. Graphing all measurements of Rho, Figure 9, the overall trend is consistent over time (shown with the most recent data point). Given that there is only 25 years of history, conclusions could be premature, but only further measurements in the future could prove or disprove any further theories. Relative to the primary star, the secondary star appears to be following a linear path. Without a sign of an arc, the trend line suggests the possibility that these stars are not binary.

In Aladin10, Figure 1, the proper motion vectors, displayed from GAIA data, are visible for each star. It is further suggested that the stars may not be gravitationally bound as the paths are divergent, given that the error estimate for RA was 0.02196 and the error estimate for DEC was 0.02264. Adding GAIA data for parallax, the primary star's parallax was 2.813. However, because of the low precision of GAIA's instruments, this figure may not be significant. The secondary star's parallax was 5.294, as shown in Table 4. Converting to lightyears (and parsecs) from Earth, the primary star is approximately 1158.89 lightyears, or 355.49 parsecs from Earth, while the secondary star is approximately 615.83 lightyears, or 188.9 parsecs from Earth, Table 5. Noting the stars' separation from each other, and lack of parallactic overlap, this adds to the belief that OSO 51 AB is an optical double, and not a gravitationally-bound physical binary.

Conclusion

The star system, OSO 51 AB, was studied to study whether a double star or gravitationally bound system. After independently collecting data, the average position angle was 299.33° and the average separation was 11.5". These measurements were compared alongside historical data, and it was seen that the position angle changed while the separation remained relatively con-

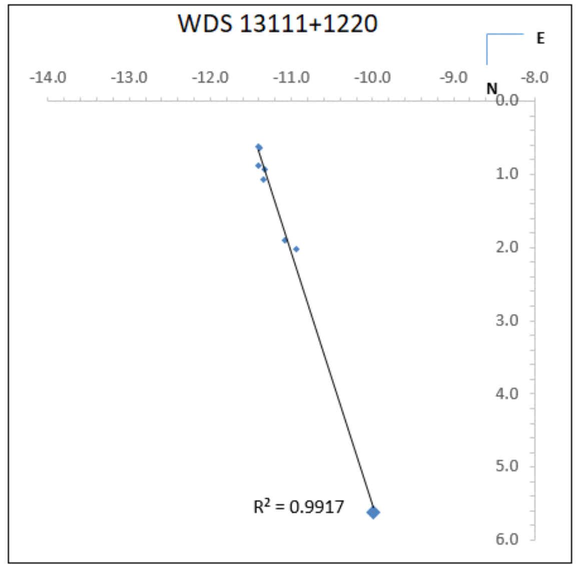

Figure 7. Historical data with average of new data along with linear trend line.

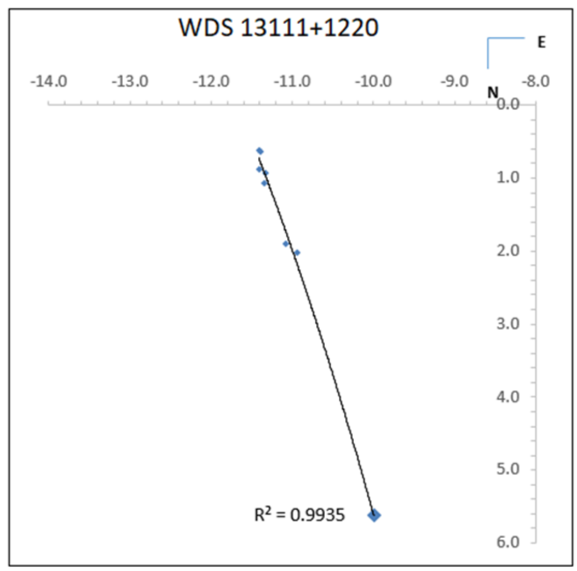

Figure 8. Historical data with average of new data along with polynomial trend line.

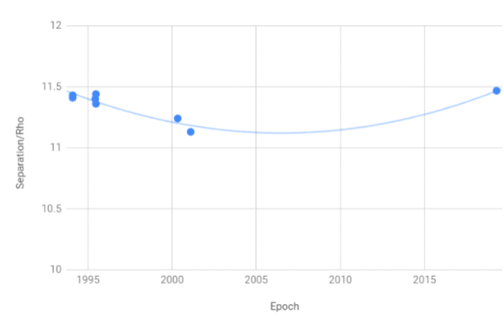

Figure 9. Graph showing Rho decreasing and then increasing over time.

Inputs	Parallax	Parallax Error
Star A	2.812	0.025
Star B	5.294	0.216

Table 4. Parallax and parallax error for OSO 51 AB.

Star	Min Distance	Midpoint	Max Distance
Primary	352.31	355.49	358.72
Secondary	181.49	188.9	196.95

Table 5. Distance from Earth for the primary and secondary stars expressed in parsecs.

stant. The addition of the European Space Agency's Gaia archives parallax data seems to support the position that these are not gravitationally bound stars based on a parallax assessment. After considering multiple factors, it is proposed that OSO 51 AB is most likely not a physical double.

Acknowledgments

The team would like to thank the Boyce Research Initiatives and Education Foundation (BRIEF) for their teaching, support, and guidance through this whole project. The team would also like to thank their mentors, Hilde Van den Bergh and Ana Parra for their encouragement and advice. Finally, the team would like to thank Better Education for Women in Science and Engineering (BEWiSE) for providing the gateway for the team to get involved in the program. Dates were converted from Gregorian date to Julian date using the USNO Julian Date Converter.

This work has made use of data from the European Space Agency (ESA) mission Gaia (https://www.cosmos.esa.int/gaia), processed by the Gaia Data Processing and Analysis Consortium (DPAC, https://www.cosmos.esa.int/web/gaia/dpac/consortium). Funding for the DPAC has been provided by national institutions, in particular the institutions participating in the Gaia Multilateral Agreement.

References

Fernique, F; Boch, T; Oberto, A and Bonnarel, A; Strasbourg astronomical Data Center, Aladin Sky Atlas 10

Gaia Collaboration, 2018, "Gaia Data Release 2: Summary of the contents and survey properties". ArXiv e-prints.

Gaia Collaboration, 2016, "The Gaia mission", *A & A* **595**, A1.

Las Cumbres Observatory; Haleakala Observatory, Hawaii

Luri et al. (2018): On the use of Gaia parallaxes.

Fitzgerald, M.T. (2018, accepted), "The Our Solar Siblings Pipeline: Tackling the data issues of the scaling problem for robotic telescope based astronomy education projects."; Robotic Telescopes, Student Research and Education Proceedings

Washington Double Star Catalog. Stelle Doppie Web Double Star Database https://www.stelledoppie.it/index2.php

Astronomical Applications Department. USNO Julian Date Converter https://aa.usno.navy.mil/data/docs/JulianDate.php

Discovery of a Wide Binary in the Solar Neighborhood

Wilfried R.A. Knapp

Vienna, Austria
wilfried.knapp@gmail.com

Abstract: During the work on a report with the topic of star systems in the solar neighbourhood up to 10 parsecs a so far unknown wide binary was discovered at a distance of ~8.1 parsecs from the Sun. This comes rather as a surprise as stars in the solar neighborhood are most likely the best investigated stellar objects

Part of the work on a report on star systems in the solar neighborhood up to 10 parsecs (currently in progress) was the selection of GAIA DR2 objects with parallax > 100mas and parallax error < 0.5% and Gmag < 18. The resulting 34 objects at a distance up to 10 parsecs included a pair so far not listed in the WDS catalog or other catalogs with binaries/multiples in the solar neighborhood.

The primary is TYC 3980-1081-1 (Gaia DR2 2202703050388170880) at J2000 position RA 21 51 38.297 Dec +59 17 38.456 with Gmag 9.3832 and parallax 123.0568 mas with error 0.5944 which means a distance of ~8.1 parsecs from the Sun. The secondary is UCAC4 747-070768 (Gaia DR2 2202703050401536000) at J2000 position RA 21 51 40.108 Dec +59 17 34.854 with Gmag 14.3852 and parallax 118.1243 mas with error 0.0208. Using the DR2 data for a Monte Carlo simulation calculating spatial distance between the components (see Appendix) results in a minimum distance of ~33,000 AU, a median distance of ~70,000 AU and a maximum distance of ~105,000 AU suggesting strongly a potential gravitational relationship (see Figure 1).

It seems a bit surprising to detect a new likely physical pair this close to the Sun, but this might be explained by the rather large delta parallax of ~5 mas between the two components making a potential gravitational relationship not very obvious at first glance.

Even more surprising is the fact that not even the primary is listed as close to the neighboring object in, for example, the RECONS project – this asks for additional research. Finch et al. 2016 give a parallax of 154.8 mas with a rather large error of 12.1 mas and for this reason this object was not included in the Henry et al. 2018 paper on new discoveries within 10pc. So there might be some caveats regarding this object but nonetheless the currently given data suggests a so far not identified physical system at a distance within 10 parsecs from the Sun even if DR2 proper motion data are somewhat different.

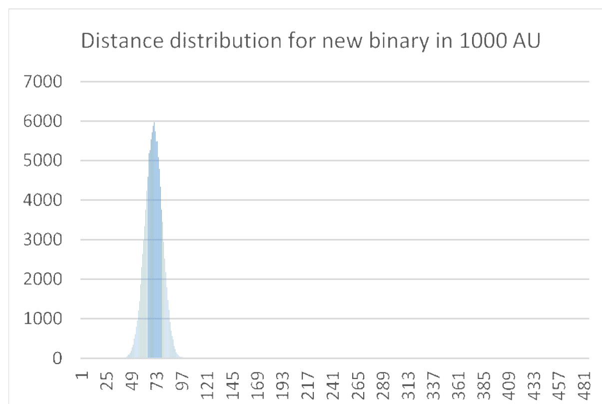

Figure 1. Distance distribution for newly detected binary in 1000 AU.

Gaia DR2 lists neither for the primary nor for the secondary a duplicated_source indication but the RUWE value for the primary is > 16 suggests that the Gaia DR2 single-star model does not provide very good fit to the astrometric observations – in this case just indicating for good reasons that the source is a non-single object.

Discovery of a Wide Binary in the Solar Neighborhood

The Gaia DR2 StarHorse catalog (Anders et al. 2019) provides a median mass for the primary of ~0.5 Sun mass but no such value for the secondary – an estimation based on magnitude difference gives ~0.15 Sun mass for the secondary. Based on these values a potential orbit (see Appendix) would have a minimum period of several million years, which means that most likely no human time frame will deliver enough observations for a reliable calculation of such a long period orbit.

Data for KPP4430 (WDS 21516+5918) based on Gaia DR2 2015.5 values are as follows:

- 327.90966427 RA J2000 in degrees
- 59.29440774 Dec J2000 in degrees
- 111.954 Position angle J2015.5
- 0.003 Error position angle
- 14.64214 Separation in arcseconds
- 0.00078 Error separation
- 10.93868 Estimated Vmag primary
- 0.00286 Error estimated Vmag Primary
- 14.58762 Estimated Vmag secondary
- 0.00227 Error estimated Vmag secondary
- 123.0568 Parallax primary in mas
- 0.5944 Error parallax primary
- 8.12633 Distance primary from the Sun in parsecs
- 118.1243 Parallax secondary in mas
- 0.0208 Error parallax secondary
- 8.46566 Distance secondary from the Sun in parsecs
- -79.190 Proper motion RA primary in mas/yr
- 10.517 Proper motion Dec primary in mas/yr
- -86.799 Proper motion RA secondary in mas/yr
- -19.190 Proper motion Dec secondary in mas/yr
- 33,031 Minimum spatial distance between the components in AU
- 0.50268 StarHorse median mass for primary in Solar masses
- 0.15000 Estimated mass for secondary in Solar masses
- 7,472,048 Minimum period of a potential orbit in years

Acknowledgements

The following tools and resources have been used for this research:

- DSS2 images
- 2MASS images
- Aladin Sky Atlas v10.0
- GAIA DR2 catalog
- GAIA DR2 StarHorse catalog
- Washington Double Star Catalog
- CDS VizieR
- CDS TAPVizieR
- Gaia@AIP Services hosted by the Leibniz-Institute for Astrophysics Potsdam (AIP)

References

F. Anders, et al., 2019, "Photo-astrometric distances, extinctions, and astrophysical parameters for Gaia DR2 stars brighter than G = 18", *Astronomy & Astrophysics*, **628,** A94.

Finch, Charlie T., Zacharias, Norbert, 2016, "Parallax Results from URAT Epoch Data", *The Astronomical Journal*, **151**, Issue 6, article id. 160, 12 pp.

Todd J. Henry, et al., 2018, "The Solar Neighborhood XLIV: RECONS Discoveries within 10 parsecs", *The Astronomical Journal*, 155:265 (23pp).

Knapp, Wilfried R. A., 2018, "A New Concept for Counter-Checking of Assumed Binaries", *Journal of Double Star Observations*, **14** (3), 443.

Appendix

Description of the Potential Gravitational Relationship assessment procedure (according to Knapp 2018):

GAIA DR2 data for RA/Dec and Plx are used for a Monte Carlo simulation assuming a normal distribution for these parameters with the given error range as standard deviation. The distance between the components is calculated from the inverted simulated parallax data and the simulated angular separation using the law of cosines

$$\sqrt{a^2 - 2ab\cos\gamma + b^2}$$

with a and b = distance vectors for the stars A and B in lightyears calculated as (1000/Plx)*3.261631 and γ = angular separation in degrees calculated as

$$\gamma = \arccos\left[\sin(DE1)\sin(DE2) + \cos(DE1)\cos(DE2)\cos(|RA1 - RA2|)\right]$$

The likelihood for potential gravitational relationship (LPGR) is the percentage of simulation results < 200,000 AU (~1 parsec) out of the simulation sample with a size of 120,000 corresponding with the likelihood that the real distance is smaller than 200,000 AU with an margin of error of 0.37% at 99% confidence.

The minimum, median, and maximum distance is the smallest, median, and largest result of the simulation sample.

Ignoring the likely effects of eccentricity the smallest/median/largest distance is used as estimation for the value for the semi-major axis of a potential orbit allowing for the calculation of a minimum/median/maximum orbit period assuming zero inclination using either median mass data from Anders et al. 2019 or if not available mass estimation from other sources.

UCAC4 337-189531, Discovery of Stellar Duplicity During Asteroidal Occultation by (3130) Hillary

Carles Perello
Agrupacio Astronomica de Sabadell, MPC-619, Catalonia, Spain
International Occultation Timing Association (IOTA-ES)
rigilk436@gmail.com

Eric Frappa
Euraster, Faycelles, France
frappa@euraster.net

Tomas Janik
Usti nad Labem, Czech Rep.
Czech Astronomical Society
Teplice Observatory and Planetarium
jazzer@centrum.cz

Bjoern Kattentidt
MPC K71, Neutraubling, Germany
International Occultation Timing Association (IOTA-ES)
bjoern@kattentidt-astro.de

Jiri Polak
Observatory Rokycany and Pilsen, Plzen-Lhota, Czech Rep.
jiri.polak@centrum.cz

Michal Rottenborn
Observatory Rokycany and Pilsen, Plzen, Czech Rep.
rotmi@seznam.cz

Antoni Selva
Agrupacio Astronomica de Sabadell, MPC-619, Catalonia, Spain
International Occultation Timing Association (IOTA-ES)
antoni.selva@gmail.com

Abstract: The occultation of the star UCAC4 337-189531 by the asteroid 3130 Hillary on July 23rd, 2019 has shown the duplicity of the star. Three observations carried out from Czech Rep. and Spain enable the determination of the parameters of this double star. A separation of 193.5 ± 18.7 milliarcseconds (mas) and a position angle (PA) of 54.5 ± 18.7 degrees has been calculated. From the magnitude drop in the light curves the estimated magnitudes without filter are 12.6 ± 0.04 and 13.4 ± 0.2. We suggest that this pair be included in the WDS catalog.

UCAC4 337-189531, Discovery of Stellar Duplicity During Asteroidal Occultation by (3130) Hillary

Circumstances

On July 23, 2019 the asteroid (3130) Hillary occulted the star UCAC4 337-189531. This prediction was published in the occultation's feed IBEROC *[6] (Figure 1) and it was observable from the south-east of Spain to the north-east of Europe. UCAC4 337-189531 is a 12.2V magnitude star with the equatorial coordinates RA 19h 30m 57.37s, Dec. -22º 36' 13.26" (J2000.0).

The magnitude of the asteroid (3130) Hillary in the moment of the occultation was 15.5. This value has been obtained in the ephemeris web page of the Minor Planet Center *[3]. Also, star and asteroid magnitudes were in the prediction

Observations

Five separate sites observed this occultation: three with positive results and two negatives. Table 1 gives the geographical coordinates and instrumentation used.

All the stations recording a positive occultation had results that did not match with the predicted ones, specifically the predicted time and the predicted magnitude drop.

Data Analysis

Using the magnitudes of the UCAC4 catalogue and the MPC, the predicted combined magnitude of the target was 12.26V (star UCAC4 [12.312V] plus asteroid MPC [15.5V]) and the predicted drop magnitude was 3.24V.

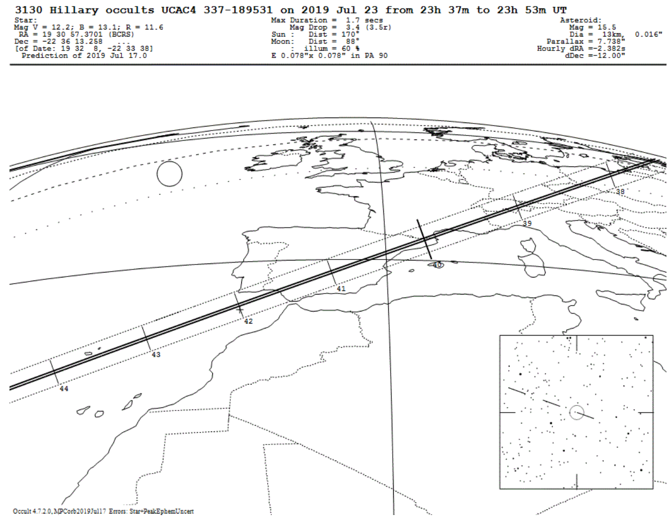

*Figure 1. Prediction map of the occultation computed with Occult *[1].*

The #1 station recorded the occultation 32.9s after the predicted time, and the event had a measured magnitude based in its light flux value of 12.50V ± 0.01 and a magnitude drop of only 0.33V. That's allow us to compute the magnitude of the star not occulted: 12.57V ± 0.04.

The #2 station recorded a delayed disappearance of 53.0s and the event had a measured magnitude based in its light flux value of 13.29V ± 0.01 and a magnitude

#	Station Team	Longitude, Latitude, & Altitude	Telescope	Equipment	Integration used
1	C. Perello & A. Selva	2° 05′ 24.6″ E 41° 33′ 00.2″ N 224 m	Newton 50 cm f/4	TV Camera Watec 910HX & KIWI inserter time	0.08s
2	J. Polak	13° 16' 30.6" E 49° 56' 02.1" N 533 m	Newton 30.3 cm f/4	TV Camera Watec 120N & TIM-10 Inserter time	0.16s
3	T. Janik	14° 02' 25,7" E 0° 40' 59,5" N 378 m	Schmidt-Cassegrain 15.3 cm f/10	TV Camera Watec 120N+ & TIM-10 Inserter time	0.64s
4	M. Rottenborn	13° 15' 37.8" E 49° 50' 09.5" N 427m	Newton 30.3 cm f/4	TV Camera Watec 120N & TIM-10 Inserter time	0.16s
5	B. Kattentidt	12° 12′ 57.3″ E 48° 59′ 23.1″ N 335m	Schmidt-Cassegrain + FR 27.9 cm f/6,3	TV Camera Watec 910HX & DL7USM-2006 V2.0 inserter time	0.16s

Table 1. Geographical coordinates and equipment of each station

UCAC4 337-189531, Discovery of Stellar Duplicity During Asteroidal Occultation by (3130) Hillary

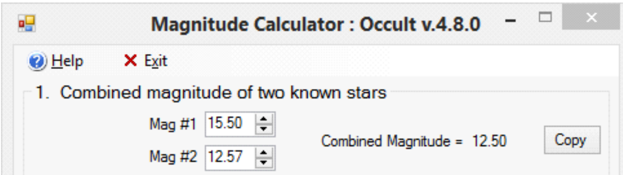

Figure 2. Estimated magnitude of the A component.

drop of only 1,07V. That's allow us to compute the magnitude of the star not occulted: 13.44V ± 0.2.

The #3 station recorded a delayed disappearance of 53.0s (the observer didn't report the delayed time in his report, he only reported a similar delay to station #2) and the event had a measured magnitude based in its light flux value of 13.27V ± 0.01 and a magnitude drop of only 1,08V. That's allow us to compute the magnitude of the star not occulted: 13.42V ± 0.2.

All the results match with the explanation that one component of the system did not be occulted. Based on the signal measured in the recorded videos we think the #1 station recorded the occultation of the B component (the fainter) and the #2 and #3 stations recorded the occultation of the A component (the brighter). The tool used to estimate the magnitude for each star based in the recording was the Magnitude Calculator Tool from Occult *[1] (Figures 2 to 4) assuming the magnitude assigned to the asteroid is 15.5V. These magnitudes are an approximation since there were no photometric filters placed in front of the detectors, and based in the predicted asteroid magnitude and the magnitude drop recorded.

We have also used the same comparison star to estimate the magnitude of the both components: UCAC4 337-189601 with a catalogue magnitude of 11.93V.

All timings obtained with TV-cameras have been corrected following the values obtained by G. Dangl * [4]. See Table 2.

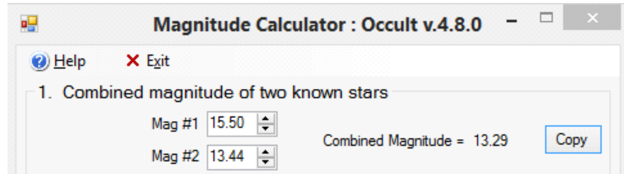

Figure 3. Estimated magnitude of the B component.

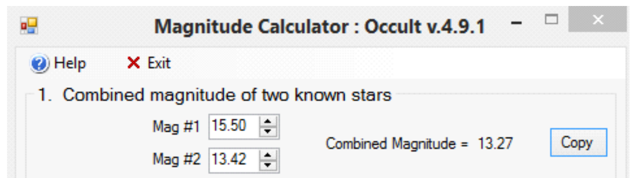

Figure 4. Estimated magnitude of the B component.

Using the software Occult *[1] we fit the circular shape limits of the asteroid, obtaining a result of ~24.4 km being the negative result of the #4 station a good reference for the shadow limit (see Figure 9) but not enough to be fully reliable about the shape. A separation and position angle of the occulted double star were also obtained and the values are listed in Table 3.

Conclusions

The casual occultation caused by an asteroid of the star UCAC4 337-189531 revealed its duplicity. The number of observers registered was enough to allow us to determine the parameters of this binary system.

(Text continues on page 92)

#	D2	D1	R2	R1
1	23 40 38.47 ± 0.08	-	23 40 41.39 ± 0.04	-
2	-	23:39:24.08 ± 0.16	-	23:39:25.84 ± 0.16
3	-	23:39:19.32 ± 0.32	-	23:39:21.56 ± 0.32

Table 2. Timings of the occultation. D1 and R1 are the disappearance and the reappearance of the brighter component of the double star, while D2 and R2 are, respectively, the disappearance and the reappearance of the secondary component.

Distance (mas)	193.5 ± 18.7
PA (degrees)	54.5 ± 18.7
Mag. (A)	12.6V ± 0.04
Mag. (B)	13.4V ± 0.20

Table 3. Parameters of the double star UCAC4 337-189531

UCAC4 337-189531, Discovery of Stellar Duplicity During Asteroidal Occultation by (3130) Hillary

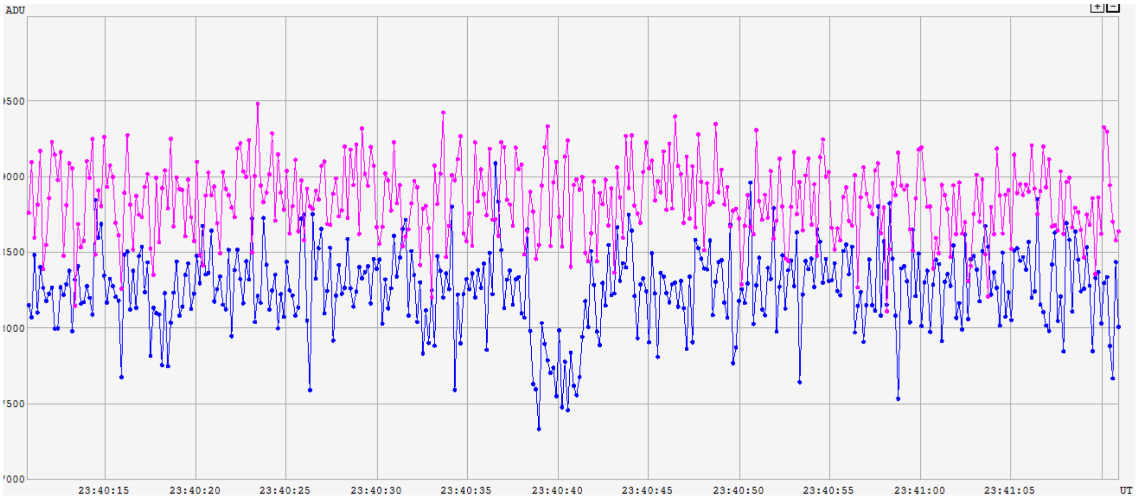

*Figure 5. A. Selva and C. Perello light curve obtained with Tangra *[2].*

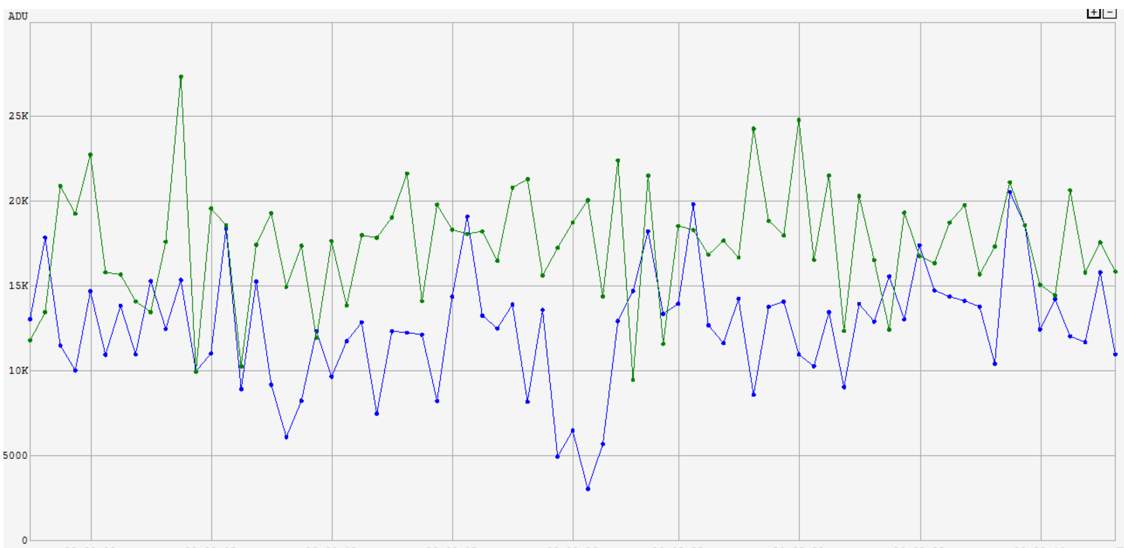

*Figure 6. T.Janik light curve obtained with Tangra *[2].*

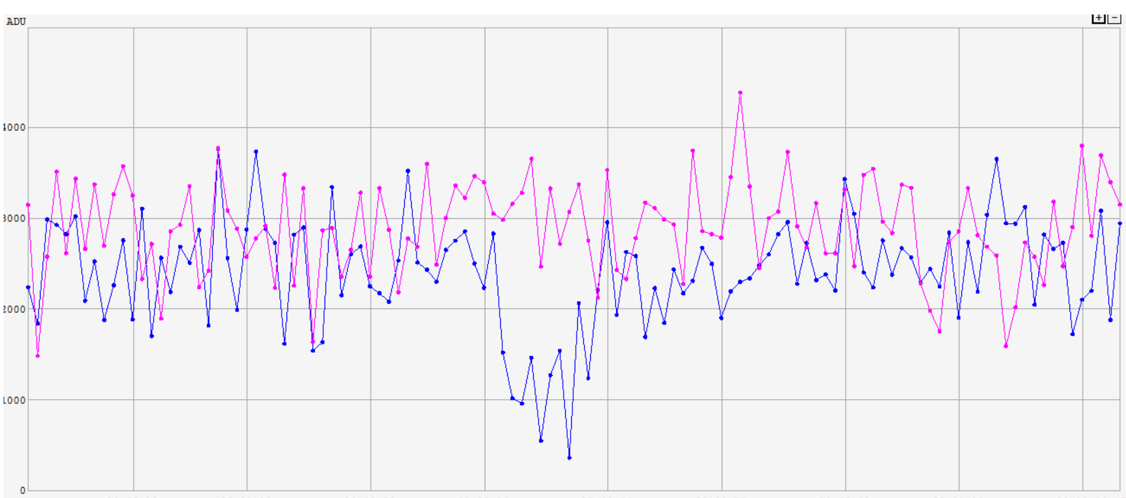

*Figure 7. J. Polak light curve obtained with Tangra *[2].*

UCAC4 337-189531, Discovery of Stellar Duplicity During Asteroidal Occultation by (3130) Hillary

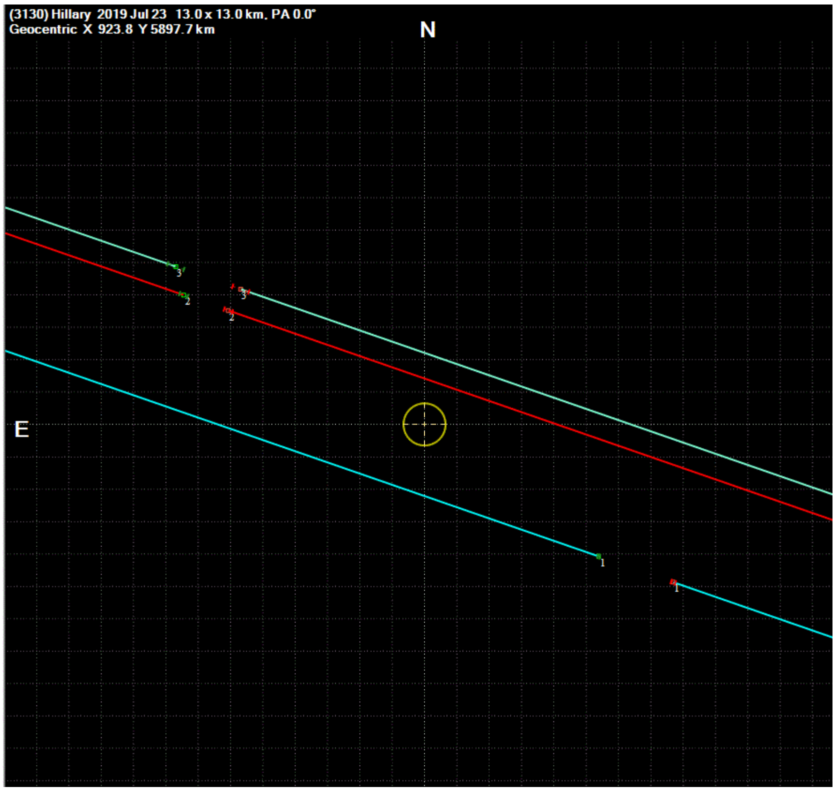

*Figure 8. Chart obtained with Occult *[1] before double star settings applied. The line is present if the star is visible.*

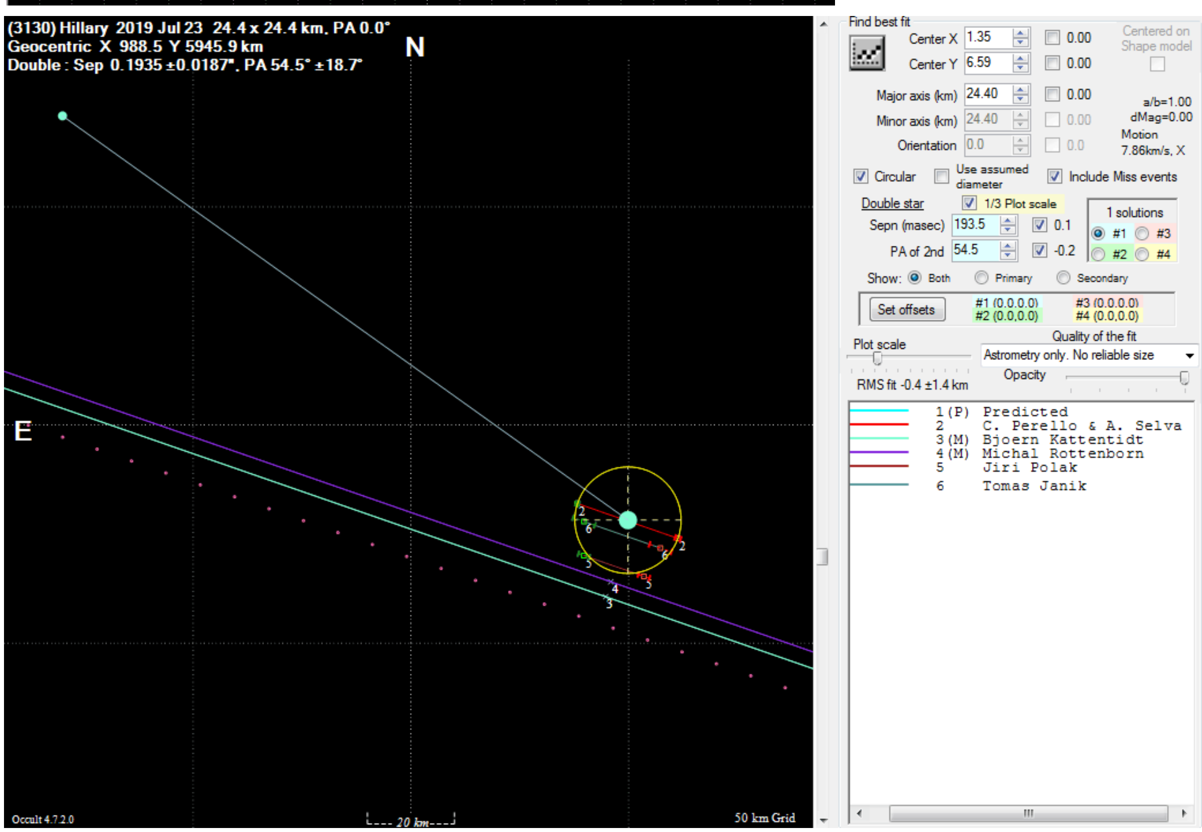

*Figure 9. Double star solution obtained by Eric Frappa with Occult *[1]. See *[5] for more information. The chords in the circle are the time that the star is occulted by the asteroid for the different observer's station. The continuous line below are the two negative chords (star always visible) and the dotted line is the predicted path.*

UCAC4 337-189531, Discovery of Stellar Duplicity During Asteroidal Occultation by (3130) Hillary

(Continued from page 89)

*References

Occult v4.7.2 (last stable version is v4.9.1) Occultation prediction software by David Herald, http://www.lunar-occultations.com/iota/occult4.htm

Tangra 3.6.17 software for reducing astronomical video observations, http://www.hristopavlov.net/Tangra3/

Minor Planet Center as a feed of orbital elements used to create the predictions, https://minorplanetcenter.net/

Dangl, Gerhard, Video exposure time analysis from recordings with video time insertion, http://www.dangl.at/ausruest/vid_tim/vid_tim1.htm

Herald, Dave, et al., "New Double Stars from Asteroidal Occultations, 1971 – 2008", *Journal of Double Star Observations*, **6**(1), 88-96, 2010. http://www.jdso.org/volume6/number1/herald.pdf

IBEROC Occultation Feed for Occult Watcher, maintained by Carles Perelló and available at http://ocultacions.astrosabadell.org/IBEROC/

Astronomical Association of Queensland 2017 Program: Blue Star Observatory Measurement of Six Neglected Southern Multiple Stars

Peter N. Culshaw, Diane Hughes, John Hughes, Des Janke, Graeme Jenkinson

Astronomical Association of Queensland, Australia.
bluestars@iprimus.com.au

Abstract: This paper presents the final results of a 2017 programme of photographic measurements of six southern multiple stars. All results were obtained using an Atik 460EX mono CCD camera used in conjunction with an equatorially mounted 400mm F4.5 Newtonian reflector.

Introduction

These latest results are part of an ongoing programme commenced in 2008 by the Double Star Section of the Astronomical Association of Queensland. The target stars were selected from the Washington Double Star Catalogue (WDSC) and were observed in Queensland, Australia from a latitude of approximately 27° S.

The results are presented in Table 1. The mean 95% confidence intervals for the new measures were ± 0.638º in PA and ± 0.128" in separation.

Method

Nightly sets of one hundred images were obtained with the equipment described above, after which the images were stacked using Atik DAWN software and then analysed using the astrometric double star program REDUC (Losse, 2008). Approximately ten stacked images of each target were taken per night for seven nights and the results averaged to obtain measures of separation and position angle with sufficient confidence.

Full details of the method are given in Napier-

(Text continues on page 97)

System	Last listed measure			New measure			Comment
	PA °	Sep. "	Epoch	PA °	Sep. "	Epoch*	
RSS331	254	8.2	1976	255.77	7.90	2017.396	Minimal change in 43 years
I 1250	149	4.6	1932	149.06	4.88	2017.448	Little probable change
B2777	106	5.7	1934	85.24	3.73	2017.456	Clear movement
CPO453	337	3.2	1928	334.29	3.53	2017.525	Slight changes
DON779	294	6.0	2015	299.10	5.90	2017.530	Change in PA
DON779	n/a	n/a	n/a	235.05	11.64	2017.530	New "C" component?
B2385	228	6.3	2015	229.94	6.17	2017.552	Minimal change
B2385	n/a	n/a	n/a	26.30	8.35	2017.552	New "C" component?

Table 1. Measurements of Nine Southern Multiple Stars

* Epochs of new measures given in Besselian years as the average of the observations making up the measure.

Astro. Assn. of Queensland 2017 Program: Blue Star Observatory Measurement of Six Multiple ...

RSS331 ***Centaurus***	**RA. 14 22.7** **MAG. 9.89 & n/a**	**DEC. -30 36** **PA. 254°**	**Last Measure 1976** **SEP. 8.2"**
Date	**No. images**	**PA°**	**Sep"**
16 May 2017	10	256.16	8.111
24 May 2017	10	255.80	7.939
25 May 2017	10	255.86	7.834
26 May 2017	10	255.77	7.793
27 May 2017	10	255.97	7.873
30 May 2017	10	255.05	7.856
02 June 2017	10	255.75	7.861
Mean		**255.766**	**7.895**
Std. dev.		0.346	0.105
95% CI +/-		0.320	0.097
P(t) movement		0.000	0.000
COMMENTS Slight increase in PA. Little probable change in separation.			

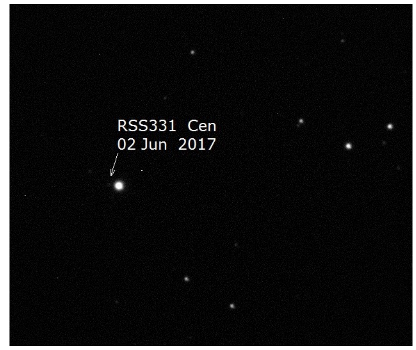

I 1250 ***Centaurus***	**RA. 14 43.6** **MAG. 8.11 & 12.7**	**DEC. -39 39** **PA. 149°**	**Last Measure 1932** **SEP. 4.6"**
Date	**No. images**	**PA°**	**Sep"**
02 June 2017	10	148.97	4.895
04 June 2017	10	149.8	4.794
09 June 2017	10	149.98	4.783
20 June 2017	10	149.33	4.76
21 June 2017	10	148.86	4.796
23 June 2017	10	148.89	4.93
25 June 2017	10	147.57	5.222
Mean		**149.057**	**4.883**
Std. dev.		0.792	0.162
95% CI +/-		0.733	0.150
P(t) movement		0.000	0.000
COMMENTS Very little if any apparent movement since the first measure in 1925.			

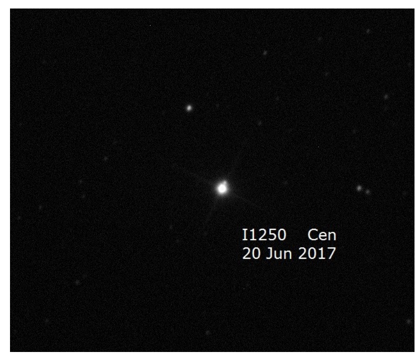

B 2777 ***Centaurus***	**RA. 14 56.0** **MAG. 8.52 & 14.1**	**DEC. -33 04** **PA. 106°**	**Last Measure 1934** **SEP. 5.7"**
Date	**No. images**	**PA°**	**Sep"**
02 June 2017	10	84.56	3.632
04 June 2017	10	85.66	3.585
21 June 2017	10	85.63	3.744
23 June 2017	10	84.57	3.74
25 June 2017	10	85.77	3.782
30 June 2017	10	85.26	3.892
Mean		**85.242**	**3.729**
Std. dev.		0.552	0.109
95% CI +/-		0.579	0.115
P(t) movement		0.000	0.000
COMMENTS Reductions in PA and separation are consistent with the two previous measures of 1930 & 1934.			

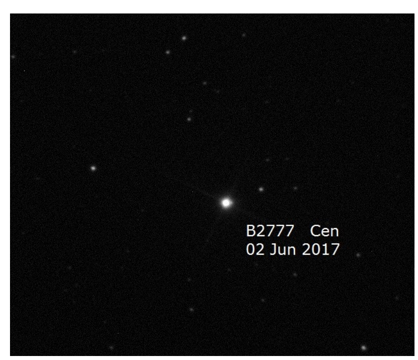

CPO453	RA. 16 04.7	DEC. -49 15	Last Measure 1928
Norma	MAG. 11.21 & 13.0	PA. 337°	SEP. 3.2"
Date	**No. images**	**PA°**	**Sep"**
30 June 2017	10	334.21	3.548
02 July 2017	10	335.19	3.606
17 July 2017	10	334.43	3.485
18 July 2017	10	333.4	3.509
21 July 2017	10	335.17	3.588
22 July 2017	10	334.37	3.515
23 July 2017	10	333.28	3.48
Mean		**334.293**	**3.533**
Std. dev.		0.756	0.049
95% CI +/-		0.699	0.046
P(t) movement		0.000	0.000

COMMENTS
PA has decreased in contrast to slight increase between previous measures in 1902 & 1928. Probable slight increase in separation over same period.

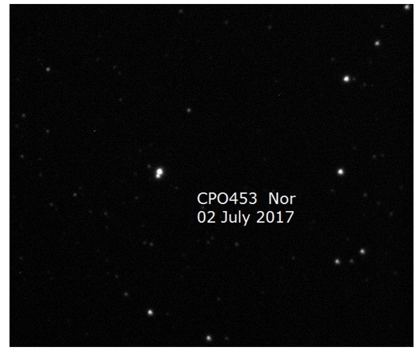

DON779	RA. 16 10.9	DEC. -66 21	Last Measure 2015
TrA	MAG. 8.09 & 14.1	PA. 294°	SEP. 6.0"
Date	**No. images**	**PA°**	**Sep"**
02 July 2017	10	299.75	5.438
11 July 2017	10	299.12	6.129
17 July 2017	10	299.77	5.842
18 July 2017	10	298.73	5.772
21 July 2017	10	298.10	5.929
22 July 2017	10	299.13	6.097
23 July 2017	10	299.12	6.083
Mean		**299.103**	**5.899**
Std. dev.		0.579	0.245
95% CI +/-		0.535	0.226
P(t) movement		0.000	0.000

COMMENTS
Clear change in PA. Little probable movement in separation.

DON779	RA. 16 10.9	DEC. -66 21	Last Measure n/a
TrA	MAG. 8.09 & n/a	PA. n/a	SEP. n/a
Date	**No. images**	**PA°**	**Sep"**
02 July 2017	10	234.69	11.572
11 July 2017	10	234.59	11.383
17 July 2017	10	234.15	11.72
18 July 2017	10	234.98	11.621
21 July 2017	10	235.59	11.863
22 July 2017	10	235.65	11.786
23 July 2017	10	235.71	11.522
Mean		**235.051**	**11.638**
Std. dev.		0.611	0.165
95% CI +/-		0.566	0.152
P(t) movement			

COMMENTS
Possible “C” component not previously recorded.

Astro. Assn. of Queensland 2017 Program: Blue Star Observatory Measurement of Six Multiple ...

B2385	RA. 16 26.0	DEC. -44 43	Last Measure 2015
Norma	MAG. 9.06 & 13.1	PA. 228°	SEP. 6.3"
Date	**No. images**	**PA°**	**Sep"**
11 July 2017	10	228.44	6.203
21 July 2017	10	230.16	6.215
22 July 2017	10	231.61	6.154
23 July 2017	10	231.11	6.198
29 July 2017	10	229.98	6.106
30 July 2017	10	229.11	6.24
01 August 2017	10	229.14	6.09
Mean		**229.936**	**6.172**
Std. dev.		1.139	0.057
95% CI +/-		1.054	0.053
P(t) movement		0.000	0.000

COMMENTS
Minimal changes evident since the original 1901 measure.

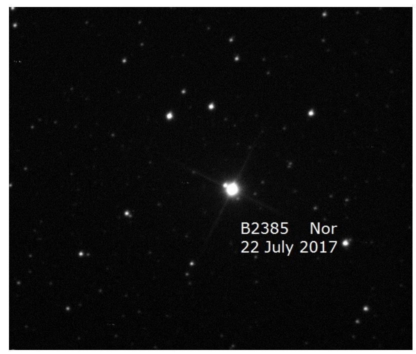

B2385	RA. 16 26.0	DEC. -44 43	Last Measure 2015
Norma	MAG. 9.06 & 13.1	PA. 228°	SEP. 6.3"
Date	**No. images**	**PA°**	**Sep"**
18 July 2017	10	26.26	8.251
21 July 2017	10	27.00	8.087
22 July 2017	10	26.54	8.364
23 July 2017	10	25.12	8.249
29 July 2017	10	26.76	8.632
30 July 2017	10	25.91	8.310
01 August 2017	10	26.50	8.557
Mean		**26.299**	**8.350**
Std. dev.		0.625	0.189
95% CI +/-		0.578	0.174
P(t) movement			

COMMENTS
Possible new “C” component not previously recorded.

(Continued from page 93)

Munn and Jenkinson (2009). Subsequent work on the errors inherent in the method is described in Napier-Munn and Jenkinson (2014). As proficiency has grown in the use of this equipment with the 400mm reflector, close doubles with considerable magnitude difference between the components have been successfully measured.

Fellow AAQ members Culshaw, Hughes and Hughes provided invaluable assistance with image processing using Losse's REDUC software, and Janke with processing the original FITS image files into JPEG photographs.

Results

For all of the systems shown below the WDSC information is first reproduced, showing the epoch 2000 position, magnitudes, separation, PA, and the last recorded measurement. The new measurements are then given in tabular form, including the mean and standard deviation and 95% confidence limits. Any uncertainties between the images and the last recorded measurements are discussed. Finally a conclusion is given as to whether any movement of the component stars has occurred in PA or separation, based on the P-value for the t-test comparing the new mean values with the catalogued value ($P < 0.05$ is considered as evidence of change).

As detailed in the tabulated results above possible previously unlisted "C" components were found and imaged for both DON779 Triangulum Australe and B2385 Norma.

The pair CPO453 Norma shows a slight decrease in PA in comparison to an increase recorded in previous measures of 1902 and 1928.

Please note that all attached images are aligned with North to the bottom and East to the right.

Acknowledgements

This research has made use of the Washington Double Star Catalog maintained at the U.S. Naval Observatory.

The Edward Corbould Research Fund administered by the Astronomical Association of Queensland for granting of funds to upgrade imaging camera and observatory computer to suit.

References

Losse, F. Reduc software, V4.5.1. http://www.astrosurf.com/hfosaf/uk/tdownload.htm

Napier-Munn, T.J. and Jenkinson, G., 2009, "Measurement of some neglected southern multiple stars in Pavo", *Webb Society Double Star Section Circular*, **17**, 6-12.

Napier-Munn, T.J and Jenkinson G., 2014, "Analysis of Errors in the Measurement of Double Stars Using Imaging and the Reduc Software", *Journal of Double Star Observations,* **10** (3), 193-198.

Argyle, R.W., 2012, *Observing and Measuring Visual Double Stars 2nd edition*, Springer.

Astrometric Measurement and Analysis of Celestial Motion for Double Star WDS 02176+5920

Marielle Cooper[1], Theophilus Human[1], Grady Boyce[2], Pat Boyce[2], Jae Calanog[1]

1. San Diego Miramar College
2. Boyce Research Initiatives and Education Foundation (BRIEF)

Abstract: Our team observed and analyzed the double star system WDS 02176+5920 (STI 1828) using the Las Cumbres Telescope network. The data was analyzed in AstroImageJ to measure position angle and separation. A mean position angle of 140.0° ± 0.2° (theta) and separation of 11.76" ± 0.05" (rho) was measured on Julian date 2458426.85100 The historical trend shows relatively no change in position angle and separation. However, the Harshaw calculation of the pair is low at 0.0017 (Harshaw 2014) and measurements on the proper motion of the right ascension and declination suggest the stars are moving in the same direction. These combined data points suggest a high probability that STI 1828 is common proper motion pair.

Introduction

The purpose of our research was to observe and analyze the position angle and separation of a double star system. The data was then analyzed to determine the nature of the selected double star to see if it could be classified as a physical or optical pair. A subcategory of physical double stars are common proper motion pairs which share similar proper motions but have very little relative change in separation over time (Greaves 2004). Classification of a physical binary can allow the total mass of the system to be determined, if an orbital solution is obtained and the distance to the system is known. As the nature of the STI 1828 system (shown in Figure 1) is unknown, the term double star shall be used throughout this paper.

To study double star pairs and determine their nature, the position angle (θ) and distance (ρ) between the stars is measured and compared to historical values. Graphing these values over time, it can be determined whether the stars may be gravitationally bound. Our research focused on WDS 02176+5920 (STI 1828). STI 1828 is in Cassiopeia and was selected as it met the requirements of falling between 00-08 RA hours, (02h 17m RA), having a separation greater than 5" (arcseconds), and a magnitude difference less than 3. Right Ascension was restricted between 00-08 RA as this is the portion of sky visible at night during October -November. The constraints of separations of greater than 5" and magnitude difference less than 3 were applied to ensure stars could be visibly separated in the telescope images. Additional selection criteria included a desire for magnitude visible through binoculars and a position in the Northern Hemisphere.

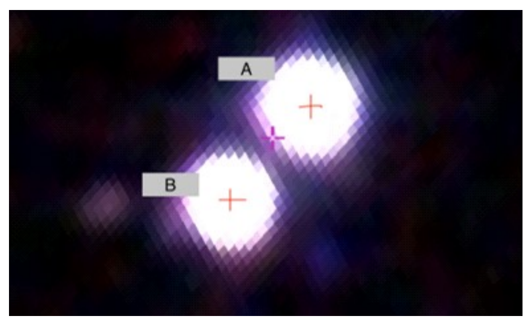

Figure 1. WDS 02176+5920 A is the primary star and B is the secondary

The first observation of this double star was recorded in 1908 by Johan Stein at the Vatican observatory with (θ) of 139.4° and (ρ) of 12.499". Since 1908 elev-

(Text continues on page 99)

Epoch	Position Angle	Separation
1908.05	139.4	12.499
1909.5	140.0	12.0
1910.97	140.2	11.408
1919.94	139.6	11.5
1921.85	138.9	11.66
1999.71	139.5	11.70
2003.68	139.8	11.742
2007.175	139.17	11.76
2010.5	140.0	11.76
2012.585	140.07	11.866
2013.066	140.13	11.776
2015.000	139.863	11.745
2018.843	140.0	11.76

Table 1: Historical Values of Position Angle and Separation Distance for STI 1828 02176+5920. Position angle is in degrees and Separation Distance in arc seconds. (Mason 2018)

en more observations have been recorded. The most recent measurement was in 2015 with (θ) of 139.8°, (ρ) of 11.745", and a difference in magnitude of 0.60.

Observations and Analysis

The Las Cumbres Observatory (LCO) was used for observation as its global network of telescopes allows for continuous visibility across the night sky. A 0.4-meter telescope was used mounted on a C-ring equatorial mount. The scientific camera used was an SBIG STX6303 mounted at the Cassegrain focus. Light was detected with the CCD capable of capturing 2048 x 3072 pixels with a resolution of 0.57 arcseconds per pixel. Default binning of 1 x 1 was used. The first data set was collected from the Haleakala site with telescope 2 (telescope id kb82) in Hawaii, USA. The second data set was collected from the McDonald Observatory using telescope 1 (telescope id kb92) in Texas, USA.

Two data sets were collected. The first one consisted of 18 images with the second having 15 images. The filters selected for the first data set were SDSS r', SDSS g', and clear. Filters were selected as the primary star had a spectral classification of G5V. For the second data set the same selection plus Bessel-B was used. Bessel-B was added to compare filter effects. Exposure times ranged from under a second for the clear to 12 seconds for the red filter. Due to telescope tracking issues for the images in the first data set, only the second data set was included for analysis. 15 images were analyzed from the second data set.

Data was returned after being processed through the Our Solar Sibling Pipeline (Fitzgerald 2018) which attached WCS coordinates, removed hot pixels, image artifacts, and flat fielded the images. The software AstroImageJ (AIJ) was used to analyze and measure the images.

The position angle and separation distance between the double stars was measured. 15 images were analyzed, four with SDSS red filters, four with SDSS green filters, three with Bessel blue filters, and four with no filter. The red filters at 12 seconds produced the clearest images while no filter and blue were lower quality images. AIJ then provided a measurement of position angle in degrees, separation distance in arcseconds, and delta magnitude between the stars. From the data the average standard deviation, and error were calculated for both position angle and separation. All data points were included as there were no obvious outliers and there was confidence in the measurement capabilities even at lower image qualities. For Epoch 2018.821 the average position angle was 140.0° ± 0.2° and 11.76" ± 0.05".

Discussion

The collected data was added and analyzed against historical data. Historical data suggested that no significant movement (movement greater than a standard deviation from the 2018 measurements) between the two stars had occurred in the past century. The data shown in Table 2 supports this conclusion. The movement recorded (Figures 2 and 3) through the century follows no obvious trend and it seems likely given the small differences that most or all movement falls within a standard deviation of each observation's measurement.

Epoch	Number of Images	Mean Position Angle (°)	Standard Deviation (°)	Mean Separation Distance (")	Standard Deviation (")
2018.843	15	140.0	0.2	11.76	0.05
2015.000	-	139.863	0	11.745	0

Table 2. Summary of the measurement of Position Angle and Separation Distance for STI 1828 02176+5920 from this paper compared to the last reported measurement in 2015. (Mason 2

Astrometric Measurement and Analysis of Celestial Motion for Double Star WDS 02176+5920

Of the 12 past observations, eight of the position angles recorded fall within the standard deviation of the 2018 position angle and seven within the standard deviation of the separation distance, Tables 1 and 2.

Graphs comparing position angle over time, separation over time, and the proper motion (Figures 2-4) demonstrate no clear relationship between the data points. Comparing the position angle data (Table 1 and Figure 2) from the early portion of the 20th century to the early 21st century, the range of the position angle remains within about one degree, with no obvious movement (Figure 2). While it is possible that there was a significant movement in both directions that then averaged out, it seems more probable that the accuracy of measurements improved over time, resulting in smaller standard deviations.

Graphing the separation distance against time , Figure 2, showed very little movement. Data from the late 20th/early 21st century is consistent, showing little change.

Figure 3 shows that separation distance in approximately the last 20 years has moved less than 0.2 arc seconds. While the early 20th century measurements show more variable separation distances, when combined with the modern measurements no clear pattern emerges.

The parametric graph also shows no clear movement in separation, Figure 4. Dates are marked on the

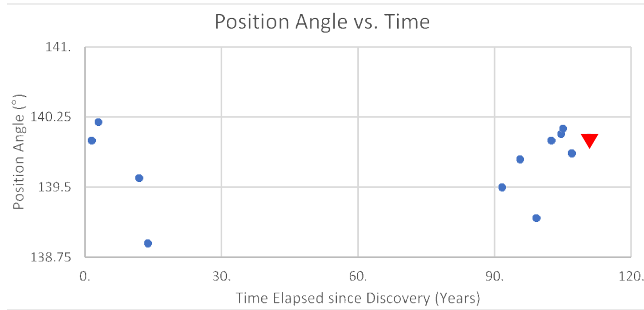

Figure 2. Graph of position angle (°) against the time passed since the first observation in 1908.05 including historical data and observations conducted. The red triangle marks the most recent data.

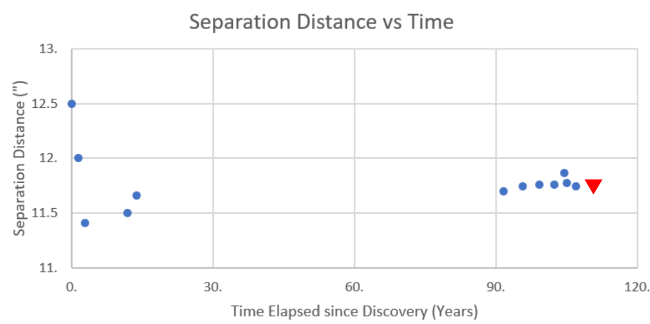

Figure 3. Graph of separation distance (") against the time passed since the first observation in 1908.05 including historical data and observations conducted. The red triangle marks the most recent data.

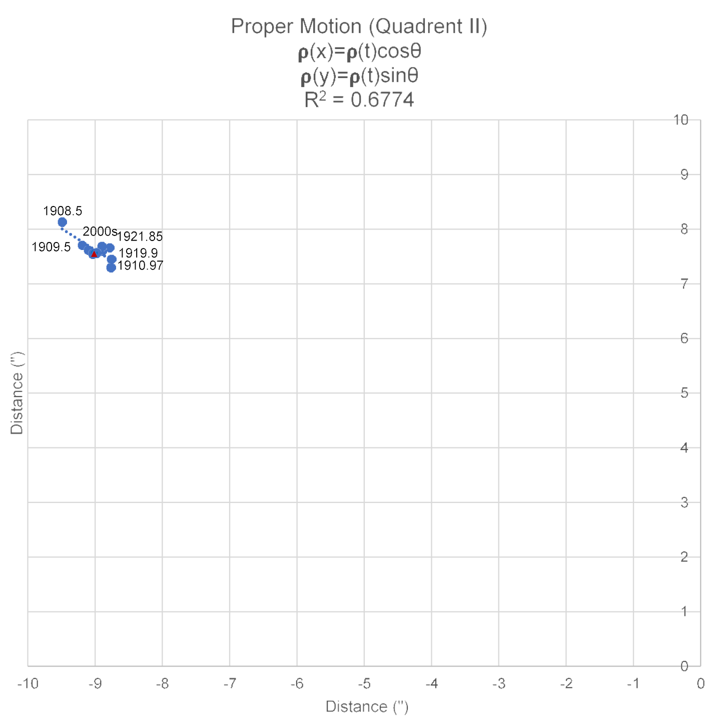

Figure 4: Graph of STI 1828 movement relative to the primary. The red triangle marks the most recent data. The R^2 for a linear fit is 0.6774 which does not fit a linear model.

Astrometric Measurement and Analysis of Celestial Motion for Double Star WDS 02176+5920

Figure 5. Graph showing potential distance overlap ranges between primary and secondary star.

graph to show the progression of time. The data is irregular, with 1998-2018 datapoints occurring clumped together while other epochs are spread apart. Analysis of the graph suggests a poor fit for either a linear or elliptic curve model, however it does fit a common proper motion pair model. As the movement is over a small range of values it is possible most movement is due to standard deviation in recording.

The proper motion of the star was also collected from Gaia release 2 data. It is summarized in Table 3.

Comparison shows that both the proper motion of the right ascension and declination of the primary and secondary are relatively close. This suggests that they are moving in the same direction.

There is evidence of stars having stellar companions (i.e. currently or previously gravitationally bound) with a distance of up to 8 parsecs between them (Shaya & Olling 2011). Gravitationally unbound stellar companions may be part of a stellar association, a very loose star cluster whose stars share a common origin but have become gravitationally unbound. Stellar companions with large distance between them are considered wide or very wide physical pairs (depending on distance). If the GAIA suggested 1.1 parsec separation between the primary and secondary star of STI 1828 is accurate it could comfortably fall into the wide binary range. Wide binaries often share similar proper motions making them common proper motion pairs or multiples (Shaya & Olling 2011). Common proper motion pairs are stars that have very similar proper motions but little to no relative motions between themselves over timescales of a century. The similarity of space motion however suggests they are related by origin. Additionally, it is common for their separation to be large enough to cause uncertainty of whether they orbit one another (Greaves 2004). STI 1828 seems to fit the categorization of common proper motion pair as it has a high degree of similarity between the star's proper motions.

The Harshaw Method (Harshaw 2014) was used to provide further analysis. There is a correlation between values close to zero being physical binaries and values close to 1 tending to be optical doubles. The result of the Harshaw calculation 0.0017 which suggests that STI 1828 is a physical double star though this method cannot predict the nature of the double's gravitational link.

There is a strong possibility that STI 1828 is a common proper motion pair as the proper motion suggests both stars are moving in the same direction. the Harshaw calculation predicts a physical pair, and the position angle and separation distance are relatively constant. The stars could also be gravitationally bound as the parallax suggests that the stars are close enough for a gravitational link to be possible. It is suggested that the position angle and separation distance be taken every five to ten years, to confirm consistency in the distance between the stars.

Conclusion

The data on STI 1828 suggests that stars are physically bound in a common proper motion pair. The new data acquired continued the trend of little movement in both position angle and separation distance over the last twenty years. The parallax data suggests the stars are close enough for gravitational linkage while the proper motion suggests the stars are heading in the same direction. The Harshaw analysis of this movement also suggests that that the primary and secondary star are physically bound.

Acknowledgements

This paper would not have been possible without the aide and support of the Boyce Research Initiatives and Education Foundation (BRIEF), Theophilius Human, Pat Boyce, Grady Boyce, and Jae Calanog. I thank them all for their time and feedback. The analysis and

Star	Proper Motion Right Ascension (mas/yr)	RA Proper Motion Uncertainty	Declination Proper Motion (mas/yr)	Dec Proper Motion Uncertainty
Primary	-43.411	0.06	-43.705	0.078
Secondary	-43.481	0.125	-43.903	0.127

Table 3: Summary of the Proper Motion of STI 1828. Data acquired from GAIA Release 2.

work contained within also relied upon the LCOGT network and made use of the SIMBAD and Aladin databases operated by the CDS in Strasbourg, France.

This work has made use of data from the European Space Agency (ESA) mission Gaia (https://www.cosmos.esa.int/gaia), processed by the Gaia Data Processing and Analysis Consortium (DPAC, https://www.cosmos.esa.int/web/gaia/dpac/consortium). Funding for the DPAC has been provided by national institutions, in particular the institutions participating in the GAIA Multilateral Agreement.

References

Boyce, G. and Boyce, P. Boyce, Research Initiatives and Education Foundation (BRIEF), http://www.boyce-astro.org/home.html.

Fitzgerald, M.T., 2018, accepted, "The Our Solar Siblings Pipeline: Tackling the data issues of the scaling problem for robotic telescope based astronomy education projects.", Robotic Telescopes, Student Research and Education Proceedings.

Gaia Collaboration, 2016, “The Gaia mission”, *A & A* **595**, A1.

Gaia Collaboration, 2018, “Gaia Data Release 2: Summary of the contents and survey properties”. ArXiv e-prints.

Greaves, J., 2004, “New Northern hemisphere common proper-motion pairs”, *Monthly Notices of the Royal Astronomical Society*, **355**, Issue 2, 585–590, https://doi.org/10.1111/j.1365-2966.2004.08341.x

Las Cumbres Observatory Network https://lco.global/observatory/sites/

Mason, B, 2018. Washington Double Star Catalog. Astronomy Department, United States Naval Observatory, http://ad.usno.navy.mil/proj/WDS/.

Sordiglioni, G. 2018. Stella Doppie Double Star Catalog, http://www.stelledoppie.it/index2.php?menu=29&iddoppia=48579.

Shaya, E.J & Olling, R.P., 2011, “Very Wide Binaries and Other Comoving Stellar Companions: A Bayesian Analysis of the Hipparcos Catalogue”, *The Astrophysical Journal Supplement Series*, 192:2 (17 pp).

Harshaw, R., 2014, “Another Statistical Tool for Evaluating Binary Stars”, *Journal of Double Star Observations*, **10**, 32.

Wenger et al., 2000. "The SIMBAD astronomical database", *A&AS*, 143:9.

Journal of Double Star Observations

January 1, 2020
Volume 16, Number 1

The Journal of Double Star Observations (ISSN 2572-4436) is an electronic journal published quarterly. Copies can be freely downloaded from http://www.jdso.org.

Questions, comments, or submissions may be directed to rclark@southalabama.edu or to rmollise@bellsouth.net

The *Journal of Double Star Observations* (*JDSO*) publishes articles on any and all aspects of astronomy involving double and binary stars. The *JDSO* is especially interested in observations made by amateur astronomers. Submitted articles announcing measurements, discoveries, or conclusions about double or binary stars may undergo a peer review. This means that a paper submitted by an amateur astronomer will be reviewed by other amateur astronomers doing similar work.

Submitted manuscripts must be original, unpublished material and written in English. They should contain an abstract and a short description or biography (2 or 3 sentences) of the author(s). For more information about format of submitted articles, please see our web site at http://www.jdso.org

Submissions should be made electronically via e-mail to rclark@southalabama.edu or to rmolise@bellsouth.net. Articles should be attached to the email in Microsoft Word, Word Perfect, Open Office, or text format. All images should be in jpg or fits format.